A multi-institutional quantitative survey of multi-leaf collimator accuracy using a digital picket fence test with sub-millimetre detection capabilities.

By

Willem Petrus Engelbrecht Boonzaier

B.Sc. (Hons), University of the Free State, 2016

This thesis is presented in partial fulfilment of the requirements for the Degree of Master of Science in Medical Physics in the Faculty of Medicine and Health Sciences at Stellenbosch University.

April 2022

Stellenbosch University https://scholar.sun.ac.za

Table of content:

Stellenbosch University https://scholar.sun.ac.za

Stellenbosch University https://scholar.sun.ac.za

Stellenbosch University https://scholar.sun.ac.za

Stellenbosch University https://scholar.sun.ac.za

List of figures:

Stellenbosch University https://scholar.sun.ac.za

Stellenbosch University https://scholar.sun.ac.za

Stellenbosch University https://scholar.sun.ac.za

Stellenbosch University https://scholar.sun.ac.za

List of tables:

Stellenbosch University https://scholar.sun.ac.za

Abstract:

When patients are treated with modern radiotherapy, multi-leaf collimators (MLC) are used to shape treatment fields. With recent advances in technology, MLCs have also been used to modulate dose in certain areas inside patients to obtain better treatment outcomes. For the desired treatment outcomes to be valid, the equipment used to deliver the radiotherapy must function optimally.

This study was aimed at creating software that can measure the accuracy of the MLC independently with routine picket fence test measurements. With this in place, the software was used to conduct a national survey of the accuracy of MLC systems on various medical linear accelerators in South Africa.

Using on-board imaging and the in-house created software, MLC position and width errors could be found efficiently and with a very low degree of user input. When the results from the software were validated with measurements, other commercial software, and log files from linear accelerators, the average errors found agreed within 0.27mm, 0.49mm and 0.11mm for the measurements, commercial software and log file comparisons respectively.

A national survey could be done with data from participating volunteer centres. A distinction could be made between units with more advanced capabilities such as VMAT and SRS capabilities by including picket fence tests acquired during arc delivery and picket fence tests done as a measure of the performance of the MLC for VMAT and SRS applications.

The results showed that the software was easy and non-costly to compile. Results indicate that the software is robust enough to be used across a multitude of vendor types but sensitive enough to detect MLC errors in the order of 1 pixel of the onboard detector used. The software indicated that all units that participated in this study met the national standards of 2mm MLC accuracy. SRS capable units all had MLC accuracies under 1mm.

Stellenbosch University https://scholar.sun.ac.za

Declaration:

By submitting this thesis electronically, I (Willem Petrus Engelbrecht Boonzaier) declare that the entirety of the work contained therein is my own, original work (excluding the collection of data for routine monthly quality assurance volunteered for this study), that I am the sole author thereof, that reproduction and publication thereof by Stellenbosch University will not infringe any third party rights and that I have not previously in its entirety or in part submitted it for obtaining any qualification.

April 2022

Date

Copyright © 2022 Stellenbosch University
All rights reserved

Stellenbosch University https://scholar.sun.ac.za

Introduction:

Cancer:

What is cancer?

Mammalian cells contain chromosomes in the nucleus of the nucleus that consists of molecules called deoxyribonucleic acid (DNA). These DNA molecules are responsible for controlling cellular processes and contain the genetic information of cells. One of the very important processes is the replication of a cell. When these DNA molecules are damaged, they can bear serious implications for the cell. Depending on the severity of damage done to the DNA, the DNA might be repaired through DNA repair mechanisms. If the damage is not too severe, enough of the DNA molecule is still present and the chances of successful or complete and correct repair are very good. As the severity of the damage to the DNA of a specified cell increases, the chances of the DNA repairing correctly or completely become lower. Incorrectly repaired or unrepaired DNA molecules can lead to mutations in the chromosomes of the cell. The most severe cases of DNA damage are most likely to end in cell death(1).

Generally, cells of the human body grow and divide to form new cells as the body requires. If a cell grows too old or damaged, it has a pre-programmed way of removing itself from the body. This method is called apoptosis and it is a type of programmed self-killing that the cell initiates to create room for new, healthy cells to take their place(2).

Cancer is a collective name given to a group of diseases where this pre-programmed method has gone corrupt/mutated or is no longer present or the part of the DNA controlling it could not be repaired after damage. It usually results in some cells in the body growing or dividing uncontrollably and sometimes spreading to surrounding tissues. It is also possible for some of these cancer cells to break off from the host and spread to a remote location in the human body where it starts to grow anew. This remote spreading of cancer is called metastasis(2).

Cancerous tumours that exhibit invasion of nearby tissue or metastasis are classified as malignant. Some tumours do not exhibit this behaviour. They are referred to as benign and they usually cause harm to the body by growing so large that they interfere with the normal functioning of the body(2).

There are many differences between cancer cells and normal cells, with the most predominant being that cancer cells grow and divide uncontrollably. Because of this,

Stellenbosch University https://scholar.sun.ac.za

cancer cells are generally less specialized than normal cells and can ignore signals that would normally tell cells to stop dividing or initiate apoptosis(2).

Cancer cells are also able to "invade" the normal functioning of normal cells by inducing nearby primitive cells to form blood vessels to supply blood and by extension nutrients to the tumour to grow. It also can "hide" from the immune system which is supposed to get rid of unwanted or abnormal cells in the body(2).

In the human body, these cancer cells develop as a genetic disease, which means that it is a product of changes to the genes that control normal functions in the cells of the body – especially those genes that control functions such as growing, dividing and death of normal cells. These changes or damages to the DNA or genes can come from a multitude of factors, including exposure to environmental factors such as smoke or ionising radiations such as ultraviolet rays from the sun. The faults can be inherited from parents in some cases and in others it originates purely as an error during cell division(2).

Cancer treatment:

The treatment for cancer includes a multitude of fields with the major contributors being surgery, chemotherapy and radiotherapy.

Surgery:

Surgery forms part of several parts of oncology, including prevention, diagnosis, staging and treatment of cancer(3).

As a sole treatment of cancer, surgery is limited in a very large way. For surgery to be a successful cancer treatment, the tumour must be completely removable from the human body. This is a very effective method in the early stages of cancer, where the cells are contained to a specific part of the body, have not infiltrated too much of the normal tissue and have not metastasized to remote locations(3).

Surgery is often not a singular treatment modality but is often combined with other forms of treatment where surgery is responsible for tasks as debulking the disease, resection of metastatic disease, oncologic emergency surgery, palliative surgery or for reconstruction purposes(3).

Stellenbosch University https://scholar.sun.ac.za

Chemotherapy:

Chemotherapy can contribute to oncology treatment in many ways. Primary induction, adjuvant or neoadjuvant treatment regimens may be used(3).

During chemotherapy treatment, specific drugs are administered to the patient which can kill cells with certain functions or change characteristics of certain cells, like stopping the cells from dividing or making the cancer cells more radiosensitive(3).

Some chemotherapy drugs for example will target rapidly dividing cells as this is the main characteristic of cancer cells. This is a very targeted way of treating this disease, but unfortunately, there are normal cells in the human body that need to divide rapidly to ensure the normal functioning of the body. Some of these cells can be found in the digestive tract, hair follicles and bone marrow. When chemotherapy is therefore given as treatment, patients may experience side effects correlating to the normal cells discussed here being harmed as well(3).

When chemotherapy is given as an adjuvant treatment, its main function is to eliminate the micro-metastatic disease in addition to the primary radiotherapy or surgery. The aim of this is to prevent recurrence locally or elsewhere due to systemic spread through the body. This has the advantage to increase the overall survival of the patient(3).

Radiotherapy:

Radiotherapy is a popular treatment modality for many types of cancer. The basic principles of radiotherapy involve destroying the tumour cells by bombarding them with ionising radiation. One of the advances of radiotherapy is that it travels in a relatively straight path, which allows the treatment to be targeted to the tumour, however, due to the tumour being inside of the body, some of the normal cells will also have to be irradiated to reach the tumour(3).

Radiotherapy can be divided into external beam radiotherapy and internal radiotherapy. When using external beam radiotherapy, high energy radiation beams are used to treat the target inside or on the body from an external source. Modern external beam radiotherapy focuses on killing the tumour while doing as little as possible damage to the normal tissue. This can be delivered by many different technologies, but the Linear accelerator (linac) is probably the most popular of all(3). Figure 1 below shows a radiotherapist positioning a patient on a modern linac for radiotherapy treatment.

Stellenbosch University https://scholar.sun.ac.za

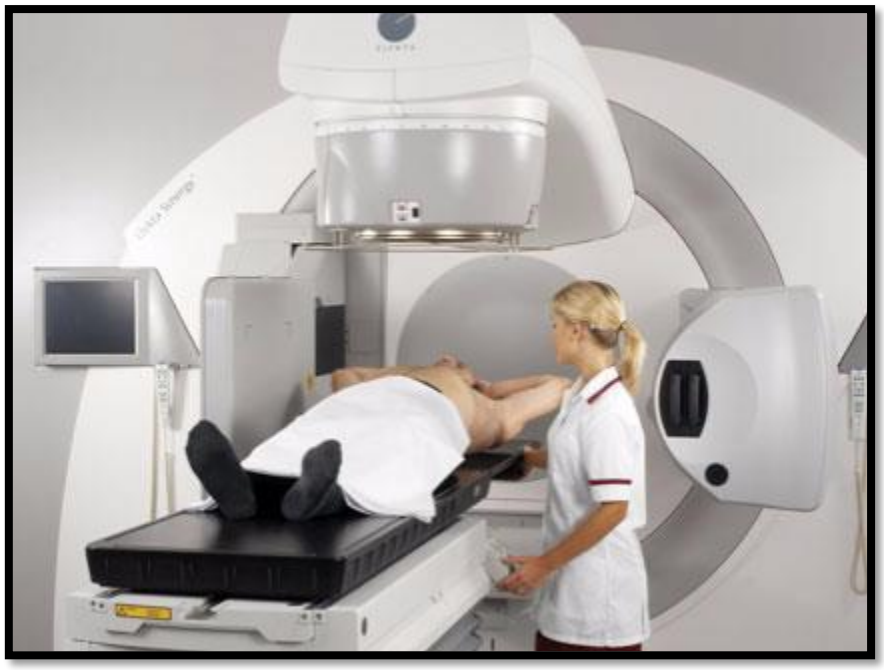

Figure 1: Image of a radiotherapist positioning a patient on a modern linac for radiotherapy treatment(4).

Internal radiotherapy also referred to as brachytherapy, is a technique where a sealed radioactive source or sources are placed in, near or inside the tumour for some time or permanently. This radiotherapy technique is effective for localised lesions that are easily accessible. Encapsulated sources used for brachytherapy usually have a sharp dose fall-off, which allows for treating tumours with high doses while giving low doses to normal tissue in the vicinity. For advanced disease, brachytherapy often provides no advantage over other techniques(3).

Role of Linear accelerators in Radiotherapy:

Linear accelerators have been around almost since the discovery of X-rays in 1895 by Roentgen. In the 1950s, H.E. Johns invented the cobalt-60 unit and revolutionised radiotherapy with high energy photons. Soon after medical linacs topped cobalt-60 units and are now at the forefront of radiotherapy(4).

Linacs are used in external beam radiotherapy or sometimes called teletherapy. This technique usually consists of irradiating the target volume with more than one beam from a source of radiation external to the patient, collimated with the use of an mutli-leaf collimator (MLC) system, which can also be used to create irregularly shaped fields or dynamically to modulate the intensity of radiation being treated with. With the help of modern linac, this can be done with a variety of options including the choice of patient setup, constant source to surface distance (SSD) or constant source to axis distance (SAD),

Stellenbosch University https://scholar.sun.ac.za

photon beams with energies that can range from 4MV to 25MV, high energy electron beams in the mega electron volt region and the variety of clinically available field sizes that can be set by the multi-leaf collimator system. Modern linacs have on-board imaging systems to verify patient setup. This can be in the form of a megavoltage detector that can be used with the radiation supplied from the treatment beam itself or an additional onboard imaging system with radiation capabilities in the kilovoltage range(4).

Stellenbosch University https://scholar.sun.ac.za

Linear accelerators:

Components of a medical linear accelerator:

To produce a clinically relevant megavoltage radiation beam for the treatment of cancer, LINACs are equipped with several components that include an injection system like an electron gun, an RF power generation system (magnetron or klystron), an accelerating waveguide, an auxiliary system, a beam transport system, a beam collimation system and a beam monitoring system. A schematic diagram of the medical LINAC design is shown in figure 2(4).

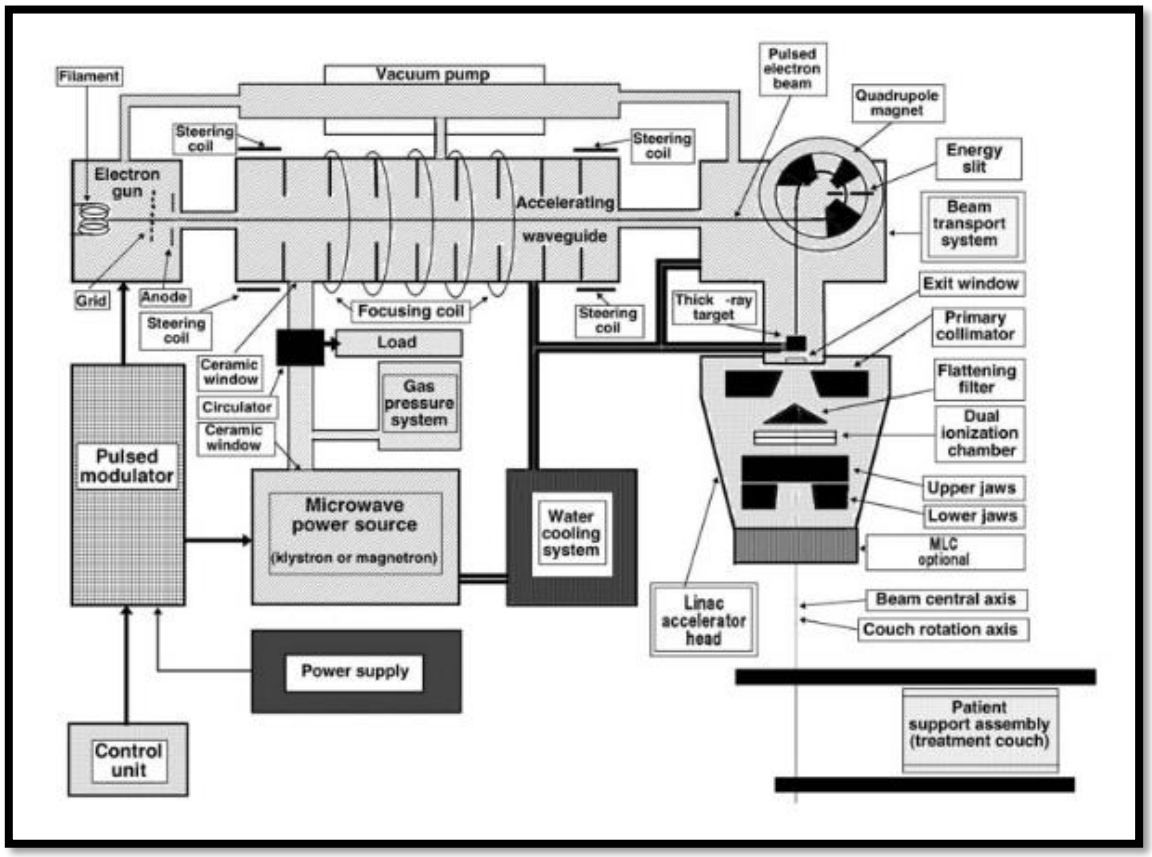

Figure 2: Schematic diagram of LINAC design(4).

Injection system:

The injection system of a LINAC is the source of electrons that are accelerated in the LINAC and is simply called an electron gun. In an electron gun, electrons are thermionically emitted from a heated cathode. The electrons are successively focused electromagnetically into a thin pencil beam by a curved focusing electrode and can accelerate to the perforated anode. The anode also serves as the entrance window to the accelerating waveguide. Electrostatic fields that focus and accelerate electrons are supplied to the anode and cathode from the pulse modulator to ensure that the electron

Stellenbosch University https://scholar.sun.ac.za

pulses are in phase with the microwaves emitted by the Radiofrequency power generation system(4).

Radiofrequency power generation system:

The radiofrequency power generation system produces microwaves that are used in the accelerating waveguide to accelerate electrons to the appropriate kinetic energy required for treating cancer. This system consists of two major components, the radiofrequency source and the pulse modulator(4).

Clinically, the radiofrequency power source is usually either a magnetron or a klystron. Both these devices use electron acceleration and deceleration in a vacuum to produce microwaves. This can be done when electrons are thermionically emitted from a heated cathode and the electrons accelerate and decelerate according to a pulsed electric field(4).

The pulse modulator is a complex system of electronic circuitry that controls the voltage, current and time factors associated with the radiofrequency power source and the electron gun. This sophisticated piece of circuitry is housed in the modulator cabinet and is responsible for ensuring that the microwaves and electron beams coincide when they enter the waveguide to allow for optimal acceleration. (4).

Accelerating waveguide:

The accelerating waveguide is an evacuated tube of cylindrical or rectangular design that is used in the transport of microwaves and electron acceleration. It consists of cavities for two main reasons, to couple and distribute microwave power between adjacent cavities and to provide a suitable electric field pattern for electrons to be accelerated. Two types of accelerating waveguides are used clinically(4).

The travelling waveguide houses microwaves that enter the accelerating waveguide on the side of the electron gun and travel to the target end of the waveguide. They are either absorbed on the exit end or transported to a resistive load where they are absorbed or fed back in phase into the waveguide(4).

In standing waveguides, the ends of the guide are closed with a conducting disc to reflect the microwave power. This results in standing waves in the waveguide that are used to accelerate the electrons(4).

Stellenbosch University https://scholar.sun.ac.za

Auxiliary system:

The Auxiliary system is composed of several components which aid in making electron acceleration possible. The vacuum pump system produces a vacuum pressure of 10^6 torr in the waveguide and the radiofrequency generator. The water-cooling system is used for cooling the waveguide, the target and the radiofrequency generator. Lastly, the auxiliary system also has lead shielding against leakage radiation built into the LINAC system(4).

Operation of a medical linear accelerator:

Basic principles of electron acceleration:

Fundamentally, to be able to accelerate particles, they must contain a charge if the acceleration is accomplished by fast-changing electric fields. With this method, electron acceleration can be achieved through different designs and techniques. Some examples of charged particle accelerators that use varying electric fields to accelerate charged particles include betatrons, cyclotrons and more recently microtrons(4).

Electron acceleration in the linear accelerator:

In LINACs, electrons are accelerated with the help of electromagnetic waves in the radio-frequency spectrum. The electron energy is usually low at the time of injection; however, these electrons gain energy as they travel down the evacuated waveguide. Very high-frequency radio waves are needed to accelerate electrons to energies that can be used clinically(4)(5).

The first important component to aid in the acceleration process is the waveguide. This is usually a metal holder of about 1 m in length with corrugations on the inside. The corrugations, or sometimes called iris diaphragms, together with the waveguide dimensions, determine the velocity at which the waves travel within the waveguide. An example of a waveguide can be seen below in figure 3(4)(5).

Stellenbosch University https://scholar.sun.ac.za

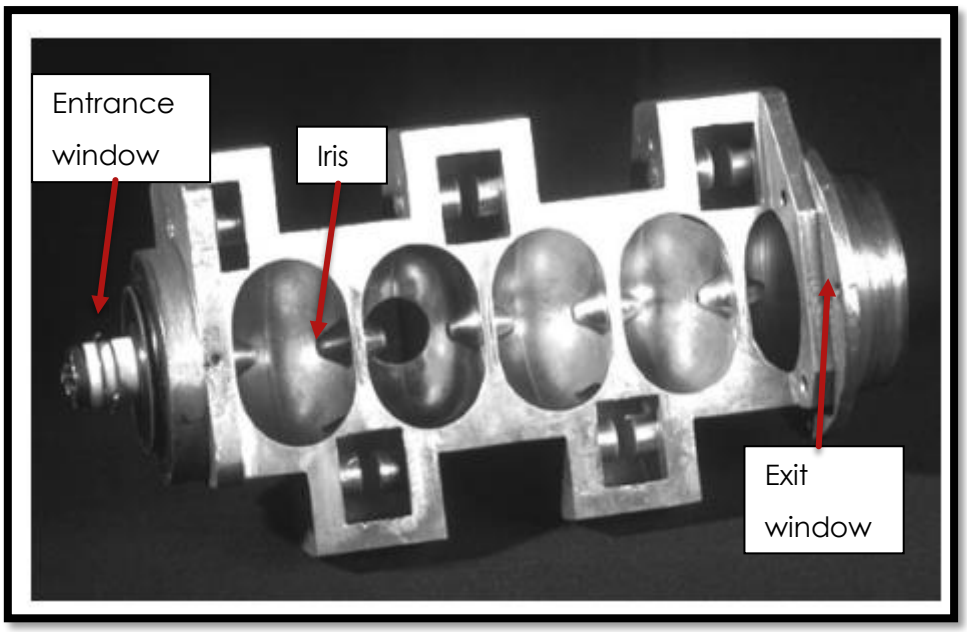

Figure 3: Annotated Image of accelerating waveguide(4).

The second component of importance is the radio wave generator, which can be a magnetron or a klystron(4)(5).

One of the most important components to ensure electron acceleration is the pulse forming network. This network is a collection of electronic components with the main function of synchronising the output from the electron gun and the magnetron/klystron. This is an essential step as the electrons need to be ejected with the right energy and at the right moment to ensure optimal acceleration(4)(5).

When all these components function together, electron acceleration can be achieved by the following process. The electric field component of the radio waves bunches the electrons into a cluster or group just after ejection. This is achieved as can be seen in figure 4 below, showing that if electrons are faster than the wave they are decelerated to the ideal velocity and if they are slower than the wave they are accelerated to the ideal velocity. This will happen until all electrons oscillate about the equilibrium position. At the same time the wave will be traversing the waveguide and with the help of the waveguide and iris designs, accelerate the electrons in a way like a wave of water accelerating a surfer riding it. This will decrease the frequency and increase the wavelength of the radio wave as energy from the radio wave is transferred to the electrons. The velocity of the wave is therefore constant as the electrons are accelerated through the waveguide. This can also be seen in figure 4(5).

Stellenbosch University https://scholar.sun.ac.za

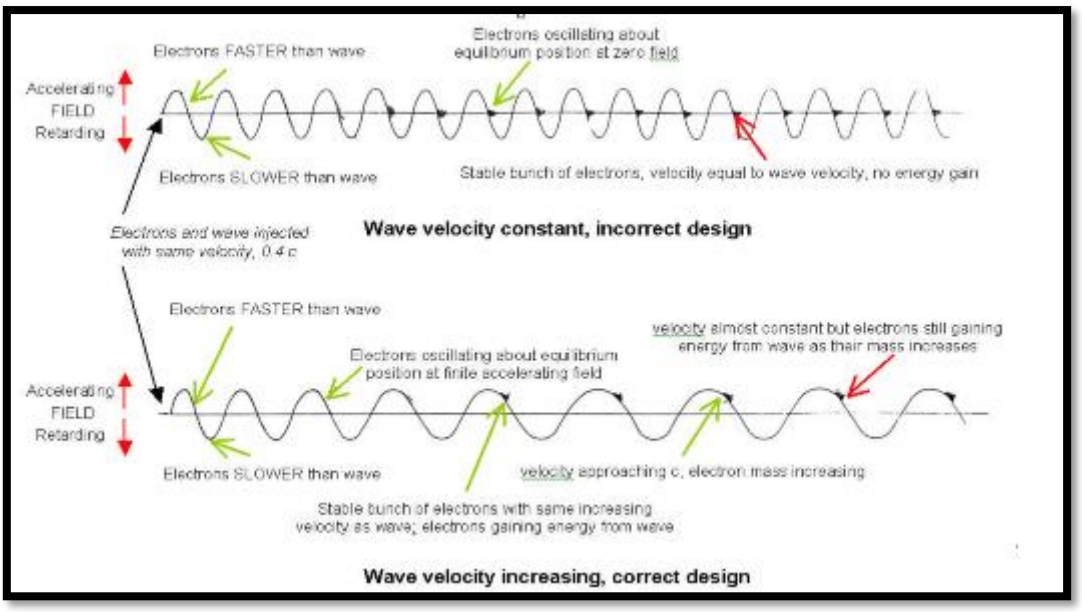

Figure 4: Diagram explaining the bunching and acceleration of electrons in an accelerating waveguide(5).

After electron acceleration is performed as described above, the accelerated electrons can then be used to treat a patient with the aid of the electron beam or with a photon beam, which is created by forcing the electron beam to hit a high atomic number transmission target, producing bremsstrahlung photons(5).

Electron beam transport:

Bending electromagnets are used in LINAC operating at energies above 6MeV. The reason for this is that the waveguide required for electrons to reach the kinetic energy to generate a megavoltage beam with energy higher than 6MeV is too long for straight-through mounting. The accelerating waveguide is usually mounted parallel to the axis of gantry rotation; therefore the electron beam needs to be bent to exit from the gantry head to treat cancer(4).

Production of clinical electron beams:

Several clinical LINACs can deliver electron beams and photon beams. Electron beams that can be generated from a clinical LINAC typically range in energy from 4 MeV to 30 MeV. The electron beam can be produced by removing the transmission target and the flattening filter needed for photon beam generation by use of mechanical systems. The currents that produce the electron beams are two to three times weaker than the currents needed to produce photon beams due to the removal of the transmission target and the flattening filter. The thin electron beam that is produced in the waveguide, exits through a small beryllium window. Beryllium has a low atomic number, which makes it ideal to

Stellenbosch University https://scholar.sun.ac.za

reduce the amount of electron scattering and bremsstrahlung production that occurs within the window(4).

From this point onward, clinical electron beams can be used in scattered electron beams and pencil electron beams. Scattered electron beams are produced by placing thin foils of materials with a high atomic number (copper or lead) in the beam. This is usually done on the level of the flattening filter in the linac head and can spread the thin electron beam to fill field size apertures of up to 25x25 cm^2(4).

Pencil electron beams are not frequently used clinically but can be achieved with two electromagnets that are subject to computerised manipulation of the magnetic field. This design enables the operator to deflect the pencil-thin electron beam across the clinical treatment field. An important advantage of this technique is that intensity modulation can be achieved, whereas with scattered electron beams only uniform electron fields can be applied(4).

Production of clinical photon beams:

Clinical photon beams are generated from clinical electron beams as discussed in the previous section. The electron beam is forced to hit a high atomic number transmission target in the linear accelerator head where the electrons interact with the target. The most important interaction for the topic of photon beam production is bremsstrahlung interactions. In this process, some of the kinetic energy is converted into electromagnetic radiation. Fundamentally, an electron with energy high enough to penetrate through the electron cloud of the target atoms will interact electrostatically with the nucleus. The attraction force of the nucleus will slow the electron down while bending the trajectory of the electron. As the electron decelerates, it loses energy. This energy is released as electromagnetic radiation in the x-ray spectrum, which if the initial electron energy is sufficient, will allow for x-rays of sufficient energy to treat cancer in patients. Figure 5 below shows a representation of three electrons undergoing bremsstrahlung interactions with a target atom(4).

Stellenbosch University https://scholar.sun.ac.za

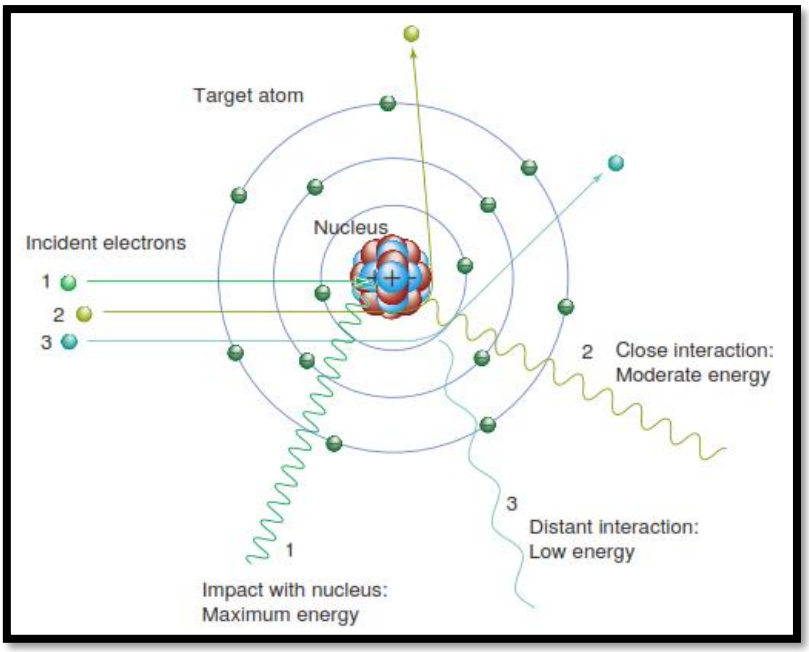

Figure 5: Diagrammatic representation of three electrons taking part in bremsstrahlung interactions with the same atom giving rise to x-rays of different energies(4).

Linear accelerator treatment head:

The LINAC head is designed for beam production, shaping, localization and monitoring of clinical photon and electron beams. These functions are performed by several retractable x-ray targets, flattening filters and electron scattering foils, primary and adjustable secondary collimators, dual transmission ionization chambers, a field-defining light and range finder, optional retractable wedges and optional Multi-Leaf Collimators (MLC) (4).

X-ray targets are used to produce photons from electron beam interactions. After this, the photons interact with the flattening filter which is designed to flatten the photon distribution profile at a reference depth in water, usually 10 cm depth (4).

Some modern medical linear accelerators give the added option of removing the flattening filter and replacing it with a flat filter of brass, stainless steel or aluminium. This produces flattening filter-free (FFF) radiation beams with increased intensity when compared to flattened beams. These beams have an intensity that is relatively flat for a small central region (1-2cm) and then decreases towards the edge of the beam, generating a large sloped region. This intensity distribution makes it very difficult to obtain a uniform dose distribution for large fields, if not modulated, but becomes significantly easier as the field size decreases. An added advantage is the increased dose rate of doubled the normal dose rate (15-30Gy/min compared to the standard 3-6 Gy/min). These characteristics make these types of beams ideal candidates for the delivery of large

Stellenbosch University https://scholar.sun.ac.za

doses per session to very small targets, which is the case for stereotactic radiosurgery (SRS) and stereotactic body radiotherapy (SBRT). (5)

Scatter foils are used to spread out electron beams as and the collimation systems are used to shape the beam using either applicators (in the case of a spread-out electron beam), secondary collimators (Jaws) or MLCs(4).

Dose monitoring systems:

Dose rate monitoring systems are one of the most important safety components of the LINAC. The IEC 60601-2-1 specifies international standards for clinical electron LINAC, which include regulations regarding the type of radiation detectors that should be used for this purpose, the display of the monitor units, the termination of radiation and the monitoring of beam flatness, uniformity and dose rate(4).

These chamber detectors that are inherent to the LINAC must have minimal effect on clinical photon and electron radiation beams (should not perturb the fluence significantly), they should be independent of environmental changes and should always be operated under saturation conditions(4).

The dose monitoring system usually consists of a transmission ionization chamber that is a built-in component that permanently monitors the clinical electron and photon beam output during treatment. It is usually positioned directly below the flattening filter or the scattering foil for photon and electron beams respectively and just above the secondary collimation system and often consists of pressurised chambers that have a response that is independent of the environmental influence(4).

It is empirical that this dose-measuring chamber is subject to strenuous quality assurance as this is the only physical radiation measurement made by the LINAC during patient treatment and because it is used to terminate the radiation beam after enough monitor units (MUs) have been delivered. For these reasons, there are often two independent ionization chambers that function with identical bias voltage supplies and electrometers. If the primary chamber, therefore, fails to terminate the beam, the second will reach the pre-set MU limit and terminate beam delivery. In the case where both of the chambers fail, the LINAC is equipped with a timer that will terminate the delivery of radiation to the patient with minimal radiation overdose received by the patient(4).

This chamber is not only used for radiation dose estimation and beam termination purposes but can also be used to measure the beam energy, flatness and symmetry at the position of the chamber. For the ionization chamber to be able to perform all these

Stellenbosch University https://scholar.sun.ac.za

measurements simultaneously, the electrodes are segmented into several sectors. The output from this chamber is used in an automatic feedback circuit to steer the electron beam through the accelerating waveguide, beam transport system and to ensure accurate beam bending onto the target or scattering foil, ensuring optimal flatness and symmetry of the beam(4).

Lastly, the dose monitoring part of the chamber can be used in dose rate monitoring of the dose rate to the isocentre as a safety interlock as well as monitoring dose rates when the LINAC employs advanced radiation treatment techniques where dose rate is varied during treatment(4).

Beam collimation:

Photon beam collimation can be achieved with three components namely the primary collimators, the secondary collimators and the MLCs. The primary collimator is a conical opening in the tungsten shielding that produces the primary radiation field. The secondary collimation system usually consists of four block jaws. Secondary collimators allow to cut or shape the primary radiation beam into larger simple rectangles or squares symmetrically and asymmetrically.

An MLC is a set of thin metal structures that can adjust dose delivery by changing the primary or secondary beam into irregular shapes or by modelling the intensity of the photon beam through a segmentation process. Intensity modulation and therefore MLCs are essential to intensity-modulated radiotherapy (IMRT) and volumetric modulated-arc therapy (VMAT) (4).

Stellenbosch University https://scholar.sun.ac.za

Treatment methods:

3DCRT

Conformal radiotherapy is a technique that arose from the need to deliver higher tumour doses to achieve better tumour control, whilst maintaining an acceptable level of normal tissue sparing. In this technique, a treatment volume is delineated from diagnostic imaging of the tumour site before the treatment by a radiation oncologist. The prescribed radiation dose is then conformed to the shape of the volume delineated. The delivery of doses with this technique is usually accompanied by a three-dimensional imaging chain, starting with volumetric imaging for delineation of the target(4).

Conformal treatment planning is most commonly done utilizing three-dimensional capable treatment planning systems, usually with the use of multiple beams in the same plan or multiple beams that are not co-planar. The planning process usually consists of standard forward planning techniques where the planner will optimize the beam parameters of a specific beam, then calculate the dose to view the effect of its changes. This will then be repeated by the use of a manual iterative procedure of finding the best beam parameters for the specific case. For more advanced conformal plans, inverse type planning can be used to achieve an intensity-modulated type treatment(4).

IMRT

Intensity Modulated Radiotherapy is a radiotherapy delivery technique whereby numerous beam segments can be formulated per beam and superimposed to achieve conformal, uniform and intensity-modulated dose distributions within the target whilst limiting dose to normal tissue. This is usually accompanied by inverse planning techniques, where iterative algorithms are used to optimise beam parameters to achieve specific goals and constraints that are set by the planner. IMRT is fundamentally delivered as multiple irregularly-shaped segments at a fixed gantry angle. Since IMRT, by definition, requires multiple irregularly-shaped segments, multi-leaf collimators, are essential to achieving this delivery technique(4).

Two major IMRT delivery techniques exist. The first is referred to as the static or the step and shoot technique and the second is the dynamic or sliding window technique. The first type of delivery is described by the word static as the MLCs are static when the beam is on. The delivery will be performed by a series of segments where the MLC moves and dose is delivered, but never at the same time. Because of this, this technique is often very time-consuming(4).

Stellenbosch University https://scholar.sun.ac.za

The dynamic technique creates multiple segments dynamically as the beam is on. With this technique, not only leaf positions need to be monitored and controlled, but also leaf speed. This makes this delivery technique more complex but saves time or allows for more segments per beam in the same period, which in turn could lead to better quality plans(4).

VMAT

Volumetric modulated arc therapy is an evolved form of IMRT where the radiation dose is no longer delivered as segments of a stationary beam, but segments while the beam arcs around the patient. When delivering a VMAT plan, the gantry speed, dose rate, and MLC positions can be altered while the beam is running(6).

Stereotactic irradiation

Stereotactic irradiation is a technique of radiotherapy, that employ extremely focal irradiation techniques and non-coplanar photon radiation to deliver a radiation dose to stereotactically localised and immobilised lesions in parts of the human body. This technique has gained the most popularity in the brain and comprises prescription characteristics of total doses of between 10 and 50 Gy to very small targets, usually in the range of 1-35cm^3(4).

Because of the extreme focal nature of this delivery, treatment is usually required to be delivered within a positional margin of 1mm. This places pressure on the need for extremely accurate, precise and effectively functioning equipment, excellent treatment planning, near-perfect immobilisation, strenuous quality assurance and extremely accurate delivery to the patient(4).

Modern Stereotactic systems include gamma knife systems, Linac based radiotherapy, which shape beams either with stereotactic cones or MLC systems, or robotic arm systems accompanied by a variety of less invasive immobilisation techniques such as vacuum fixed mouthpieces or film suppression to limit movement of the patient during treatment(4).

For such specialised techniques, micro-MLC systems have also been developed. These systems use leaves of smaller width and greater accuracy but have limited maximum field size capabilities due to the specificity of the design(4).

Stellenbosch University https://scholar.sun.ac.za

Basic principles of radiation dose delivery:

Ionising radiation is the division of radiation responsible for dose deposition and can be divided into particle radiation, usually considered as directly ionising, and photons that are uncharged and usually considered to be indirectly ionising. Ionising particles include higher energy electrons, protons, neutrons and alpha particles, whereas photons are usually X-ray or gamma photon beams(4).

Photon interactions:

Photons interact with matter in several ways including Rayleigh scattering, photoelectric absorption, Compton scattering, pair production and photonuclear interactions. Of all these interaction methods, Compton scattering is by far the most dominant interaction method at clinically relevant photon energies and is therefore the only process discussed in this document(4).

Compton scatter:

By definition, Compton scatter assumes that a photon interacts with a free electron. This means that the photon energy is larger than the binding energy of the orbital electron. In this interaction process, the photon is assumed to lose some of its energy to the electron. When the photon "collides" with this electron, the photon is deflected by a certain angle and with a changed frequency whereas the electron gains the energy lost by the photon. The electron overcomes the orbital binding energy, this is usually negligible, and then leaves the atom with the rest of the gained energy presenting as kinetic energy. This is considered an indirect way of ionisation as the photons liberate electrons that in turn ionise the atom and thus deposits dose(4).

Electron interactions:

Electrons may interact in two ways that are of clinical importance. The first is soft collisions, also called orbital collisions. The second is hard collisions or nuclear collisions(4).

Soft collisions:

Soft collisions occur when the incident electron has an energy that is lower than the energy needed to penetrate the electron cloud. This assumes that the electron will interact with an orbital electron or the electron cloud as a whole, depending on the energy of the incident electron. As the charges of both the incident electron and the electron cloud are negative and the incident electron has too low energy to penetrate this electron cloud, the electron will interact via Coulomb force interactions. These interactions may produce excited or ionised states of the atom, depending on the energy

Stellenbosch University https://scholar.sun.ac.za

of the incident electron. These directly ionising interactions are responsible for dose deposition as they change the state of the molecular composition of the material that may create free radicals that damage the cell structure or control mechanisms. These types of interactions are generally more common for low atomic number materials like water and soft tissue in the human body at clinically relevant photon energies(4).

Hard collisions:

Hard collisions are interactions where the impinging electron has enough kinetic energy to penetrate the electron cloud. In this specific case, the electron has a Coulomb interaction with the positive charge of the nucleus. The attraction force between the nucleus and the electron changes the trajectory of the electron as it passes by the nucleus through a breaking motion. When this happens, the energy lost by the electron is irradiated as electromagnetic radiation/photon. This type of hard collision is called breaking radiation or Bremsstrahlung. The probability for such an interaction increases with an increasing atomic number of the material the electron is interacting with. This type of interaction usually increases in probability with an increase in the atomic number of the material at the clinical photon energies(4).

A summary of the radiation interactions discussed above and their relationship to dose deposition is shown in figure 6 below.

Stellenbosch University https://scholar.sun.ac.za

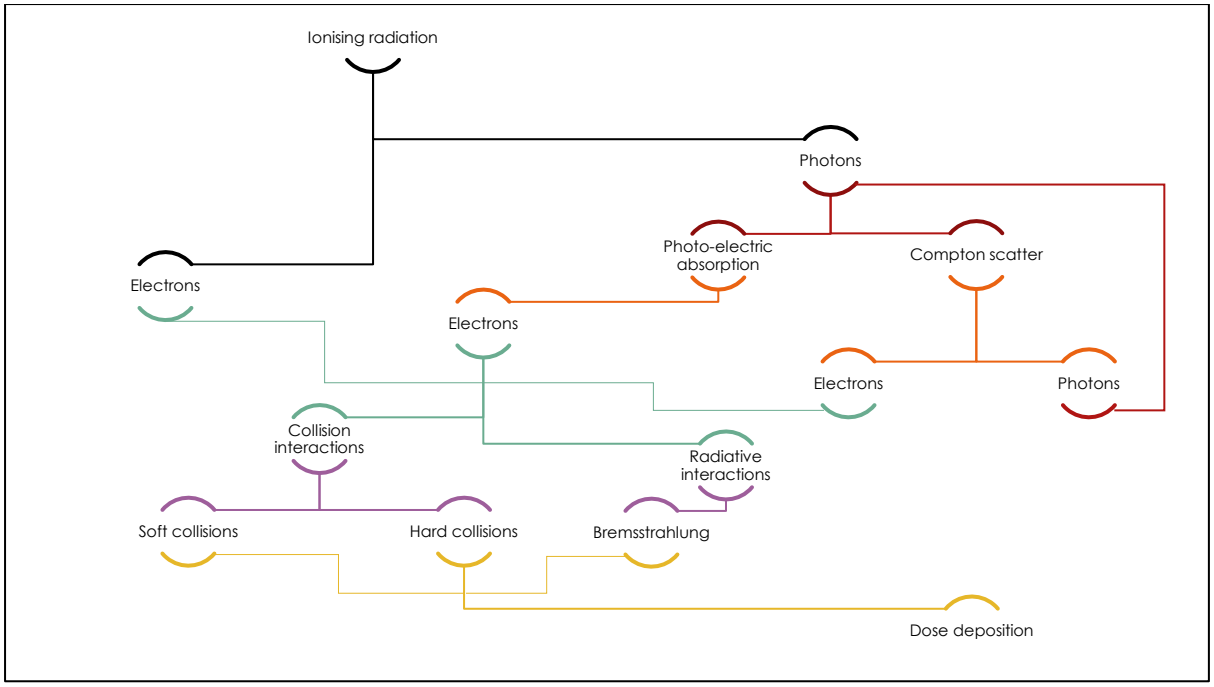

Figure 6: Flow diagram explaining the dose deposition of radiation in the clinical environment.

Stellenbosch University https://scholar.sun.ac.za

Radiation detectors:

Many radiation detectors are used in modern radiotherapy for quality assurance purposes. Each detector type presents a unique set of characteristics giving rise to its advantages and disadvantages.

Solid-state dosimetry:

Various types of solid-state detectors are available however, none of these detectors can perform absolute dosimetry without the calibration of the detector by an external system. The most widely used solid-state detectors are thermoluminescent dosimeters (TLDs), diodes and film(7).

TLD dosimetry:

When a crystal with thermoluminescent properties is irradiated, a small amount of the absorbed energy is deposited in the lattice of the crystal. This stored energy can later be released in the form of visible light if the crystal is heated sufficiently. The light output from the TLD is proportional to the radiation dose that was absorbed by the crystal. This light output is called a glow curve(7).

Lithium fluoride dosimetry:

The atomic number of lithium fluoride (8.2) is close to that of soft tissue (7.4), which makes it a good candidate for clinical dosimetry. These detectors can also be manufactured to be smaller than the electron range of clinically used beams and therefore the Bragg-Gray cavity theory can be used for this type of scenario(7).

Silicon diodes:

As with solid-state dosimeters, these p-n silicon detectors are used for relative dosimetry. The advantages of this type of detector are that they are very sensitive, have a small size, have a quick response and are relatively rigid. They are mostly used for electron beam measurements, output consistency checks and in vivo patient dose measurements. These detectors are however dependent on a variety of environmental and non-environmental factors. This detector is composed of a silicon crystal that is mixed or doped with impurities. Radiation induces a current in this detector which can be related to the absorbed dose(7).

Energy dependence:

Silicon detectors have a high atomic number (Z=14) compared to that of water and therefore has a severe degree of energy dependence when using them in photon

Stellenbosch University https://scholar.sun.ac.za

dosimetry. In electron dosimetry, the silicon diodes are not energy dependent as the ratio of electron stopping power of silicon to water does not change with electron energy to a significant extent. This ratio does not change with depth to a significant extent either. This is still however dependent on the diode and its design(7).

Angular dependence:

The response of diodes varies significantly with angle and this must be taken into consideration when using this type of detector clinically(7). This angular dependence is due to asymmetry in the design characteristics regarding the three dimensional physical size and dimension of the detector and the build-up region(4).

Temperature dependence:

Silicon diodes are not very sensitive to temperature change and this factor can often be ignored; however, it should be taken into consideration when the temperature has significantly changed since the calibration to the time of measurement(7).

Radiation damage:

Very high doses of radiation can induce radiation damage to these detectors. This is mostly due to the fact by displacement of silicon atoms in the lattice of the crystal. The severity of the damage is dependent on the type of radiation, the energy of the radiation and the total radiation dose(7).

Radiographic film:

This type of film consists of a base coated with an emulation containing very small crystals of silver bromide. When this film is exposed to ionising radiation or visible light, a chemical reaction occurs in the exposed film, forming what is called the latent image. During the development of the film, the crystals that were changed chemically by the radiation will form small grain of metallic silver. The unaffected granules are removed from the film by the developing solution. This leaves the film clear in the areas that weren't exposed and dark in the areas that were. The amount of darkening in the film is also dependent on the amount of radiation energy absorbed(7).

The blackening degree is measured by the determination of the optical density as measured with a densitometer. This device measures light transmission through the film. The optical density can be defined by equation 1 below:

$$OD = \log\left(\frac{I_0}{I_t}\right) \qquad 1$$

Stellenbosch University https://scholar.sun.ac.za

In equation 1, I_0 is the amount of light if there is no film in the densitometer and I_t is the amount of light transmitted through a part of the film with a certain darkening(7). This quantity is usually corrected for background or "fog" on the film and the net optical density is used. The speed of the film is a parameter that can be described as the amount of radiation needed to cause a certain amount of film blackening and can vary among films(7).

The radiographic film is a well-established dosimetric tool for electron beams. It is however not often used in dosimetry of photon beams as Compton scattering is the predominant mode of interaction at clinically applicable energies and determining a correlation between optical density and the absorbed dose is tenuous. There are many uncertainties associated with film measurements and this makes absolute dosimetry impractical. This film is however used for routine relative dose measurements for quality control purposes(7).

Radiochromic film:

Radiochromic film is made of an immensely thin colourless radiosensitive dye bonded to a thick mylar base, which gives it stopping power properties similar to that of water. The dye changes blue colour intensity with increased ionising radiation exposure as a result of a polymerization procedure. The advantages of this type of film are that it is tissue equivalent, it has a high spatial resolution, a large dynamic range, low to no energy dependence, it is not sensitive to light photons (excluding ultraviolet radiation) and no chemical processing is needed(7).

The colour is recorded with a spectrophotometer with commercially available laser scanners and CCD microdensitometer cameras. These measurements are also analysed by optical density. It is however essential to not scan the film directly after exposure as development stability occurs after 24 hours(7).

These films must also be calibrated before they can be used for dosimetry and they show a linear response with increasing dose up to a level beyond an increase of dose no increase in response is noted(7).

Ionisation chamber:

Ionisation chambers are used regularly to measure radiation dose. It is composed of a gas-filled cavity, an anode and a cathode. For the standard cylindrical ionisation chamber, the anode is a central collecting electrode with the cathode forming the wall of the chamber. A basic design of a cylindrical ion chamber can be seen below in figure 7(4).

Stellenbosch University https://scholar.sun.ac.za

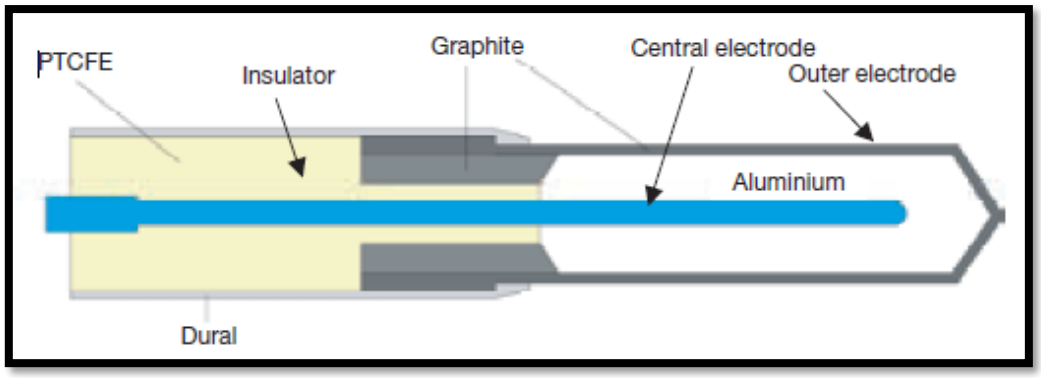

Figure 7: An image of the basic design of a cylindrical ion chamber(4).

When ionisation chambers are irradiated, the gas becomes ionised and ions are collected by either the anode or cathode, depending on the charge of the ion. Through calibration and appropriate corrections, the very small current of electrons formed can be converted to a radiation dose. Electrometers can be coupled with these ionisation chambers to measure these very small currents(4).

Ionisation chambers that are not sealed from the atmosphere and allow surrounding air in, are called open-air ionisation chambers. For these chamber types, temperature and pressure corrections need to be applied to the measurements(4).

Ionisation chambers are available in a variety of designs, each designed for a specific function. These include cylindrical, parallel plate, well type and extrapolation chambers(4).

Electronic portal imaging devices:

Portal imaging devices are used with medical linear accelerators primarily to validate the patient setup before treatment by comparing onboard images to reference images taken during or at the time of the simulation. Online portal imaging has developed with the need to have an immediate correction for the setup error of the patient before treatment(4).

The most clinically used electronic portal imaging devices in the modern era are composed of amorphous silicon diode arrays. Advantages of this type of configuration are that it is flat and therefore does not take up a lot of space, the detectors are very sensitive and can produce an image with only a small amount of radiation and that the signal can be digitized into an image, which produces quick image formation for on-line image formation and evaluation(4).

Since these detectors are often mounted on a retractable arm, the mechanics and by extension the panel can sag at non-zero gantry angles(8).

Stellenbosch University https://scholar.sun.ac.za

It has been shown through measurement that the EPIDs, on a variety of clinically used machines, move 0.4 mm on average in the cross-plane and 1.6 mm in the in-plane directions due to sag(9).

Since the amount of sag varies from one gantry angle to the next, a correction should be applied if absolute position measurements will be made from EPID images(8).

Stellenbosch University https://scholar.sun.ac.za

Digital image processing:

Components and properties of a digital image:

The standard digital image is composed of a two-dimensional array of picture elements. These picture elements are called pixels. As a standard, pixels have three major properties(1).

Pixel spacing:

The first is called pixel size or pixel spacing. This indicates the size of only one of the sides of the pixel in distance units, as pixels are typically square elements or the distance from the centre of one pixel to the centre of the next. In three-dimensional datasets, like Computed Tomography (CT) or Magnetic Resonance Imaging (MRI), images consist of a slice through the human body with a determined slice thickness. Since the picture elements now have a third dimension or thickness, they are referred to as volume elements or voxels(1).

Pixel value:

The second property is called pixel or voxel value. This property can be presented as a number that correlates to an intensity value. Usually, the intensity is an indication of the colour of the pixel, but in the medical imaging environment, images are often displayed as greyscale. This means that the colour scale used for allowed pixel values are between shades of grey, stretching from black to white(1).

Pixel depth:

The last property that pixels or voxels have is depth. The depth of a pixel or voxel refers to the number of different intensity or colour elements available to display the image. As this value increases, more colours or intensities can be used to display the image. If the pixel depth is too small, pixels with different pixel values will be grouped into the same colour or intensity and may be displayed as if they had the same intensity, which is incorrect. Pixel depth is usually encoded bits represented by some power function of two. An 8-bit image for example will have a pixel depth of 256, which means that the pixel value can be any number between 0 and 255(1). Figure 8 below show the same digital image displayed with decreasing pixel depths from A to D.

Stellenbosch University https://scholar.sun.ac.za

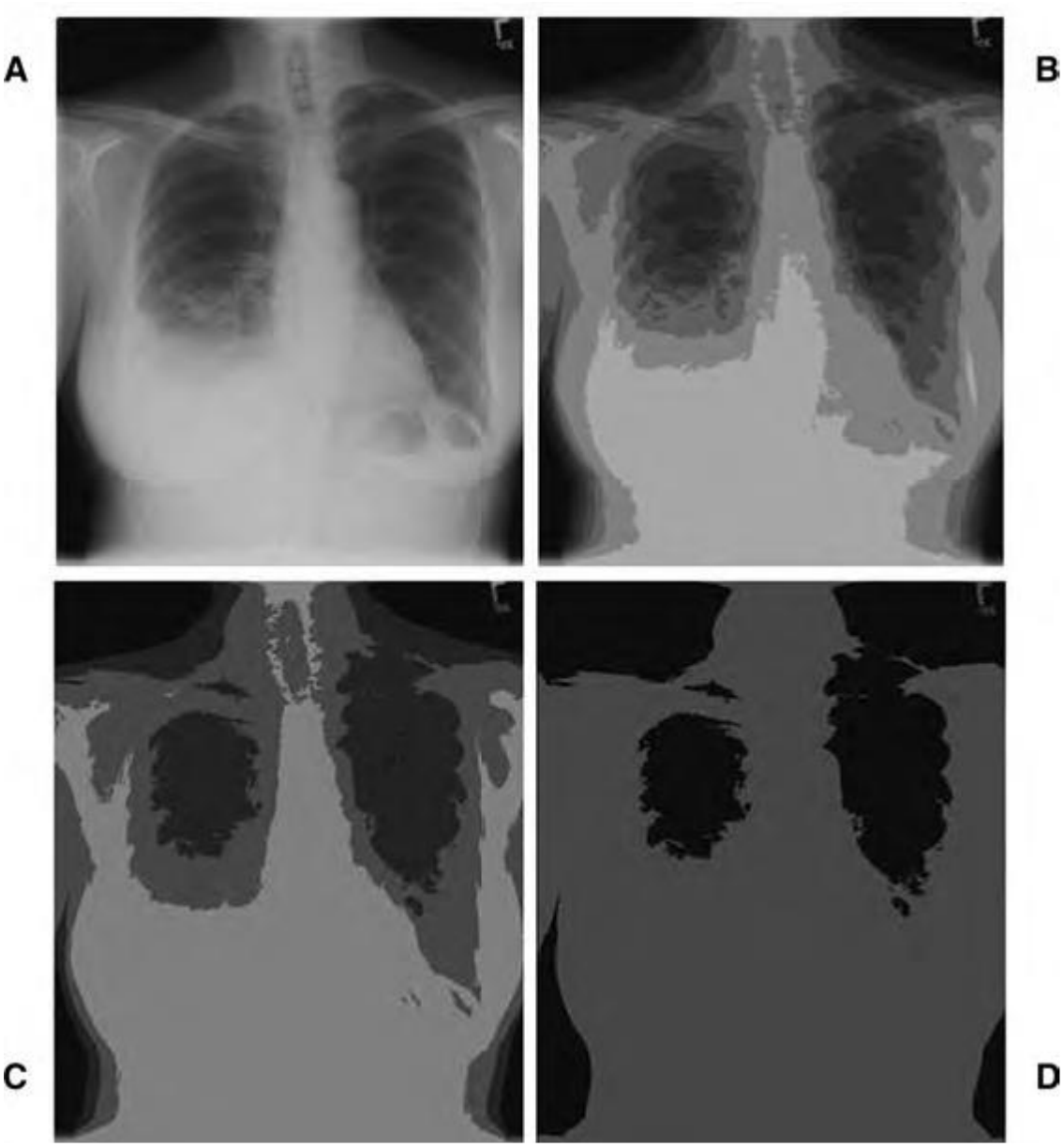

Figure 8: An example of a digital image displayed with decreasing pixel depth(1).

Display of a digital image:

When a digital image is displayed, three main factors are considered. The first is the physical meaning of the pixel value. This becomes increasingly important for medical images. For X-ray images, the pixel value correlates to optical density. for CT imaging, the voxel value correlates to Hounsfield units, which is a measure of the relative density of the material imaged. With MRI, the voxel value indicates some property of the magnetic spin of the protons in the material. The meaning of this value often defines what the maximum and minimum possible values should be to display such an image as well as an appropriate depth(1).

Stellenbosch University https://scholar.sun.ac.za

As the human eye may not be able to discern small changes in intensity that may provide important diagnostic or clinical information, certain manipulations may be made to the display of the image to aid the user in identifying small differences. These include special functions like zooming, rotating or panning, but also intensity-based manipulations which play around with what is called the window width and window level(1).

For a greyscale image, the window refers to a range of grey values chosen to display the image. The larger the window width, the smaller the changes from one colour to the next, but the larger the range of values represented. The smaller the window width, the smaller the represented range, but the larger the changes from one colour to the next(1).

The window level is a measure of where on the pixel depth scale this window is centred. A window with a width of 10 can be centred at different positions on the pixel depth scale to discern different properties from an image. For a CT image, for example, a window with a width half of the pixel depth will give good information on differences between air and soft tissue but it will not be able to discern soft tissue from dense tissues such as bone well when centred low on the pixel depth scale. When it is however positioned at the high end of the pixel depth scale, the user will be able to discern small differences in density better for higher density structures than for lower density structures(1). An example of differences in display due to window level can be seen in figure 9a and 9b below:

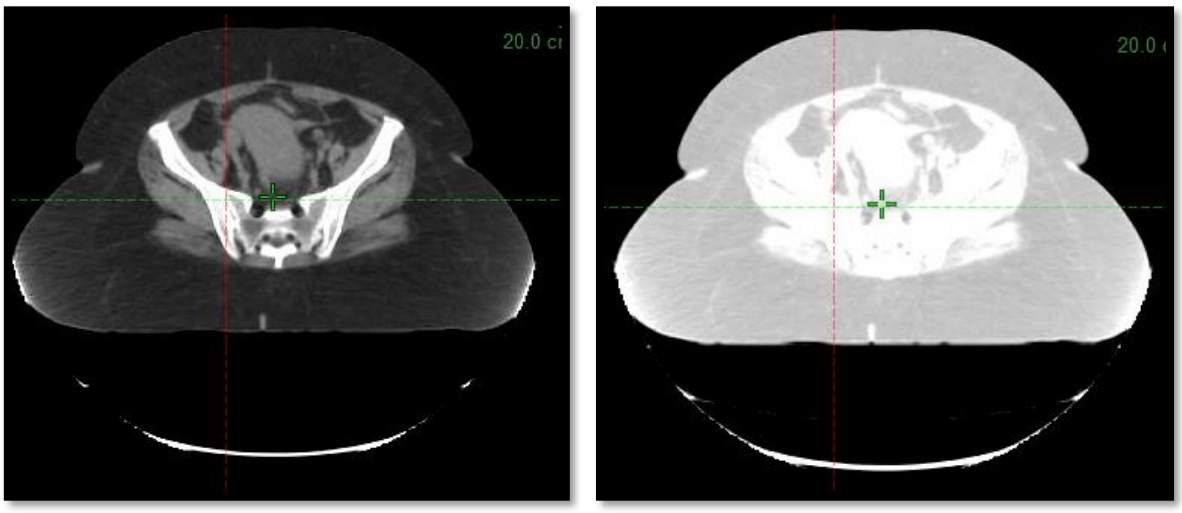

Figure 9: a) Planning CT with a Pelvis window applied (-160 to 240HU) and b) The same planning CT with an adapted lung window applied (-473 to 0HU).

An image manipulation technique, known as thresholding, is a manipulation of the window width and level. If an image is manipulated by thresholding, all values below the threshold are set to the minimum possible value and all values equal and above the threshold are set to the maximum possible value. For greyscale images, this creates a true

Stellenbosch University https://scholar.sun.ac.za

black and white image, where pixels are either displayed as black or white. This is a handy technique in identifying intensity differences around a threshold value(1). An example of an MRI image and what it looks like after thresholding can be seen in figure 10 below:

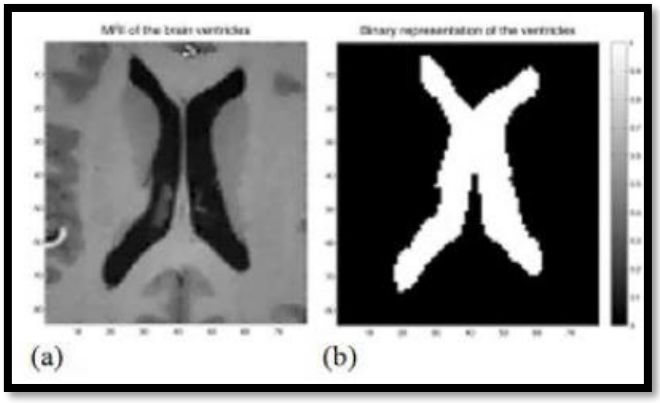

Figure 10: An example of an MRI image before (a) and after(b) thresholding has been applied(1).

Image quality measures:

To evaluate the quality of a medically acquired image, several image quality measures need to be evaluated. Four main measures govern the image quality of a digital image(1).

Contrast:

The first is called contrast. Contrast (C) is the ratio of intensity difference between two pixels (I_a and I_b), to the average intensity ($I_{average}$) in the image or section of the image being analysed(1). This can be represented mathematically with equation 2 below

$$C = \frac{I_a - I_b}{I_{average}} \qquad 2$$

If the contrast value is large, the difference between the two pixel intensity values is larger than the average intensity and the two intensities will be easy to distinguish. If the contrast is low, however, the inverse is true, and the intensities will not be easily distinguished(1).

Resolution:

Resolution or sharpness/unsharpness is a measure of the minimum size of an object that can be imaged/represented in the image. It is directly related to the pixel size and therefore also the number of pixels used to display the image. If the object being imaged is smaller than the size of a pixel, the object will be represented by the intensity of the object and that of its surroundings. This may lead to the object being missed if it is of low contrast or the size of the object being misinterpreted if it is of high contrast. This process

Stellenbosch University https://scholar.sun.ac.za

of averaging the intensity within a pixel causes a blurring artefact if the resolution is not sufficient. If the size of the pixel is low enough that the object covers enough pixels, the size and intensity of the object will be represented more accurately and with less blurring(1). Figure 11 below show a digital image displayed with decreasing levels of resolution from A to D.

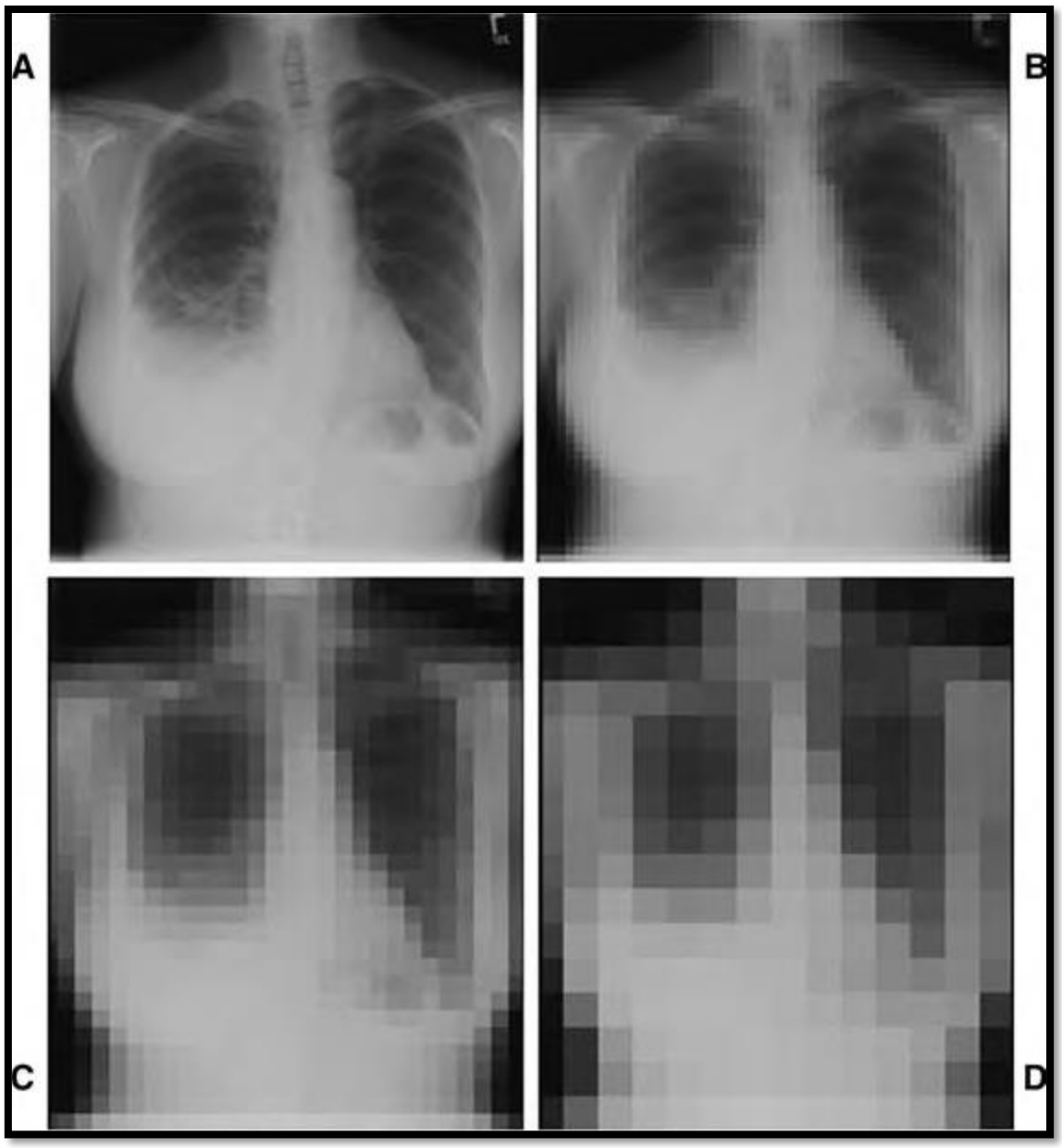

Figure 11: A digital image displayed with decreasing levels of resolution from A to D(1).

Image Noise:

Producing x-rays is a random process whereby the fluctuation of x-rays in a determined area can be described as quantum noise. This is governed by Poison statistics. Additionally, the process of converting x-rays detected into a digital image will introduce

Stellenbosch University https://scholar.sun.ac.za

additional noise. Two distinct forms of quantum noise can be defined. Primary quantum noise refers to the noise generated randomly through x-ray production. Secondary quantum noise refers to the noise generated as the image forms in the x-ray detector or by the digitisation or amplification of the signal(1).

When quantifying noise, the signal to noise ratio (SNR) is one of the most popular measures. This is simply the ratio of the signal and the noise, where the signal is represented by the average pixel value ($I_{acerage}$) in the defined area and the noise is the standard deviation (σ) in pixel value in this area(1). It can be represented mathematically by equation 3 below:

$$SNR = \frac{I_{average}}{\sigma} \qquad 3$$

If the average intensity of the pixel values is much higher than the standard deviation, the SNR will have a high value and the image has little noise, however, if the average intensity of the pixel values is much lower than the standard deviation, the SNR will be low and the image has a lot of noise(1).

Image artefacts:

Image artefacts are misrepresentations of measured data formed in the digital image that can be a result of the object being imaged, the imaging system or inaccurate calibration thereof as well as the processing of the image post-acquisition. These are areas or individual pixels with pixel values that do not represent the object imaged but is altered or replaced. Imaging artefacts degrade image quality as analysis of the image is not analogues to analysing the object imaged, which may give false impressions regarding the object(1).

Image processing

Digital images have a very important advantage in that they can be processed post-acquisition. This means that the image can be manipulated in some ways to enhance contrast, decrease noise or amplify the signal. It should be noted that image processing or manipulation can only alter acquired data. Processing cannot resolve the object that is too small to be imaged by the detector for example(10).

Noise reduction filters

For quantitative analysis of certain properties in digital images, special smoothing is often used as a method of removing or reducing random noise. Smoothing filters are often used to this end, where each pixel in the post-processed image is simply some form of mathematical manipulation of its surrounding pixels(10).

Stellenbosch University https://scholar.sun.ac.za

Although smoothing can reduce random noise, it can also alter measured information by either averaging intensity information, causing blurring, or enhancing sharp edges. This may cause the processed image to have spatially inconsistent properties to the original image(10).

Gaussian filter:

The Gaussian filter is an image smoothing filter that reduces noise in the image by changing the selected pixel to a weighted average of the pixel's value itself as well as its neighbourhood. The larger the distance of the neighbouring pixel from the chosen pixel, the smaller its weight will be to the new value of the chosen pixel(11).

In medical images, this filter is partially useful for filtering images that have a lot of noise. It has also been noted that for images with inherent high SNR, the gaussian filter could worsen image quality, however, it has proven quite handy for images with low SNR(11).

Mean filtering:

The mean or average filter reduces image noise by smoothing the selected pixel with its neighbours. In this process, the selected pixel value changes to the mean of the pixel itself and the pixels directly surrounding it. The mean filter is poor at maintaining sharp edges in an image. Image blur is a by-product of mean filtering(12).

Median filtering:

Median filters are considered non-linear and tend to preserve sharp edges when smoothing an image. When using the median filter, the values of the pixel chosen, and its immediate surrounding pixels are sorted by magnitude and the median of these magnitudes is taken as the new pixel value. This makes the median filter very good at removing noise but maintaining large sharp edges. Since this filter is good at maintaining the integrity of sharp edges, it does not lead to as much image blurring(12).

Peak detection algorithms:

Peak detection algorithms have been part of medical physics history, specifically in spectroscopy. The simplest method for detecting peaks is composed of logical (TRUE/FALSE) processing and could be applied in small computers by 1990. This technique uses a sliding window approach comparing the intensities at the beginning, the centre and the end of the window constantly. Simple techniques include minimum thresholds above which a peak qualifies as a "true" peak and is not considered image noise anymore. A true peak can be identified by the logical rule that the beginning and the end of the window should have lower intensities than the centre of the window. And by

Stellenbosch University https://scholar.sun.ac.za

searching for these areas where peaks are in the order of the expected width, can filter out “false” peaks(13).

Stellenbosch University https://scholar.sun.ac.za

Statistical considerations in data analysis:

The science behind statistics is one of probability. Probability distributions provide us with the ability to link the probabilities and the possible outcomes in a randomised experiment. This becomes helpful in the field of medical imaging knowing that the production of x-rays is a randomised process and that additional random noise is induced when detecting and digitising these x-rays(10).

Types of data sets:

Discrete random variables:

Discrete random variables are variables that are best used when describing outcomes that are discrete or countable. In digital imaging, pixel values belonging to discrete pixels can be seen as discrete random variables. A pixel value can only belong to a discrete pixel. If a line profile of a series of pixel values are taken from an image, this creates a discrete probability distribution

Pixel values are available only for integer pixel numbers, but not for decimal pixel numbers, as decimal pixels are not physically possible.

Continuous random variables:

Continuous random variables are variables that are used to describe possible outcomes that cannot be counted. Medically speaking, an example might be the amount of medication needed to cure a disease. These variables can take on any value in an applicable range and are not limited to discrete values. These variables are best described with continuous probability distributions(14).

In theory, if the example of a single line profile is used again but the intensity is expressed as a function of position from the starting point, the discrete probability function can be used to develop a continuous probability function with intensity values for positions correlating to non-integer pixel numbers(14).

Figure 12 below shows an example of discrete measurements of Hounsfield units for known electron density values, as indicated by points on the curve. A continuous dataset was achieved by linear interpolation to achieve datapoints in between measured data points which is indicated by the solid line(15).

Stellenbosch University https://scholar.sun.ac.za

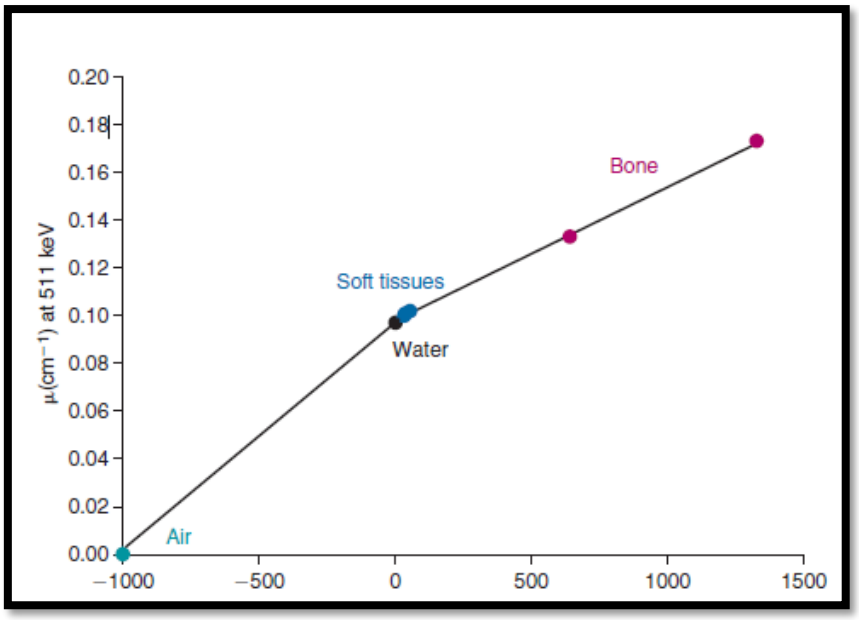

Figure12: Graphical representation of the difference between discrete and continuous datasets(15).

Interpolation:

Interpolation is a mathematical method used to find a continuous function that mimics a discrete dataset, usually in the form of experimental measurements. This is desirable when the function value is required at an interval that is not defined for the discrete function(16).

Interpolation also refers to the finding of these continuous functions between existing discrete data points. If the continuous function is allowed to predict the behaviour of the discrete dataset beyond the limit of the discrete dataset, it is called extrapolation(16).

Linear interpolation:

Linear interpolation is the term used to define interpolation done by assuming that the relationship between 2 datapoints is linear and can be connected simply with a straight line(16).

If 2 theoretical data points exist (x_0, y_0) and (x_1, y_1), any point between these two points can be found by interpolating using equation 4 below.

$$y = mx + c \qquad 4$$

Where m represents the gradient of the straight line and c represents the y-intercept(16).

Stellenbosch University https://scholar.sun.ac.za

Gaussian interpolation:

Gaussian functions can be used to describe many discrete datasets and have a form that can be expressed mathematically with equation 5 below(10).

$$y = Ae^{-\frac{(x-\mu)^2}{2\sigma^2}} \qquad 5$$

Where μ represents the centre of the curve, A the height of the peak and σ, the variance, controlling the width of the peak. Figure13 below show how the gaussian curve would change in proportion with variation in each of these input parameters. F(x) and g(x) would have the same centre and therefore μ value, however, the height (A) would be more for f(x) than g(x). Curve h(x) has the lowest height (A) value, while having a larger variance (σ) making it wider and a larger value for μ, indicating that the centre has shifted to the right of the others(15).

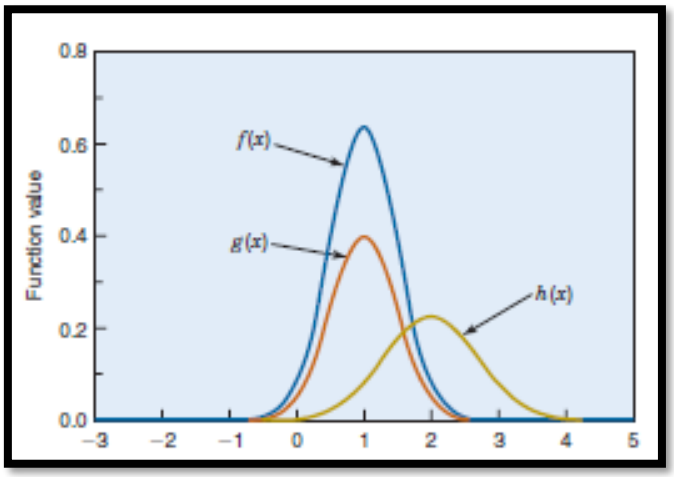

Figure 13: Graphical representation of changes in the shape of a gaussian curve based on changes in the function of the curve(15).

Statistical properties of datasets:

Range:

The range is a term used in the science of statistics to define the extent of the data points in a dataset. It can be most easily described as the difference between the highest and the lowest values in a dataset(10).

Stellenbosch University https://scholar.sun.ac.za

Arithmetic mean:

This parameter describes the average distance that values in a dataset can be found from the mean value in a dataset(10). It can be represented mathematically by the following equation 6, where $\bar{x}$ is the mean value, n is the number of datapoints in the dataset and x_i is the datapoint if the i-th position:

$$arithmetic\ mean = \frac{\sum_N fi|x_i - \bar{x}|}{N} \quad 6$$

Standard deviation:

The standard deviation of a given dataset describes the variability of the data points from the arithmetic mean(10). It can be displayed mathematically in equation 7 below where $\bar{x}$ is the mean value, n is the number of datapoints in the dataset and x_i is the datapoint if the i-th position:

$$Standard\ deviation = \sqrt{\frac{\sum_{i=1}^{n}(x_i - \bar{x})^2}{n}} \quad 7$$

FWHM:

The full width at half maximum (FWHM) is a property that is used to describe the width of peaks in a dataset. It is simply defined as the width of the peak at the height which is equal to half of the amplitude of the peak(15).

For a gaussian shaped curve, the FWHM is related to the standard deviation (SD) by the relation shown in equation 8 below:

$$FWHM \approx 2.35\ SD \quad 8$$

Stellenbosch University https://scholar.sun.ac.za

Problem statement:

The speedy development and application of new technology with specific application to MLC are a topic of concern internationally. MLCs are no longer just used for irregular field shaping, as discussed in the introduction, but is now used for intensity modulation treatments as well. Building on this, the modern linac has moved from static delivery approaches such as step and shoot IMRT deliveries to dynamic MLC IMRT and VMAT delivery techniques that have increased degrees of modulation. The authors of task group 40 of the American Association for Physics in Medicine (AAPM), in 1993, express that the QA of MLC is beyond the scope of standard practice at the time of the publication. The report further mentions that as experience with new technological innovations increases, new guidelines for QA of these systems should be addressed(17)(18).

Internationally, there has been pressure on the medical physics community to adapt to ensure safe and accurate delivery of these treatments as with the technology before. In 2007, the AAPM task group 142 published a new report for QA for medical linear accelerators with a specific section on MLC QA where a distinction is made between non-IMRT and IMRT capable machines. Furthermore, a distinction is made between the test procedure and tolerance for static IMRT and dynamic IMRT deliveries on an annual basis(19).

In 2015, the Canadian Partnership for Quality Radiotherapy published recommendations regarding National standards for QA of medical linear accelerators. In this publication, a distinction also is made between static MLC QA and dynamic MLC QA testing procedures and tolerances for monthly MLC QA(18). This shows that there is a need to test MLC accuracy not only more frequently and accurately, but also with adapted methodology and considering the clinical capability of the LINAC in question.

Unfortunately, many medical physics communities have stagnated using old quality assurance techniques, that might have been applicable with older delivery techniques, but are lacking with modern linac capabilities. This is shown through the current MLC QA recommendations in South Africa, published in 2016. For non-VMAT capable LINACs, even if they are IMRT capable, the only recommendation is that MLC accuracy should be checked with an irregular single field leaf pattern every second month by comparing the light and radiation field to a template that involves all leaves. This is the only MLC positional accuracy test required with a tolerance of 2mm. In contrast, task group 142 of the AAPM publication in 2007 recommends that for non-IMRT capable machines MLC position accuracy to be checked using 2 independent MLC template patterns monthly(18)(20).

Stellenbosch University https://scholar.sun.ac.za

For VMAT capable machines, the current South African standard is that a picket fence test pattern must be done at various gantry angles and during an arc monthly. This is on par with Canadian standards with regard to test frequency. Regarding the accuracy of the positioning, no distinction is made between static and dynamic MLC capabilities, whereas Canadian standards recommend lowering the tolerance for MLC accuracy for dynamic deliveries from 2mm to 1mm(18)(19)(20)(21).

This study was designed to primarily be a start to addressing the need for specified MLC quality assurance requirements for units with varying capabilities. Additionally, this study aims to show that a high level of accuracy and confidence can be achieved by using logical steps, simple mathematical processes and a clear fundamental understanding of the equipment used in the clinic.

Stellenbosch University https://scholar.sun.ac.za

Aim:

This work aims to develop a quantitative method to accurately and digitally measure the MLC positional error on LINACs grouped into the following three main categories:

1. LINACs not capable of VMAT treatments
2. LINACs capable of VMAT treatments
3. LINACs and additional MLC systems used for SRS treatments

And to then use this method and compile a national survey of MLC performance in South Africa.

Additional objectives include:

1. Creating an easy, quick, and non-costly but accurate method in measuring the accuracy of MLCs on LINACs.
2. Developing an independent software solution that can analyse the measurement and provide accurate and user-independent analysis of the MLC accuracy timeously.
3. Validate each MLC type available by measurements.
4. Compile a baseline for MLC accuracy per MLC type or machine using an auditing process.
5. Investigate the correlation between measured MLC errors and those recorded in log files.

Stellenbosch University https://scholar.sun.ac.za

Background and Literature review:

Design, physical and dosimetric properties of MLC:

The MLC can be mounted in the treatment head in various configurations. Many designs use the MLC as tertiary collimation ,with the primary collimator and the jaws being the primary and secondary collimation(22).

Modern designs also allow for the replacement of the secondary jaws with an MLC, which would make the MLC secondary collimation(22). Another modern variation of MLC replacing the secondary jaws as the secondary collimation system uses a dual-layer of proximal and distal MLC overlapping midway through the MLC width to minimise interleaf transmission and create faster beam modulation(23).

When designing MLC banks, a few physical and dosimetric properties need to be considered thoroughly. These include field-shaping limitations, material properties, transmission, interleaf transmission and leaf end shape(22).

Field shaping limitations:

The capability of the MLC in terms of shaping fields can be limited by many factors. These include the maximum possible field size, the physical leaf width and thickness, the overtravel capabilities of each leaf, the leaf speed when using dynamic MLC capabilities and the ability to create asymmetric fields or multiple fields within the primary open field. If these factors are not adequately considered in the design process, it can limit the ability of the MLC severely(22).

Material properties:

The composition and linear attenuation coefficient of the material used to construct the MLC is critical. Not only does this determine the structural integrity or strength of the MLC, but it also determines how well it can stop the primary beam and therefore its value as a collimator. Tungsten alloy is most popular for designing MLCs due to its high density, low cost and ease with which it can be manufactured into the desired configuration. As pure tungsten can be brittle, alloys are generally formed to achieve better mechanical integrity. Care is taken not to lower the density too much by this process as a high atomic number and high density will allow for better linear attenuation properties(22).

The main three vendors offering clinically usable MLC systems are Varian, Elekta and Siemens. All three of these vendors use tungsten alloy as MLC material(24)(25)(26).

Stellenbosch University https://scholar.sun.ac.za

MLC transmission:

MLC transmission is critical when attempting to keep the out of field dose to a minimum. When the secondary jaw is replaced with an MLC, the MLC transmission becomes a critical component in the planning and design of the MLC. When this design is used, the same requirements in terms of transmission are expected from the MLC as for the standard jaw configuration. The transmission is largely determined by the composition of the MLC, the thickness of the leaves and the energy and type of radiation to be used (22).

If the MLC is installed as tertiary collimation, it only needs to achieve the transmission abilities similar to customised blocks (<5% or between 4 and 5 Half value layers (HVL)) (22).

Interleaf transmission:

Interleaf transmission has posed major difficulty to the engineering of MLC banks. As we aim to have each leave move independently, radiation transmission through the gaps between these leaves needs to be addressed. This becomes increasingly important when the MLC alone is to be used as secondary collimation. Sophisticated planning in this regard will allow for smooth leaf motion as well as a continuous quality of attenuation over the leaf bank. (22).

In an attempt to account for this, each vendor has a specific MLC leaf design ensuring that adjacent MLC leaves overlap somewhat. Each leave would for example at the top have a protruding section named the tongue and a retruding section at the bottom called the groove which in turn would overlap with the tongue of the next leave(27).

Figure14 below shows a head-on representation of adjacent MLCs for Siemens, Varian and Elekta MLC designs(28).

Stellenbosch University https://scholar.sun.ac.za

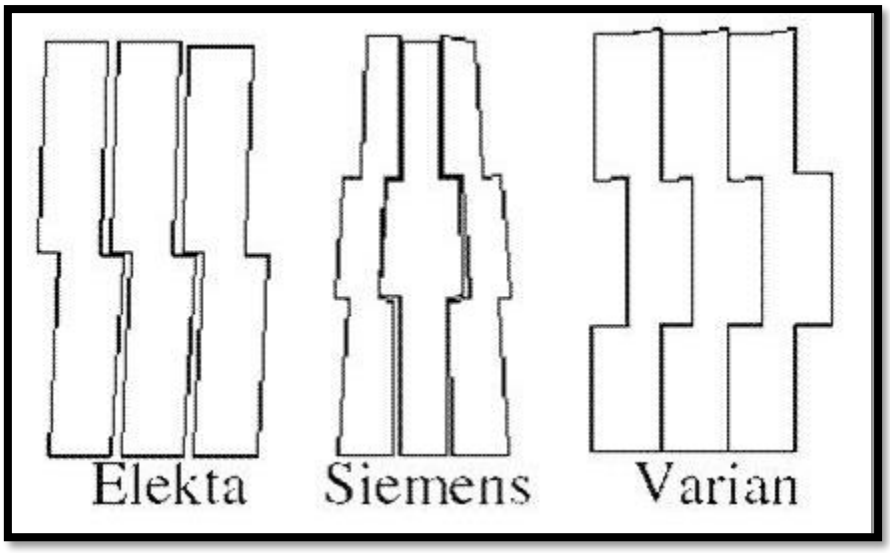

Figure 14: Diagram of differences in tongue and groove designs for various vendors(28).

Historically, interleaf transmission has been a design characteristic that needed special attention due to the clinical significance thereof. Clinically, this MLC dosimetric characteristic could lead to a difference in planned and delivered dose in shielded off areas. This was mainly due to limitations in the beam modelling software available at the time. In 1998, LoSasso et al, showed that when accounting for this effect through measured data during the treatment planning stage, the difference between planned and measured transmission in this area becomes non-detectable for dynamic MLC treatments(29).

Modern treatment planning systems (TPS) can accurately account for this phenomenon and model it well. Some modern TPS systems such as Elekta`s Monaco TPS, allows the user to measure an express package of dynamic MLC test patterns after modelling occurs to ensure that all dosimetric and positional MLC characteristics such as this are accounted for(30).

Additionally, some studies that have employed computerised algorithms with older MLC models to analyse the picket fence test have made use of a Fourier first harmonic fit out of field to detect the interleaf leakage and determine the MLC heights from this(31). For modern MLC systems like the Elekta Agility MLC system and the Varian HDMLC system, the leakage between the leaves is too small and this technique is not be applicable anymore(32)(33).

Stellenbosch University https://scholar.sun.ac.za

Leaf end shape:

Leaf end shape is a design feature that emanated from the divergent nature of the beam. To overcome this problem, two designs have been considered(22).

In the first design, the MLC tip is flat and can be positioned and mounted in such a way that it moves along the circumference of a circle that has its centre at the x-ray target. This allows that the collimator is always tangent to any diverging beam(22). This design is used for some Siemens MLC products(34).

Alternatively, the MLC can be restricted to move only in a fixed plane that is perpendicular to the central beam axis, while a small piece of the front face of each collimator is tilted to achieve an agreement with beam divergence at all positions off-axis. This method requires two sets of jaws and is difficult to apply in cases where irregular or complex shapes are created by the MLC(22).

The second design keeps the motion of the MLC in a fixed plane perpendicular to the central axis of the beam but it relies on the shaping of the leaf tip to provide an acceptable and constant penumbra over the usable range of the MLC(22).

Due to the rounded leaf end design, however, the coincidence of the light and radiation fields may differ due to the radiation transmitted through the rounded leaf tip(35). This can be seen in figure 15 below:

Stellenbosch University https://scholar.sun.ac.za

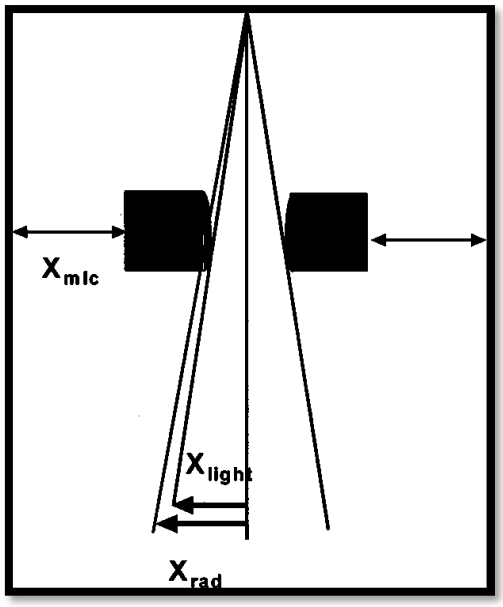

Figure 15: Diagram showing the difference in radiation and light field edge due to rounded leaf edges(35).

It should be noted that with a change in photon energy, the transmission through the rounded leaf edge would change and therefore the shape and size of the penumbra of the beam(36).

Furthermore, dose errors in the order of 5%-20% for a typical prostate plan can be expected when not accounting for treatment head scatter for small fields, collimator transmission and transmission through the rounded leaf edges(29).

Operation of MLC:

MLC systems operate in different ways, depending on the design and implementation, but should have systems in place for allowing confirmation of the accuracy of leaf position accuracy over time(22).

This can be achieved with high precision potentiometers or with an independent optical tracing of the leaves in the field and the accurate calibration of these systems when the leaf driving mechanism is fully functional(22).

Different vendors use different methods of tracking MLCs in providing accurate positioning. The Varian and Siemens MLC control system records MLC positions based on the motor current feedback, while Elekta`s Agility MLC system uses real-time data by tracking the physical MLC positions with an optical tracking system in the linac(37).

Stellenbosch University https://scholar.sun.ac.za

Quality assurance of MLC

Since the introduction of radiotherapy, beam collimation has been an area of great development. After the standard jaw or block collimation, there has been an evolution of 2D radiotherapy to 3D conformal radiotherapy, with the introduction of MLC systems due to the need for sparing of dose to organs at risk(38).

Later, inverse planning immersed, allowing for IMRT delivery techniques, which allowed the MLC to not only be used as a collimator but as a vital tool in intensity modulation. Additionally, the MLC on modern linacs can move while the radiation beam is on, allowing for dynamic MLC treatments such as VMAT. Lastly, micro MLC systems have been developed as a solution to treating extremely small lesions as part of SRS(4).

Recommended standards on MLC QA now differ from one source to the next. In South Africa, a standard MLC pattern only needs to be reviewed once every two months for LINACs that do not clinically deliver VMAT treatments. For VMAT capable units, a picket fence should be done at various gantry angles and during an arc delivery every month. Accuracy of MLC positioning should be within 2mm for units that do not perform stereotactic treatments and within 1mm for stereotactic treatments(20)(21).

This still lacks in comparison to the standards of the American Association of Physics in Medicine (AAPM) with the report from task group 142, which recommends MLCs to be checked with a picket fence test weekly and to include gantry angle as a variable monthly due to the effect of gravitational forces on the MLC positioning accuracy(19).

Regarding the requirement of the accuracy of the positioning of the MLC, most standards agree that the positional accuracy of the MLC should be under 2mm, however, the AAPM recommends from the report from task group 142 that if the machine is IMRT capable, the leaf position accuracy should be within 1mm for the 4 cardinal gantry angles(19).

Stellenbosch University https://scholar.sun.ac.za

MLC QA tests

In the literature, two basic tests are described. The first is the abutting field test. When the abutting field test is performed, the user creates fields that abut in the MLC direction and run them successively on the same detector. Ideally, this should create a uniform fluence on the detector. If the field size is calibrated too large, abutting fields will overlap and overdosing will be present on field junctions. If the field size is calibrated too small, abutting fields will not reach each other and an underdose region may be identified at the field junctions. If any of the fields are mispositioned to the other fields, overlap and or an absence of fluence will be noted ant the field junctions(39)(40).

This method is great in detecting field size errors but might not identify a systematic offset error because of calibration, for example, if both banks are offset.

The second test that can be used, is the picket fence or garden fence test. This test is described in the literature to be composed of equally size fields spaced a known distance apart and measured on the same detector in a single session. The result is an image or dose map of equally spaces slits(40).

When a dose profile is taken in the MLC direction of the fluence map, a series of peaks or troughs can be noticed. These indicate the open versus closed leafed regions of the test. The ideal picket fence has equally spaced peaks, that corresponds to the separation set when delivering and the FWHM of these peaks/troughs that is equal to the field size of the fields used(40).

In 2008, Mamalui-Hunter, M et al, published their approach to acquiring and analysing the picket fence test digitally using an onboard EPID. In this publication, they discuss necessary image processing, accounting for rotation differences between the collimator and EPID as well as a sub-pixel gaussian fit for improved precision in detecting MLC errors(41).

In 2016 Christophides, D et al, presented in a poster session their research which showed that by implementing a range of corrections similar to what was used by Mamalui-Hunter, M et al in 2008, MLC errors ≥ of 0.5 mm could be detected automatically by a software package from a picket fence test pattern(42).

In 2017, practical implications for the quality assurance of modulated radiotherapy with the use of point detector arrays was published by Steffi et al. Solutions for testing the MLC accuracy for modern systems include the picket fence test(43).

Stellenbosch University https://scholar.sun.ac.za

Effect of gravity on plan delivery:

When using the onboard EPID as a detector, the sag of the detector and gantry due to gravity with gantry angle should be accounted for. Rowshanfarzad et al in 2012 reported that they had developed a method for correcting for EPID and gantry sag in the inline and crossline planes(44).

Clarke et al reported in 2008 that the reproducibility of MLC position error with gantry angle was within 0.11 mm for an Elekta MLC(45). Another publication assessed two independent methods for measuring MLC errors due to gravity and reported that there were no significant differences in leaf position errors found at gantry angles 90 and 270 degrees(46).

Varian millennium MLC system and maintenance guide recommend that MLC QA tests be done at various gantry angles as the MLC control system has to compensate for the effects of gravity(47).

Additionally, research done by Lee, et al, states that their research "conclusively reveals that the DMLC gravity affects IMRT dose distributions"(48).

Stellenbosch University https://scholar.sun.ac.za

MLC log file in MLC error detection:

In 2019, at the ESTRO 38 meeting, Picioli, M et al presented their research into dynamic MLC parameters recorded in a dynamic log file. They concluded that although Elekta log files are not generally known in the clinical domain, they possess reliable information regarding the positioning of each MLC in a static field and the MLC speed for dynamic MLC shaped fields in compliment to the simple visual MLC picket fence inspection(49).

Karan, T et al, investigated MLC accuracy from log files in lung SBRT and the effect thereof on patient-specific QA. This study concluded that most patient-specific QA methods employ limited resolution and will most likely not be able to identify a dose discrepancy due to a small MLC displacement. It was found that in one of the lung SBRT plans, an MLC error of 5mm was detected with no significant dose impact on the patient-specific QA(50).

Calvo-Ortega, J.F. et al. validated the use of Varian Dynalog files for IMRT QA purposes by tracking the MLC positions over time. The research team still expressed their concerns that Dynalog files only reflect MLC errors that are not a by-product of a miscalibration or errors that arise because of the absolute calibration of the linac and that this method is not an absolute reflection of the components on the linac at the time of measurement(51).

When using systems that track the MLC using motor currents, mechanical MLC faults cannot be detected, whereas optical tracking would allow for detecting mechanical faults (37).

For the Elekta Agility MLC, many studies have looked into using a type of MLC log file to track the MLC movement and accuracy over time. Some studies use machine mapping capabilities that exist in the service functions of the machine, others use an extension of the linac control computer and the Elekta iCOM software communication links with Elekta linear accelerators. All these methods employ logging of the state of machine components at regular intervals(37)(52).

Rowshanfarzad et al. has suggested that independent verification of any MLC tracking system is essential. In their study, intentional offsets were introduced and verified by measurements on the EPID. Similarly, Kasmayanti et al. confirmed their findings from logging data with EPID measurements(52)(31).

Hirashima et al showed in 2018 from a study of Varian log files, linked with a dose reconstruction technique used for all fractions of 15 patients, that the largest dosimetric error in a single treatment was 2.5%. The largest accumulated dosimetric error reported for an entire treatment course was 1.6%(53).

Stellenbosch University https://scholar.sun.ac.za

Clinical impact of MLC errors:

In 2012, Moiseenko, V et al, showed by inducing systematic MLC errors that the biological impact of MLC errors is more pronounced for high modulation plans. In this study, the efficiency of 3D gamma analysis as a patient-specific QA tool was also investigated. The results show that using the criteria of 3 mm/3% and a pass rate of 95% is sufficient to ensure no under- or overdosing of the PTV. The results further show that this does not ensure an overdosing of the OARs. In some head and neck IMRT cases, the plans that passed above 99.5% with the 3mm/3% criteria still lead to roughly 5% dose differences in the spinal cord and parotid doses and were observed in this study around 1 mm systematic MLC offset(54).

In 2012, Oliver et al concluded that to maintain the dose to the PTV70Gy in their eight head and neck VMAT plans within 2%, MLC errors should be under 0.6 mm in size(55).

Several studies have investigated the dosimetric impact of MLC errors and this has driven the increasing need for a way to quantitatively check the MLC as part of routine quality assurance. One such study, published in 2015 by Karthikeyan Nithiyanantham et al., entitled "Analysis of direct clinical consequences of MLC position errors in volumetric-modulated arc therapy using 3D dosimetry system" concluded that systematic MLC errors beyond ±0.3 mm influenced the intensity-modulated dose distributions significantly(56).

Similar studies done locally at the University of the Free State in Bloemfontein, South Africa by Strauss and Shaw, found that their VMAT plans exhibited significant dosimetric changes when systematic MLC errors of ±0.5 mm and more were introduced(57).

Stellenbosch University https://scholar.sun.ac.za

Materials:

For sections 1-6 (relating to the development of a suitable QA tool), the following materials were used:

- Elekta Synergy platform linear accelerator with:
  - Agility 160 leaf MLC.
- Elekta IviewGT EPID.
- PTW 1500 ion chamber array.
- PTW – Verisoft 7.2 for measurement and analysis.
- RTQA2 Gafchromic film.
- HP LaserJet Pro MFP M426fdn scanner/printer.
- ImageJ1.48 software for viewing and processing images.
- Visual studio 2019 – for programming of the in-house software.
- Microsoft Excel for data analysis and calculations.
- Samsung stopwatch application for time measurements.

For section 7, the in house created software was validated and compared to the delivered values. For this section 1 linac of each MLC type was used. This included the following:

- Elekta Synergy platform linear accelerator with:
  - Agility 160 leaf MLC
- Siemens Artiste linear accelerator with
  - Siemens 160 MLC
- Varian VitalBeam Linear accelerator with
  - Millennium 120 MLC
- Varian Halcyon linear accelerator with
  - Varian Halcyon MLC

The following software was used for analysis or comparison of results:

- IBA myQA picket fence module.
- In-house programmed software, developed in this study for:
  - MLC error determination as through sections 1-6.
  - Visual studio software to read and display Varian MLC dynalog file information.
  - C++ programmed software for capturing and viewing Elekta iCOM information.

Stellenbosch University https://scholar.sun.ac.za

For sections 8-10, the in house created and validated software was used to test the MLCs on all units participating in the study.

These included MLC types as stated below:

- Elekta Synergy platform linear accelerator with:
    - Agility 160 leaf MLC
    - Elekta APEX microMLC
- Siemens Artiste linear accelerator with
    - Siemens 160 MLC
- Varian VitalBeam Linear accelerator with
    - Millennium 120 MLC
- Varian Halcyon linear accelerator with
    - Varian Halcyon MLC
- Varian TrueBeam Linear accelerator with
    - HDMLC

All units that participated in the study were compliant with SASQART regulatory requirements for all linac, EPID and MLC QA. For VMAT capable units, this included monthly picket fence tests at various gantry angles and a picket fence during arc delivery. All positional MLC measurements were made in a relative manner and therefore no absolute dose calibrations were necessary.

All units that participated in this study were subject to routine maintenance and calibrations for clinical use as specified by each of the vendors of the units. All calibrations were checked and verified to be correct and safe for clinical use prior to data collection for this study.

Stellenbosch University https://scholar.sun.ac.za

Methods:

Phase 1: Creating the test procedure and analysis software.

Uncertainty and possible bias in measurements were identified for phase 1 as follows:

- Measurements were only made by one observer.
- The experience level of the medical physicist with each of the sets of equipment (stopwatch, detectors and software).
- The personal preference of the medical physicist doing the tests.

These factors were addressed in the following ways to limit uncertainty and the influence of possible bias on the results.

- Measurements made by only a single observer were reviewed by an independent medical physicist that was a volunteer in the study.
- All the software and the equipment used in this section were in clinical use in the department where the tests were done. The medical physicist doing the tests was familiar with all of the equipment and worked with it on a regular basis.
- As far as possible, qualitative analysis methods was used to prevent influence of observer bias. In areas where this was not possible, methods were used to quantify qualitative results based on a predefined Likert scale.

Stellenbosch University https://scholar.sun.ac.za

Section 1: Selection of a suitable test

After considering literature and what has been done in similar studies, two tests were considered in the selection process for a test.

The first, was the picket fence test and the second was the abutting field test.

Each test was delivered on a Synergy platform Elekta Agility linear accelerator with a 6MV photon beam delivered only on the onboard imager (IviewGT). After this, the images were exported and evaluated on the following grounds:

1. The time required to do the test.
2. Image contrast.
3. Relation of image anomalies to physical errors.

The time required to do the test was measured from the start of the test to the stop of the test with a Samsung stopwatch application by a qualified Medical Physicist.

To evaluate how easily errors could be detected mathematically, a contrast factor was calculated with the equation below:

$$Contrast\ factor = \frac{Maximum\ intensity\ in\ "in\ field"\ region}{Minimum\ intensity\ in\ "in\ field"\ region} \quad 9$$

This factor represents the change in signal between the lowest and highest signals in the "in field" region. This gives an idea of the contrast in the image and how easily the independent algorithm could distinguish between true signal differences in the image and image noise.

How each test characterised an MLC error and how this correlates to the physical position or properties of the MLC were considered.

Stellenbosch University https://scholar.sun.ac.za

Section 2: Selection of a suitable imaging modality:

Radiochromic film (Gafchromic RTQA2 film), Elekta IviewGT EPID imaging and a PTW 1500 ion chamber array were evaluated as possible imaging modalities for MLC QA tests.

Each detector was evaluated by its ability to fulfil the following criteria:

1. Viability.
2. Time efficiency and digital compatibility.
3. Resolution.
4. Image quality.

Since not all the categories listed are composed of quantitative data, the detectors were scored with a Likert scale. The score was defined with the scale in Table 1 below by how suitable each of the options was for determining the accuracy of a modern MLC digitally.

Table 1: Likert scale for score determination

Score	Meaning of score on the scale
0	Unsatisfactory
1	Usable
2	Good
3	Excellent

In this way, all data regardless of nature, could be combined in a primitive quantitative manner in a simple attempt to find the most suitable detector for this study.

Viability:

The viability section consisted of evaluating how easily the test can be detected by the detector and digitized afterwards. Factors that contributed to higher scoring were features such as being able to detect the pattern easily at non-zero gantry angles, the ability to output the image in a digital format and how readily available the detector is in general in the department.

Time efficiency and digital compatibility:

For the time efficiency and digital compatibility section, the time required to deliver and digitize the image with each of the detectors were considered. The fastest detector was awarded the highest score.

Stellenbosch University https://scholar.sun.ac.za

Resolution:

The resolution of each of the detectors was considered and evaluated with a line profile across the MLC direction. The detector with the best digital resolution (smallest digital pixel size) was ranked the highest. Any detector with a resolution worse than the tolerance of the MLC test (2mm) was automatically scored a zero for this test. This information could be achieved with the ImageJ software from the image header information as well.

Image quality:

Lastly, the signal to noise ratio was considered as a measure of the image quality. For measuring the signal to noise ratio, a square region of interest (ROI) with a width of 1.5 cm was drawn on the central 2cm picket for all images in a position where the entire square was in a high-intensity region. The detector with the highest SNR scored the highest.

Section 3: Noise removal:

1D testing of filters:

The following noise reduction filters were chosen for investigation:

1. Mean
2. Median
3. Gaussian

In this section each of the noise reduction filters was assessed on the following 2 criteria:

1. The ability to remove inherent noise in the image.
2. The ability to maintain the trend of the data.

To assess both these characteristics at the same time, a line profile was taken from a specific location of a picket fence imaged with an Elekta IviewGT EPID. The image was then filtered by each filter in the Image J software and line profiles were taken at the same location of the post filtered image.

The pre- and post-filtered profiles were compared visually and assessed on the smoothness of the curve (as an indication of the smoothing ability) as well as its proximity to the original profile (as a measure of how much data is changed by this filter). The level of smoothing was deemed less important than the ability of the algorithm to not significantly alter the measured information.

Stellenbosch University https://scholar.sun.ac.za

The pre- and post-filtered profiles were compared further mathematically in Microsoft Excel by subtracting the post-filtered profiles from the pre-filtered profile. The result with the smallest difference identified the filter that would alter the original data the least.

2D verification of findings:

After the single-dimensional investigation, the filters were each applied to a picket fence pattern acquired on the IviewGT EPID. The unfiltered and post filtered images were then subtracted to verify that the measured info is not changed significantly. Qualitative visualisation of the resultant images was used to evaluate the best filter in two dimensions. If a resultant image showed edges of the pickets, significant edge smoothing occurred, blurring the edges in the post filtered image. If no edges could be seen, the trend of the data was maintained, and no edge smoothing was detected. The size of the edge that was created by the smoothing algorithm has a direct corelation to how much the data was changed.

In situations of uncertainty, the size of the smoothed edged could be measured by use of the ImageJ software using a single line profile. The smallest edge would indicate the smallest difference from the measured data. Since this section is merely a visual 2D verification of the quantitative results already obtained in the previous part of this section, qualitative analysis was not done.

Section 4: Peak detection algorithm:

The simplest peak detection algorithm was evaluated on a full pixel line of a picket fence image. The maximum of each peak could easily be detected with a maximum number function, however, for determining the minimum two methods were investigated. The determination of the maximum and minimum of each picket is critical in finding the FWHM correctly.

The first method of finding the minimum was designed to find the minimum of the image to remove the background signal. This method corrected for EPID imaging background signal, but not for MLC transmission.

Method 2 was designed to detect the picket minimum between pickets for each picket. In this way, this method could correct for EPID imaging background signal as well as MLC transmission.

A single profile study was conducted to evaluate the difference in signal between these methods and successively the influence of it on the accuracy of determining the FWHM.

Stellenbosch University https://scholar.sun.ac.za

Logical filters together with a sliding window technique helped discriminate against peaks with inadequate heigh or unexpected width.

Section 5: Interpolation:

As an optimal resolution is critical to evaluating the accuracy of MLCs, sub-pixel interpolation methods were investigated. A single-pixel profile of a single picket was used and each of the interpolation methods was evaluated for the following:

1. The simplicity of applying the interpolation
2. Accuracy in finding:
    a. Centre of the peak
    b. FWHM of the peak

The least square fit technique of interpolation was used in Microsoft Excel for:

1. Linear interpolation
2. Gaussian interpolation
3. Second-order polynomial interpolation

All interpolation techniques were applied to a single line profile acquired from an EPID image of a 2cm wide picket on the central axis, acquired in the previous sections. Where no pre-configured Microsoft Excel software exists for least square fit of these functions, the solver plug-in was used.

Section 6: Elimination of errors not caused by MLCs

Accounting for collimator rotation:

The accuracy of a straight-line interpolation technique, through least square fit, was investigated for accounting for small collimator rotation errors between the collimator and the EPID. The ability of this technique to find collimator rotation implemented was evaluated by inducing small collimator rotations and measuring them from a picket fence image on all 5 pickets. Collimator angles of 0.1 – 0.5 degrees in 0.1-degree increments were applied and a full picket fence image was taken for each setting.

Width filtering of errors:

For this section, the peak detection algorithm discussed in section 4 was used. The algorithm was used to eliminate all error peaks of width smaller than half an MLC width. Half an MLC width was used as most of the systems use rounded leaf edge MLC and therefore the error on the image is often smaller than the full width of the MLC. In this way noise that the other algorithms may have induced or may have not been removed

Stellenbosch University https://scholar.sun.ac.za

completely by the filtering algorithm was eliminated and only errors that relate to the MLC were considered.

Stellenbosch University https://scholar.sun.ac.za

Phase 2: Implementation.

Section 7: Accuracy validation of software:

For the first part of the validation study, all previous techniques were employed to create an end product that should estimate the accuracy of picket fence position and width formed by an MLC. Micro MLC systems were not included in this section. Appendix B shows a flow diagram of the flow and some specifics of the software for reproducibility purposes.

Errors of 0.5 mm, 1.0 mm, 1.5 mm and 2.0 mm were introduced via the record and verify system on the leftmost, central and rightmost pickets at 3 different height levels. The accuracy by which the software found these offsets were measured as the difference between the set error and the average measurement error across the entire picket fence image.

For the second stage of validation, the software was compared with a commercial IBA picket fence analysis tool for Elekta agility MLC as well as Varian Millennium 120 MLC. The in-house software was adapted to report the same physical characteristics, of the IBA software. The method in which these characteristics were calculated was not changed. For example, the in-house software relates picket position to the centre of the central picket, where the IBA software relates it to the centre of the acquired image.

For the third stage of validation, the relative analysis results from stage 2 were compared to Elekta machine log files or Varian Dynalog files.

Section 8: National survey of MLC data using software looking at 3DCRT and IMRT capable LINACS:

A survey was done of a group of participating LINACs in public and private sectors of radiotherapy in South Africa, by analysing the routine QA picket fence images with the created software. Instructions were given on how the Picket fence was to be constructed, to maintain a standardized test among all LINACs. The maximum width and position errors were recorded for each image.

In all sections, physicists could volunteer their routine QA for inclusion into the study. In section 8, data were evaluated for 1 Varian Vital Beam unit with Millennium 120 MLC, 1 Varian Halcyon, 1 Varian Truebeam with Varian HDMLC, 5 Siemens Artiste platforms linacs with Siemens 160 MLC, 1 Siemens Oncor with Siemens 160 MLC, 8 Elekta Synergy platform linacs with Elekta Agility MLC and 4 Elekta Versa HD platform linacs with Agility MLC.

A total of 21 linacs participated in this section.

Stellenbosch University https://scholar.sun.ac.za

Section 9: National survey of MLC data used for VMAT:

A survey was done of a group of participating LINACs in public and private sectors of radiotherapy in South Africa, by analysing the routine QA picket fence images delivered at several gantry angles and during an arc with the created software. Instructions were given on how the Picket fence was to be constructed, to maintain a standardized test among all LINACs. The maximum width and position errors were recorded for each image.

For section 9, all VMAT capable linacs were included, except the Halcyon linac due to a lack of data. This amounted to 8 Linacs in total.

For this section, the first comparison was done for position and width errors due to gravity effects. A picket fence image was taken at gantry angles 0º, 90º and 270º. The difference in position and width errors from gantry angle zero was found as a measure of the MLC stability under the influence of gravity. This was done by comparing the MLC accuracy from the in-house software measured at gantry angle zero to that at non-zero gantry angles.

Additionally, the delivery of a picket fence during an arc was investigated for VMAT capable machines where data was made available by the medical physicist on-site.

Section 10: National survey of micro-MLC data used for SRS:

A survey was done of a group of participating LINACs in public and private sectors of radiotherapy in South Africa, by analysing the routine QA fence images delivered at several gantry angles and during an arc with the created software. Instructions were given on how the Picket fence was to be constructed, to maintain a standardized test among all LINACs. The maximum width and position errors within the central 10x10 cm^2 were recorded for each image.

For this section, micro MLC systems from Eleka and Varian were evaluated. MLC accuracy, as well as leaf positioning limitations, were taken into account. 1 Varian Truebeam platform linac with Varian HDMLC and one Elekta Versa HD platform linac with an Elekta Apex external MLC were considered. Only a picket fence at gantry angle zero was considered due to a lack of clinical use of the equipment or information from participating volunteers.

Stellenbosch University https://scholar.sun.ac.za

Results and discussion:

Phase 1: Creating the test procedure and analysis software.

Section 1: Selection of a suitable test

For this section, the table below shows the delivery time for a 6-picket, picket fence pattern and an 11-field abutting field pattern.

Table 2: Table of time taken and MU per segment per combination.

Test	MU per segment	Time (s)	Export time (s)	Total time (s)
Picket fence on EPID	10	147	48	195
Abutting fields on EPID	10	298	48	346

As can be noted from the table, the abutting field pattern took two times longer to deliver due to more segments needed to create this if the same MU per field and the same field size is assumed.

Below is a graphical representation of a single profile for each of the abutting fields and picket fence patterns.

Stellenbosch University https://scholar.sun.ac.za

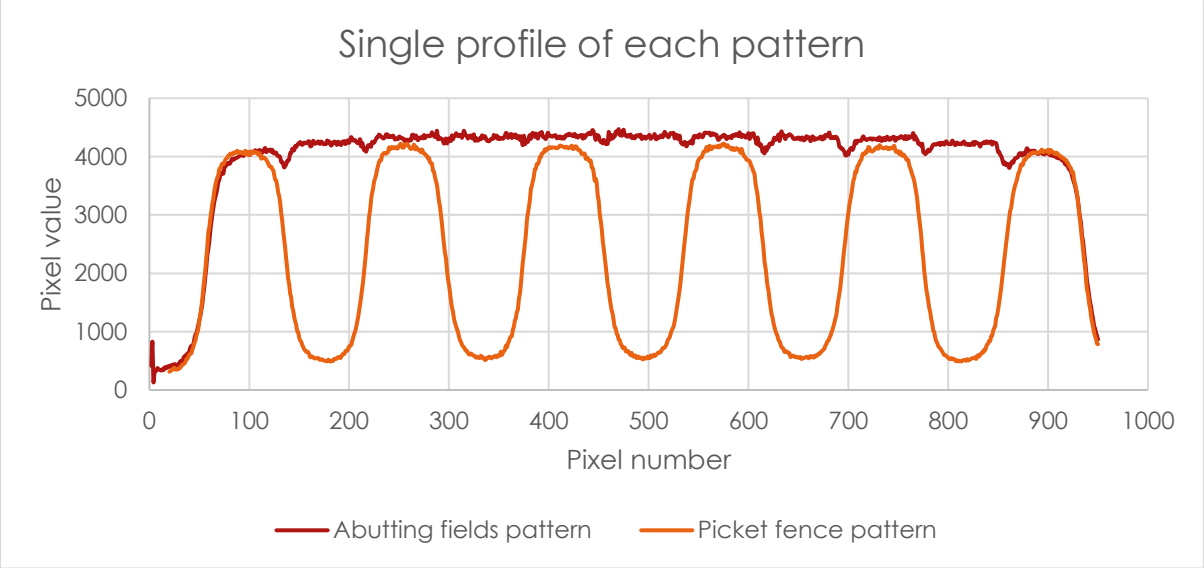

Figure 16: Graphic representation of a single profile taken through a picket fence and abutting fields test.

The contrast factor in each pattern was calculated. For the abutting fields pattern, the contrast factor was:

$$Contrast\ factor = \frac{4470}{3806} = 1.17$$

For the Picket fence pattern, the contrast factor was:

$$Contrast\ \ factor = \frac{4221}{489} = 8.63$$

The position and width of the pickets of the picket fence test correlate directly to the positioning of the MLC. An intensity dip or spike in the abutting field test correlates to a mispositioning of MLC.

The picket fence pattern was delivered in a smaller amount of time than the abutting field pattern. Both patterns extended to a maximum off-axis distance of 11cm in the MLC direction with 2cm field widths. These 2cm fields were chosen as this is a common field width in IMRT/VMAT delivery techniques and errors on these field sizes are of clinical significance when treating with these techniques.

From the single profile data, it was observed that the contrast factor values for the picket fence pattern (8.63) were much higher than that for the abutting field pattern (1.17). This increase in image contrast will allow an independent algorithm to distinguish between noise and signal much easier in the case of the picket fence than for the abutting field pattern.

Stellenbosch University https://scholar.sun.ac.za

Parameters that can be measured from the picket fence pattern include picket position, spacing and width, which correlate to field position and field size. Errors in the picket position may therefore translate directly to a mispositioned field and because the fields are shaped by MLC in this direction, by extension a fault in the MLC positioning.

For the abutting field pattern, the intensity variation from one pixel to the next is measured. This intensity variation is linked to the overlap or gap between 2 abutting fields and should be zero. There is however no numerical correlation between the intensity change and the physical error in the MLC position.

It should be noted that the time required to do the abutting fields test could be shortened by lowering the MU per field or making the segments larger, however by doing this, the already low contrast will deteriorate, and less abutting segments will be created. This decreases the usability of this test.

For all the reasons discussed above, the picket fence pattern was regarded as the best test for this purpose and used from here onward in the study.

Section 2: Selection of a suitable imaging modality:

Viability:

In this test, all detector and pattern combinations could be performed on the Synergy platform Elekta Agility accelerator imaged by the detectors with a 6MV photon beam. Figure 17a, b and c below show the 3 digital images obtained from each of the imaging systems respectively.

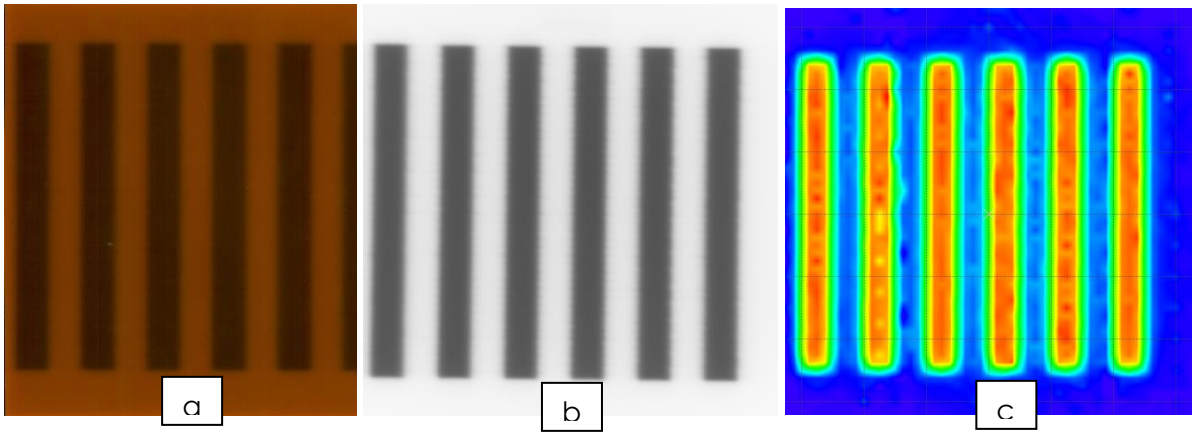

Stellenbosch University https://scholar.sun.ac.za

Figure 17: Graphic example of a picket fence image taken on a) gafchromic film b) an EPID and c) a 2D ion chamber array.

The images from the EPID are exported to the record and verify (R&V) system automatically after which a copy can be extracted to any Computer (PC) connected to the R&V system in DICOM format. For the PTW array, measured images could be exported to the PC used for measurement as a .png file. The data measured on the radiochromic film could be digitised using a flat bed scanner and a range of resolutions as a .png file.

The EPID detector was scored higher than the other detectors as it contained other DICOM data that could prove beneficial containing machine and geometry characteristics to be used in the analysis of the image such as the panel SID, gantry angle and pixel size.

The viability scores can be seen below in table 3:

Table 3: Viability and digital compatibility scores for each detector

Detector	Score
Picket fence on EPID	3
Picket fence on Film	2
Picket fence on Array	2

For this section, the EPID was the superior detector as it could image digitally and retain the DICOM info. The other two detectors were both able to image the pattern and all detectors were able to create a digital copy of the pattern.

Time efficiency and digital compatibility:

The total time to achieve a digital image was divided into two categories. The first was the time of acquisition of data from the linac and the second was the time taken to export or digitise the data into a digital image.

Due to the sensitivity variation between the detectors, the acquisition time differed between each detector as different amounts of monitor units were used for each detector. Table 4 below shows the number of MUs used per segment for each detector-pattern combination as well as the breakdown of the time taken for each part.

Stellenbosch University https://scholar.sun.ac.za

Table 4: Table of time taken and MU per segment per detector.				
Combination	MU per segment	Acquisition time (s)	Export time (s)	Total time (s)
Picket fence on EPID	10	147	48	195
Picket fence on Film	200	412	55	467
Picket fence on Array	20	144	25	169

The time efficiency scores derived from the results in table 4 are shown in table 5 below:

Table 5: Time efficiency scores for each detector	
Detector	Score
Picket fence on EPID	3
Picket fence on Film	1
Picket fence on Array	3

When the EPID was used as a detector, patterns could be imaged at any gantry angle or during an arc delivery, but for the radiochromic film and the ion chamber array, the patterns could only be accurately imaged at cardinal gantry angles. Using rotational phantoms like the Octavius 4D phantom could assist in obtaining accurate measurements at non-zero gantry angles or during an ARC, however the verisoft software will not allow for planar measurements while the rotational unit is active, and the measurement will have to be reconstructed by the user to view. As soon as this is done, the positional MLC measurements are not visible, but rather the 3D dose effect of the MLC errors in the phantom are being noted. This was not inline with the aim of this study and the availability of these phantoms were lower than that of an EPID in most departments.

Stellenbosch University https://scholar.sun.ac.za

At this stage of the study, it was observed that the PTW array acquisition and export was the fastest and the radiochromic film the slowest to acquire and the slowest to process. This was mainly due to the high MU required for adequate image contrast for radiochromic film.

Additionally, the EPID digitization was dependent on the speed of the network connection in the department and could be faster in departments with faster network speed. The difference in total time between the EPID and the PTW array was 26 seconds, which is so small that it should not make any difference to the clinical workflow.

Resolution:

The resolution of each detector was assessed from image J software`s pixel size function and specifications of each of the detectors and verified with a line profile and the known field size of the picket width.

The EPID has a pixel size of 0.4 mm at 160 cm SSD, which correlates to a digital pixel size of 0.25 mm at isocentre.

For the radiochromic film, the lowest dpi that would allow a resolution below 0.3 mm was chosen for scanning the film. This would allow for the optimal signal to noise ratio with an acceptable resolution. The optimal resolution for scanning according to these criteria was 100dpi. This results in a pixel size of 0.254 mm.

The PTW ion chamber array has chambers that are 5 mm apart. The digital resolution resulted in a 5 mm digital pixel size.

The resolution scores are shown in table 6 below:

Table 6: Resolution scores for each detector

Detector	Score
Picket fence on EPID	3
Picket fence on Film	3
Picket fence on Array	0

From the scoring criteria, the PTW ion chamber array scores a 0 for resolution as the digital resolution (5mm) is worse than the tolerance for MLC errors (2mm). The EPID and Film had similar and acceptable resolutions of 1/8th of the size of the tolerance of the MLCs and were both placed in the top position for resolution.

Stellenbosch University https://scholar.sun.ac.za

Image quality:

The signal to noise ratio was measured on all the images of the picket fence pattern. The percentage contribution of the signal and noise, as well as the signal to noise ratio, can be seen in figure 18 below.

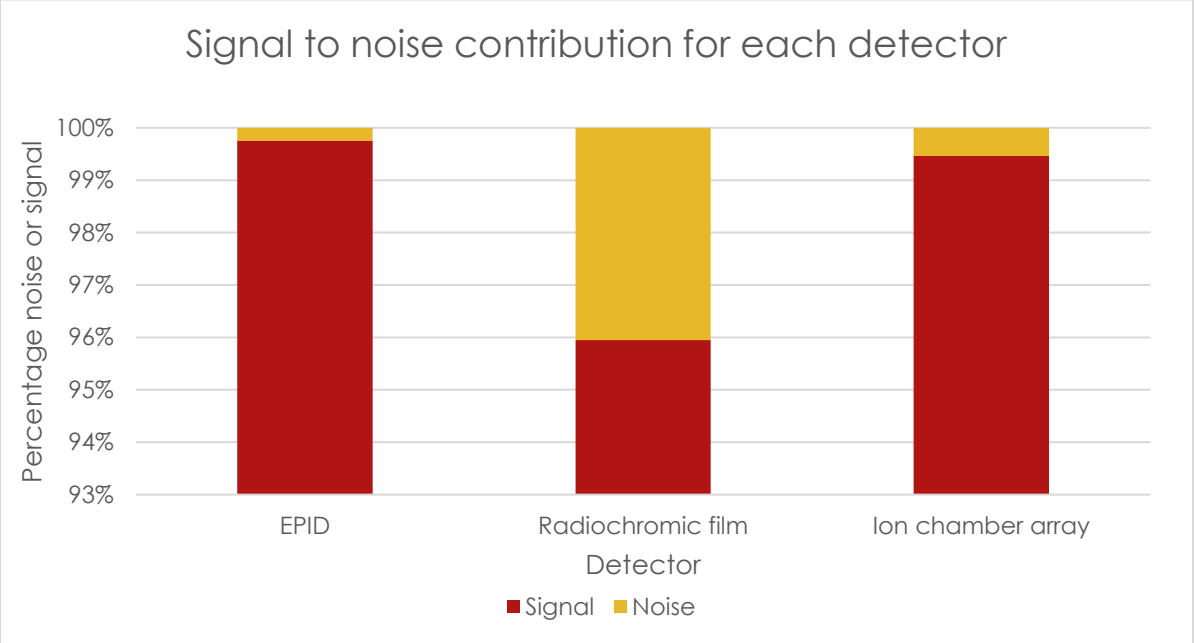

Figure 18: Graphic representation of the signal to noise ratio measured from each detector.

All detectors had a high signal percentage contribution, with the radiochromic film doing the worst at about 96% signal and 4% noise. The EPID had the highest signal to noise ratio with a noise % composition smaller than 0.5% of the total signal.

The image quality scores are shown in table 7 below:

Table 7: Image quality scores for each detector	
Detector	Score
Picket fence on EPID	3
Picket fence on Film	1
Picket fence on Array	3

Most favourable detector:

From all the data presented, the scores were combined, and the results can be seen in figure 19 below.

Stellenbosch University https://scholar.sun.ac.za

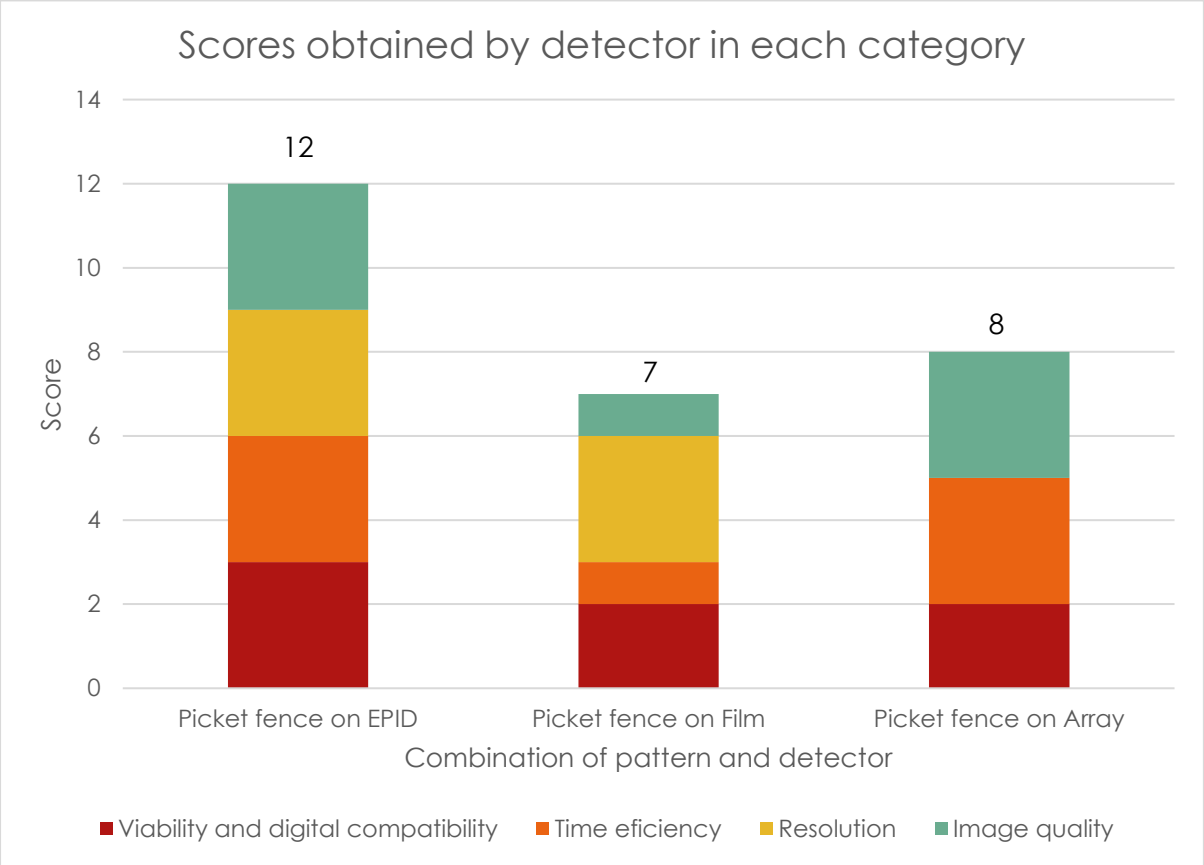

Figure 19: Graphic representation of the combined scores attributed to each detector in the form of a stacked bar graph.

From this, the EPID is the most favourable detector for this situation. The other 2 detector systems fared well but were inferior to the EPID in some cases. The biggest disadvantage of the 2D array was its resolution, while when using film, the digitisation and signal to noise ratio were disadvantages.

Only the EPID was used onward in this study.

Section 3: Noise removal:

1D testing of filters:

The single nonfiltered line profile, taken from half of the central 2cm picket of a picket fence acquired on an iViewGT EPID, was compared to filtered line profiles from the same picket fence image. This can be seen below in figure 20:

Stellenbosch University https://scholar.sun.ac.za

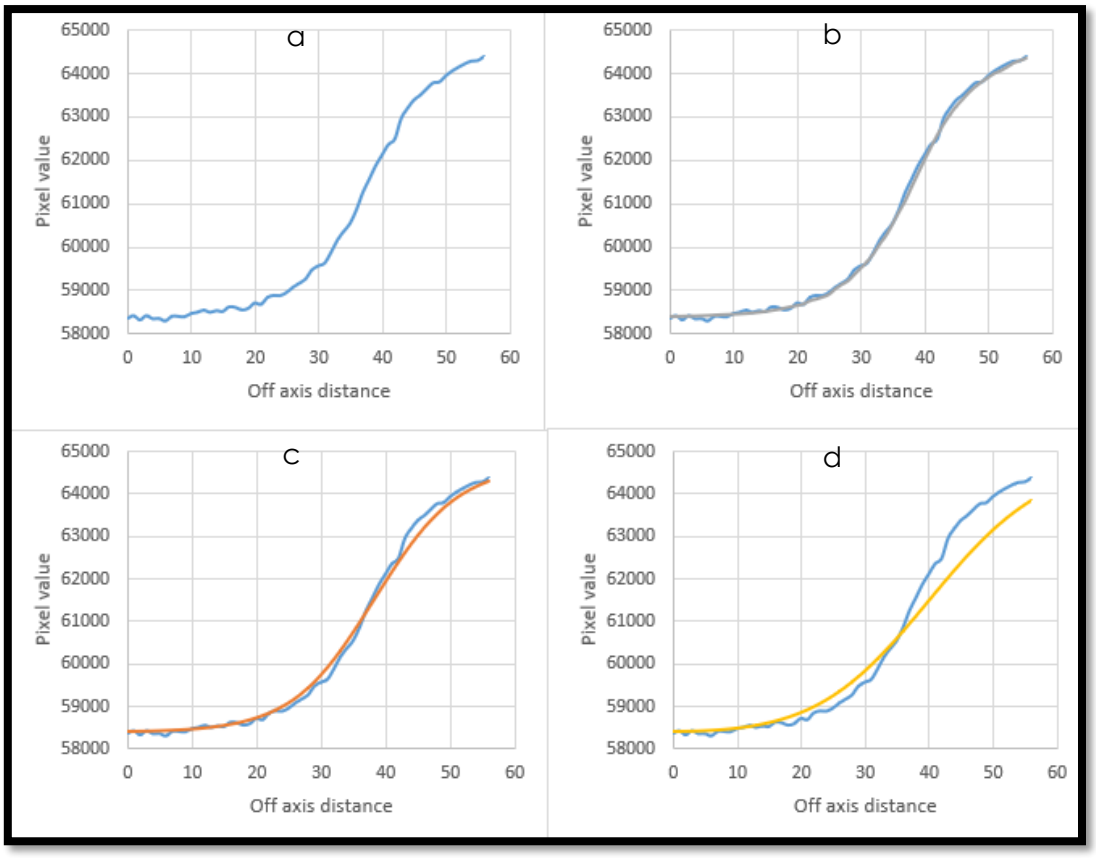

Figure 20: Graphic representation of a) a profile of the measured signal of the beam edge of a picket, b) a median filtered profile with the original profile, c) a mean filtered profile with the original profile and d) a gaussian filtered profile with the original profile.

In each of the graphs, the measured data is represented in blue and the filtered dataset in another colour. From this figure, all the filters were able to smooth the noise in the nonfiltered profile.

The difference between the nonfiltered profile and the filtered profiles was determined and plotted against the off-axis distance. This can be seen in figure 21 below.

Stellenbosch University https://scholar.sun.ac.za

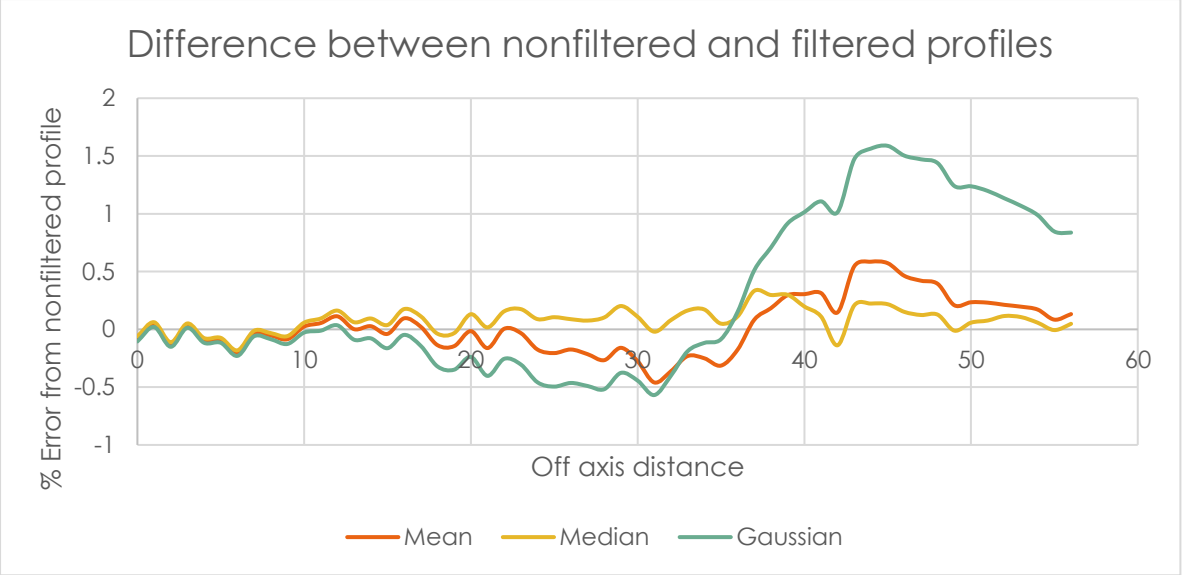

Figure 21: Graphic representation of the differences between the measured profile and filtered profiles by using each of the filters mentioned.

All filters were able to filter noise from the image without changing the nature of the data in the out of field region (where the intensity is at its lowest). The gaussian filter (figure 20d) performed the worst in maintaining the integrity of the measured data. Visually and quantitatively the mean and median filters both maintain the integrity of the measured data quite well.

From the difference profile data, the median filter displays the lowest differences, which correlate to it being the best at maintaining the integrity of the measured data.

2D verification of findings:

Figure 22 below shows the two-dimensional intensity difference between the nonfiltered and the filtered picket fence images.

Stellenbosch University https://scholar.sun.ac.za

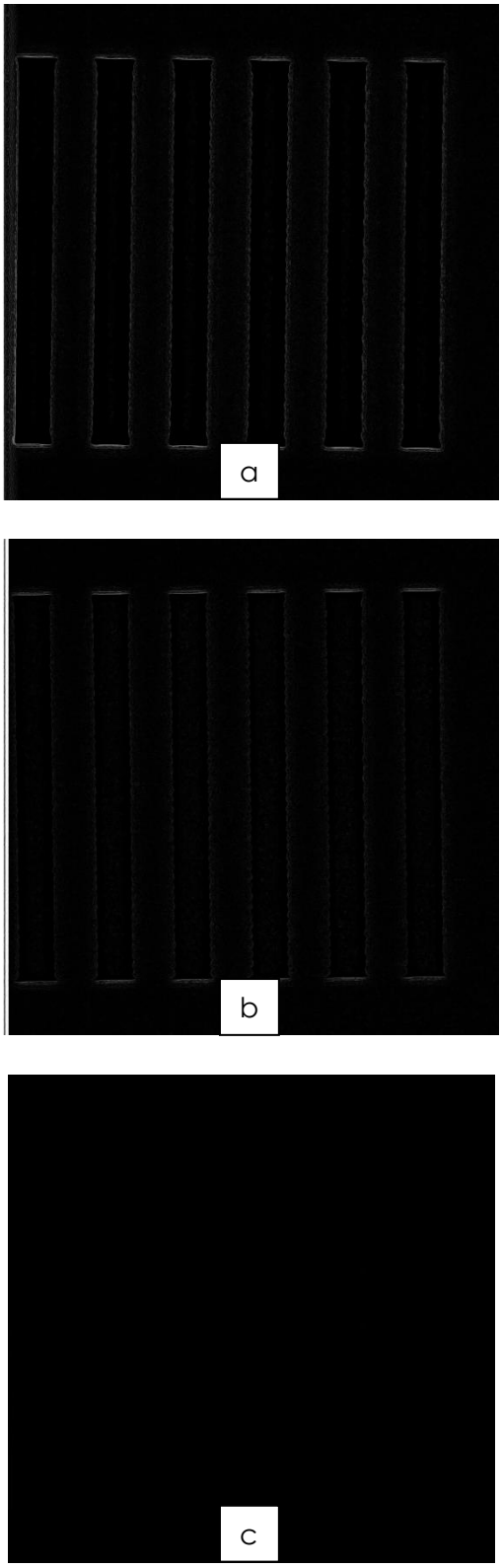

Figure22 a, b and c, show the 2D effect of smoothing with Gaussian, mean and median filters respectively.

From the two-dimensional images, the median filter has the smallest influence on the integrity of the measured data and no thickening or thinning of the pickets could be observed when subtracting the post-processed image from the original.

Stellenbosch University https://scholar.sun.ac.za

Section 4: Peak detection algorithm:

When determining the minimum signal for a peak with the two independent methods discussed in the methods section, the difference in minimum was measured to be 7.5% different depending on which technique was used. When these minima were used to determine the respective half maximum height values, the difference in half-maximum height was 6.7%. The location of the found minima can be seen graphically below in figure 23 below.

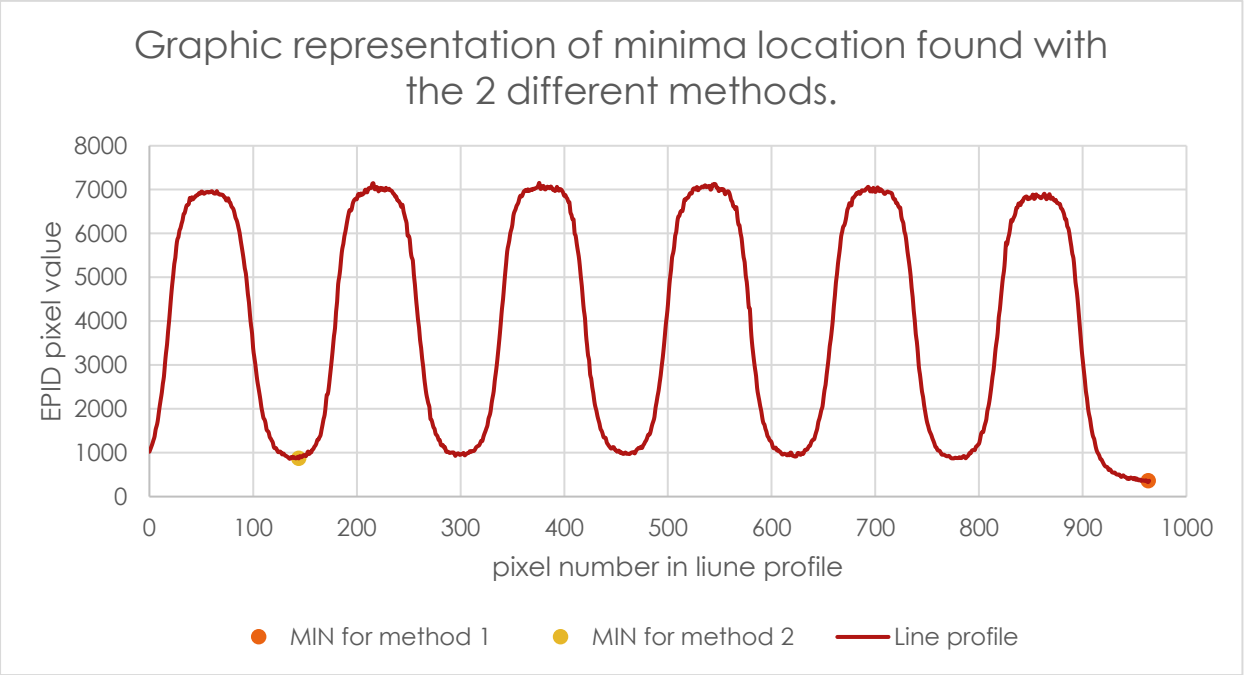

Figure 23: Graphic representation of a single line profile with the indicated minima for each method of determining the minimum.

Subsequently, the effect of this difference on the FWHM was determined. It was found that this difference in half-maximum height introduces a difference of 0.48 mm, with method 1 always having wider pickets than method 2. This can be viewed graphically in figure 24 below.

Stellenbosch University https://scholar.sun.ac.za

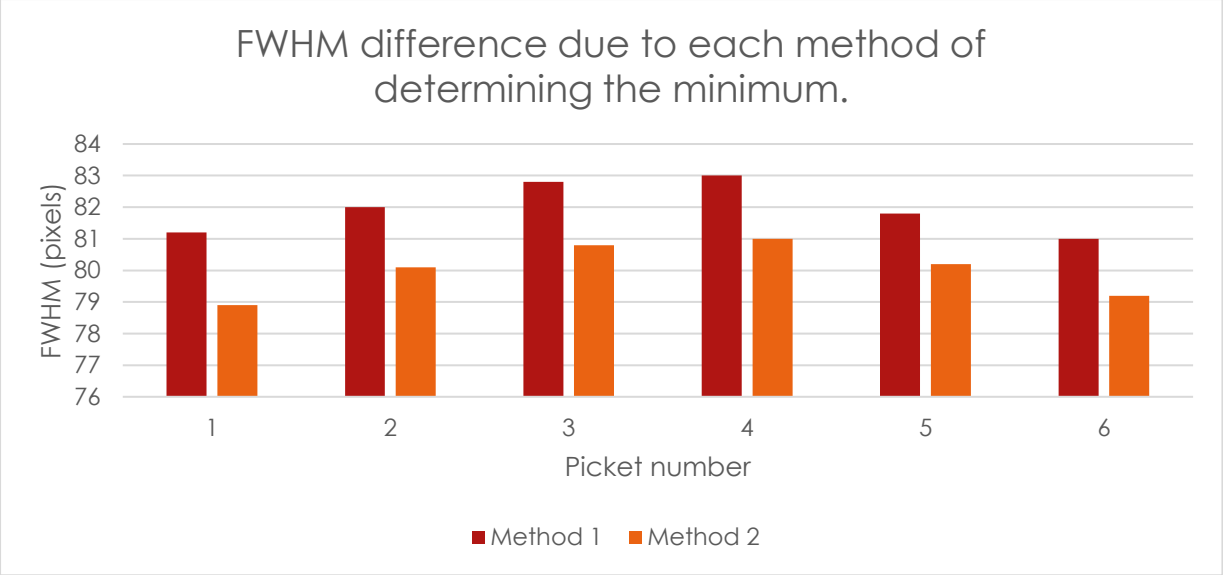

Figure 24: Graphic representation of the FWHM found from methods 1 and 2 of background determination.

From the data presented, the cruciality of finding the right minimum peak value is eminent. Graphically, it can be seen that the minimum determined through method two is a better approximation of the picket`s minimum itself (80 pixels). This method eliminates MLC transmission and EPID background imaging signals and results in FWHM values that are closer to that what was set when acquiring the image.

Method 2 for determining background and subsequently the peak position was used from here on.

Section 5: Interpolation:

A single line profile and its relationship to the centre and FWHM positions of each of the interpolations were used to assess the accuracy of each of the processes. The single line profile was taken from the central 2cm picket of a picket fence acquired on an iViewGT EPID.

During the process of interpolation, accuracy, and the degree of simplicity of each of the methods were noted.

Below is figure 25 showing the accuracy of each of the least square interpolation methods used in determining the FWHM positions as well as the central position.

Stellenbosch University https://scholar.sun.ac.za

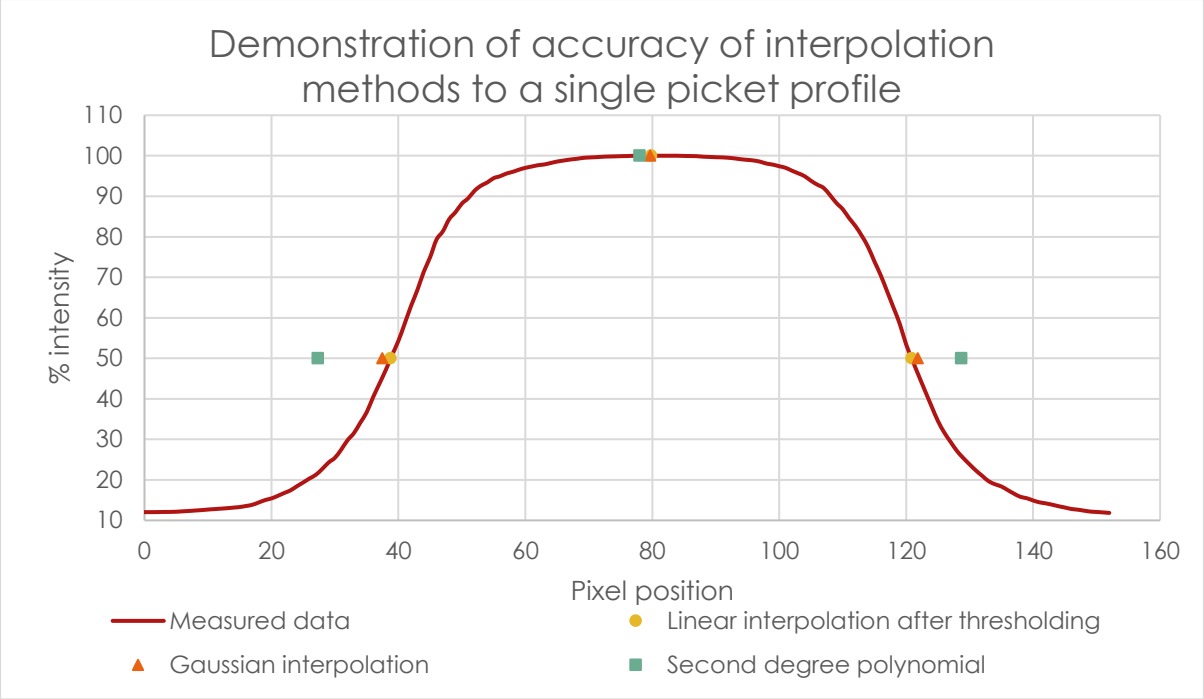

Figure 25: Graphic representation of results from interpolation methods in comparison to a single line profile of a single picket in a picket fence.

The linear interpolation with thresholding was by far the simplest technique as it only required changing the intensity level of all values and then finding the largest slope.

From the graph, it was observed that the Gaussian and polynomial interpolation methods over-estimate the width of the field and that the best fit to the actual data is the linear interpolation method after thresholding has been applied. The polynomial fit also did not estimate the centre correctly.

For the remainder of the study, the linear interpolation with thresholding technique was used.

Section 6: Elimination of errors not caused by MLCs

Accounting for collimator rotation:

Collimator angles of 0.1, 0.2, 0.3, 0.4 and 0.5 degrees were induced when imaging and the rotation of the pickets were measured for comparison.

Table 8 below shows the induced, measured and difference values for each image.

Stellenbosch University https://scholar.sun.ac.za

Table 8: Difference between measured and set collimator angles					
Collimator angle set	0.1	0.2	0.3	0.4	0.5
Collimator angle measured	0.0	0.1	0.2	0.3	0.4
Difference	0.1	0.1	0.1	0.1	0.1

From the measured data, it can be seen that the absolute collimator angle values measured differ from the set values by 0.1 degrees. The relative error from one collimator angle to the next is exactly equal to that set on the linac. It is possible that the EPID and the collimator are not aligned perfectly and that a small discrepancy of 0.1 degrees might exist as this is well below the tolerance of 0.5 degrees. Since this algorithm was simple and effective in estimating the collimator angle relative to the EPID, it was implemented in the solution to eliminate errors that are because of rotation of the collimator and not mispositioning of the MLC.

Width filtering of errors:

Errors were identified with widths of as small as 1 pixel. This shows that there is still some noise in the image that could be an effect of the processing being done or simply noise still present after smoothing.

Using this method of filtering errors through the width of an error, position errors too thin to have been created by a single MLC were dismissed.

This method proved useful in reducing errors not caused by MLC.

This method was chosen as techniques used previously employed Fourier transform fits through the leakage between the leaves, as discussed previously(58). Leakage between leaves for the system used here was not large enough to distinguish from the noise and the Fourier method could not be used to find leaf heights.

Stellenbosch University https://scholar.sun.ac.za

Phase 2: Implementation.

Section 7: Accuracy validation of software:

For the first part of this section, individual leaf width and position errors were introduced via the R&V system and the accuracy with which the software could measure it was evaluated.

Figure 26 below shows the measured versus set width errors for Halcyon, Millennium 120MLC, Agility MLC and Siemens 160MLC. The error bars indicate 1 pixel in each direction.

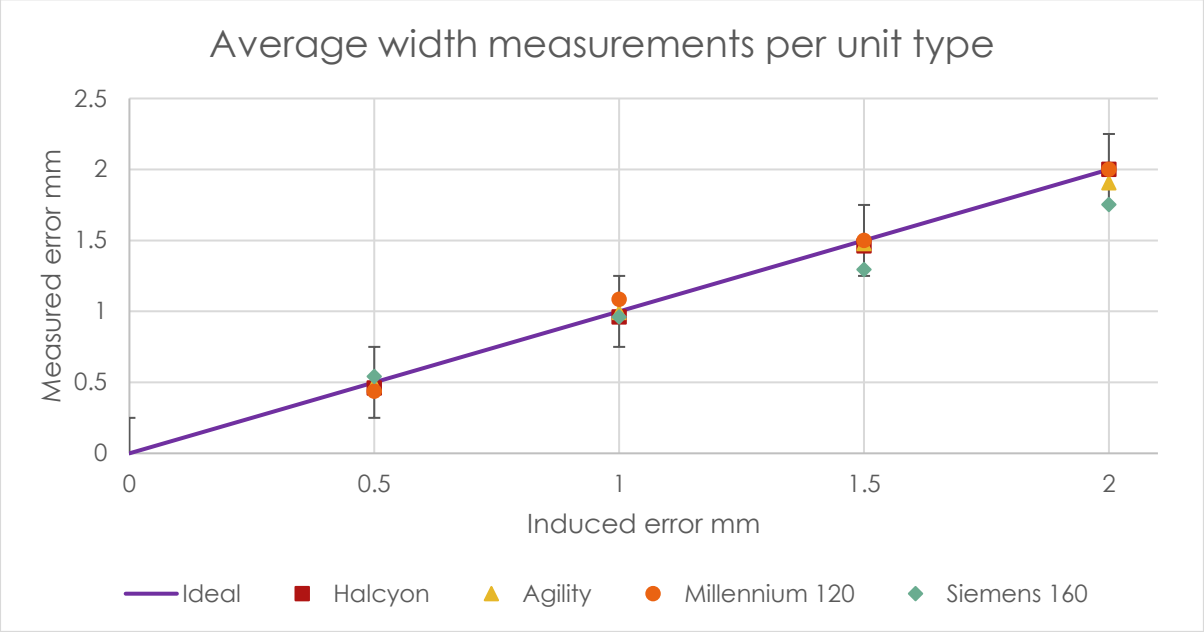

Figure 26: Graphic representation of the average width validation measurements.

Figure 27 below shows the measured versus set position errors for Halcyon, Millennium 120MLC, Agility MLC and Siemens 160MLC. The error bars indicate 1 pixel in each direction.

Stellenbosch University https://scholar.sun.ac.za

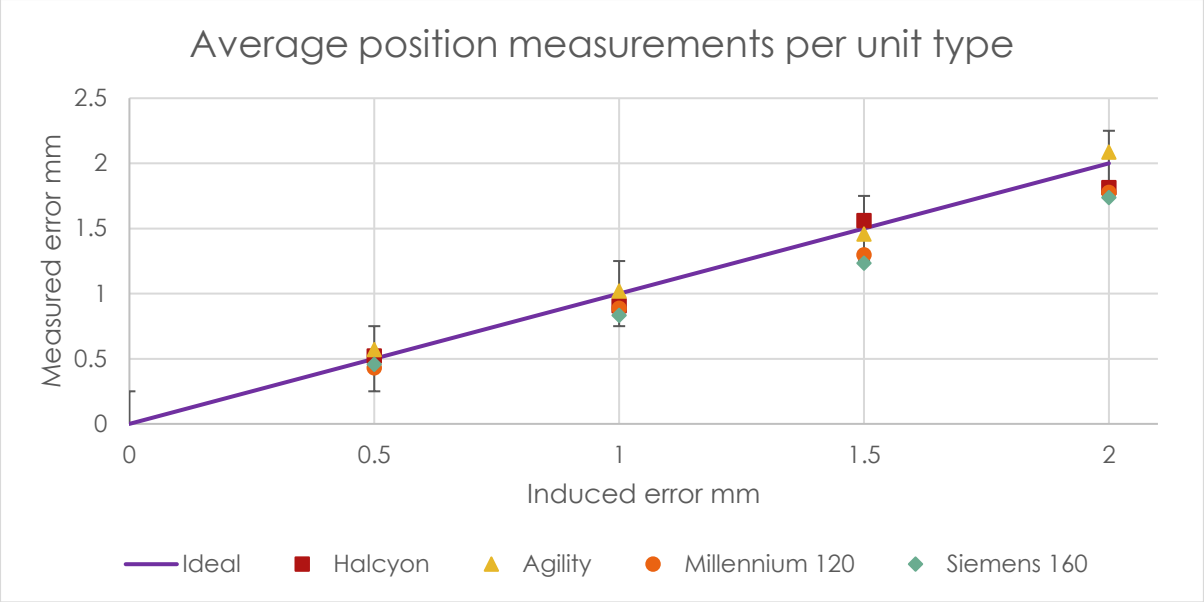

Figure 27: Graphic representation of the average position validation measurements.

In part 1 of this section, almost all relative errors induced on single MLCs could be measured with an accuracy of less than 1-pixel size. For induced width errors the absolute average errors per MLC type can be seen in figure 28 below.

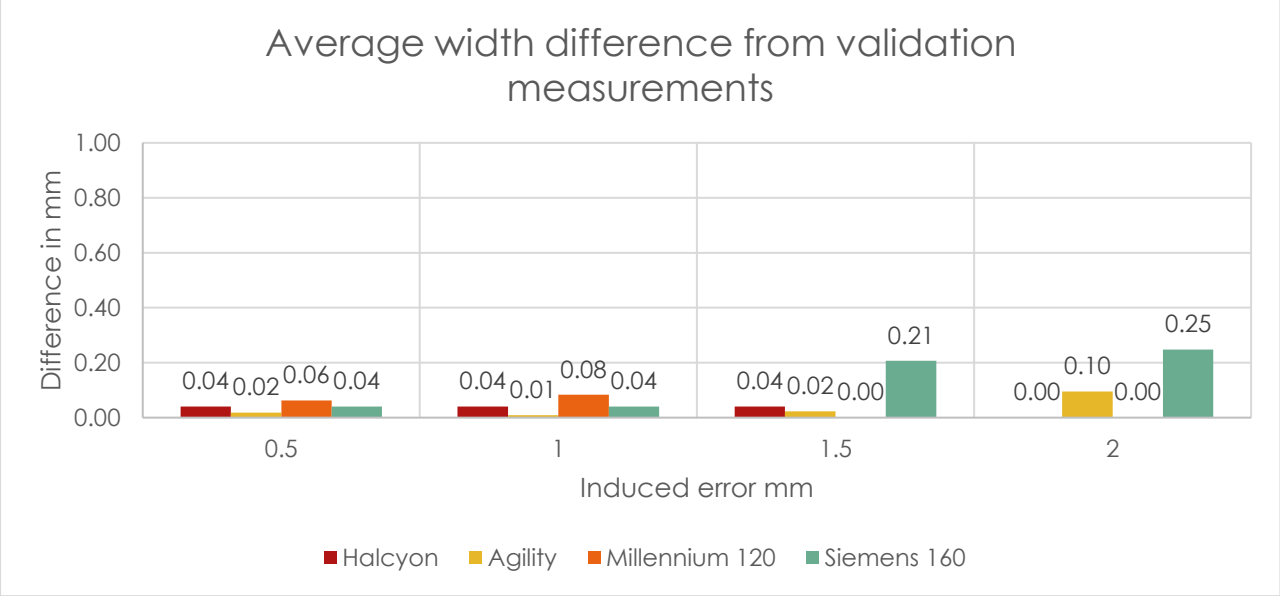

Figure 28: Graphic representation of the differences between measured and set width errors.

From this data, we can see that the software can very accurately measure errors of 1mm and 0.5mm in all MLC types. For the Siemens 160MLC, MLC differences larger than 1mm are less accurately defined, but still within 1-pixel size.

Stellenbosch University https://scholar.sun.ac.za

For induced position errors the absolute average errors per MLC type can be seen in figure 29 below.

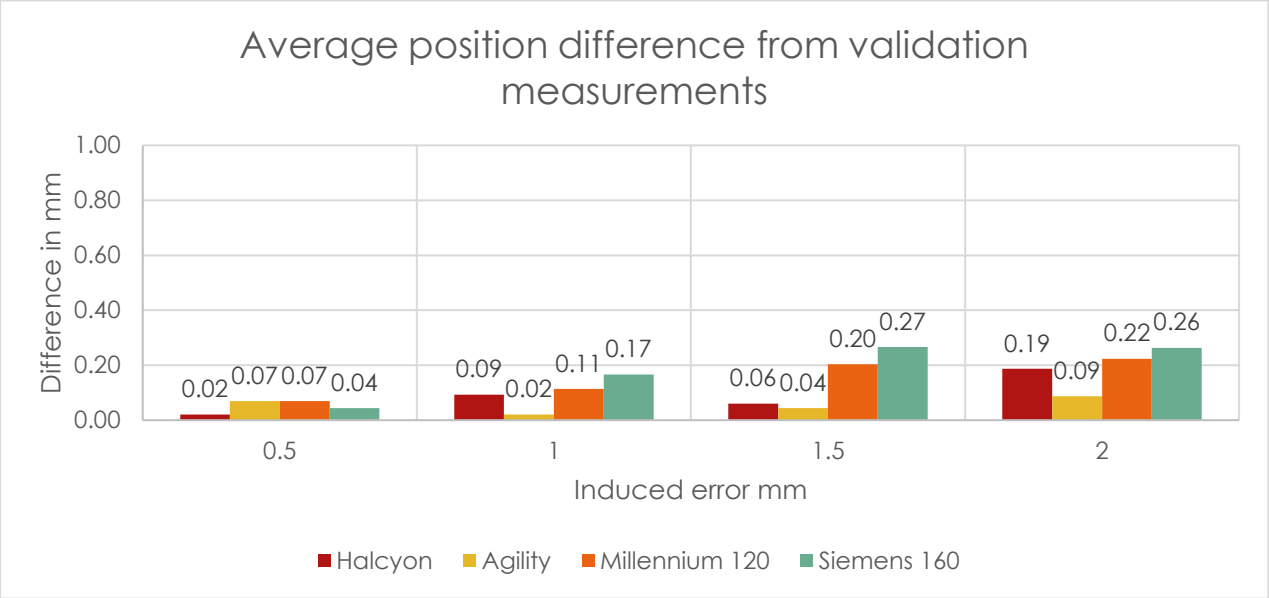

Figure 29: Graphic representation of the differences between measured and set position errors.

From this data, it can be seen that the software can very accurately measure errors of 0.5mm in all MLC types. For most MLC types it seems that the accuracy of the software diminishes as the error becomes larger toward 2mm. The effect is however not equal in size for all MLC types. For the Siemens 160 MLC, the position errors measured were only slightly larger than 1 pixel over the expected value when the induced error was larger than 1mm.

For the second part of this section, the in-house software was compared to the IBA myQA picket fence module over 3 Elekta Agility picket fences from 3 independent units. Figure 30 below shows the differences between the output of the 2 software packages for the same input.

Stellenbosch University https://scholar.sun.ac.za

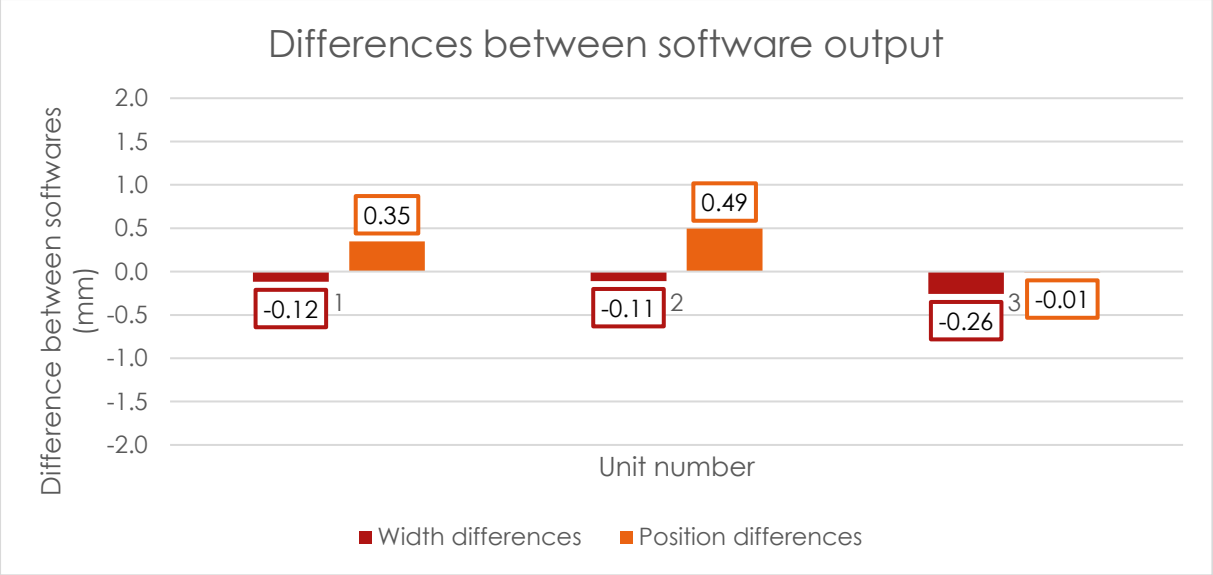

Figure 30: Graphic representation of differences measured between IBA picket fence software and in-house software on 3 linacs.

When the software was compared to the IBA myQA picket fence module in the second part of this section, the in-house software on average measured 0.28mm smaller position errors while measuring 0.16mm larger width errors than the IBA software. These errors are in the order of 1-pixel size (0.25mm) and are most likely because of the differences in the picket finding and error characterisation algorithms.

For the last section, a picket fence image was taken at gantry angles 0º, 90º and 270º while logging the relative MLC positions to what it was calibrated to. The differences in average leaf position were measured from the picket fence images and log files and compared. In this way, the differences in MLC positions due to the effects due to gravity was assessed and the log data and picket fence data could be compared directly.

Table 9 below shows the difference in picket position and width errors between the picket fence analysed from the EPID image and the Elekta iCom logs from the same session on an Elekta Versa HD linac with an Agility MLC.

Stellenbosch University https://scholar.sun.ac.za

Table 9: Differences in picket position and width errors between the picket fence analysed from an EPID image and Elekta iCom log data.				
Gantry angle	90º		270º	
Off-axis distance (cm)	Width (mm)	Position (mm)	Width (mm)	Position (mm)
-7	-0.01	0.30	0.16	-0.11
-3	-0.02	0.22	0.12	0.15
1	0.02	-0.12	0.21	0.23
5	0.18	0.09	0.20	-0.11
9	-0.28	0.04	-0.16	0.30
Average	**-0.02**	**0.11**	**0.11**	**0.09**

From table 9, the average MLC error found with the EPID and in-house software method agrees with Elekta iCom logs within 0.11 mm. the maximum difference observed between the two methods was 0.3 mm. This is congruent with the results from Sakaria et al. Their findings show maximum and average differences for Elekta log files measured from agility MLC to be 0.3mm and 0.12mm respectively(52).

Table 10 below shows the difference in picket position and width errors between the picket fence analysed from the EPID image and the Varian trajectory logs from the same session on Varian vital beam linac with a Millennium 120 MLC.

Stellenbosch University https://scholar.sun.ac.za

Table 10: Differences in picket position and width errors between the picket fence analysed from an EPID image and Varian trajectory log data.				
	90º		270º	
Off-axis distance (cm)	Width (mm)	Position (mm)	Width (mm)	Position (mm)
-7	0.00	0.00	0.06	0.18
-3	0.00	-0.01	0.01	0.11
1	0.02	-0.17	0.06	-0.06
5	0.03	0.25	0.09	-0.10
9	0.00	0.08	0.16	0.04
Average	**0.01**	**0.03**	**0.08**	**0.03**

From table 10, the average MLC error found with the EPID and in-house software method agrees with Varian trajectory logs within 0.08 mm. The maximum difference observed between the two methods was 0.25 mm.

It should at this point be noted that the Varian trajectory log file maximum error recorded differed greatly from the Elekta Icom error log maximum error. This might be due to the difference in the meaning of the MLC position in the two log files.

Table 11 below shows the maximum MLC error recorded per off-axis distance between the Varian and Elekta logs.

Stellenbosch University https://scholar.sun.ac.za

Table 11: Maximum error recorded per off-axis distance for Elekta and Varian logs				
	Elekta iCom logs		Varian trajectory logs	
Off-axis distance (cm)	Width (mm)	Position (mm)	Width (mm)	Position (mm)
-7	0.01	0.11	0.01	0.01
-3	0.05	0.09	0.01	0.00
1	0.06	0.09	0.00	0.00
5	0.07	0.13	0.00	0.01
9	0.16	0.14	0.00	0.01
Average	**0.07**	**0.11**	**0.00**	**0.01**

For Varian trajectory log files, the EPID picket fence analysed data only agrees well with the log since the errors recorded are small. It is uncertain if the recording of the MLC position in the log trajectory log file is as accurate as stated or if the EPID resolution is just not sufficient to measure the true MLC error.

This discrepancy has been observed in a previous study by Eckhause,T et al in 2015. Their study found larger variation in MLC positional error under the effects of gravity that the log files report(59).

Since the modern EPIDs are the digital detectors with the best resolution available on the market, there is no way to validate the absolute error recorded by the Varian trajectory log files by measurement. All differences and errors int the order of 1 pixel value are non-significant due to the uncertainty associated with the limited resolution of the EPID.

From comparison with log files, this data agrees with published data that Varian log files underestimate the measured MLC positional error under the influence of gravity, but that the optical tracking system used by Elekta in the Agility MLC design, reports MLC errors that are similar in accuracy to measured data(52)(59).

Section 8: National survey of MLC data using software looking at 3DCRT and IMRT capable LINACS:

A survey was done of a group of participating LINACs in public and private sectors of radiotherapy in South Africa, by analysing the routine QA picket fence images with the

Stellenbosch University https://scholar.sun.ac.za

created software. Instructions were given on how the picket fence was to be constructed, to maintain a standardized test among all linacs (attached as Appendix A). The maximum width and position errors were recorded for each image.

For all MLC designs, the average error, maximum error and standard deviation for width and position errors were measured across a 20 cm field of view. The average of all the units with similar MLC designs was determined to give a visual representation of the trends of MLC errors for units of the same make and model. Errors in this section are reported as the difference between the measured and expected positions and widths.

Figure 31 below shows the average position error, maximum position errors and position standard deviation (error bars) for all 6 Siemens 160 MLC linacs as a function of off-axis distance.

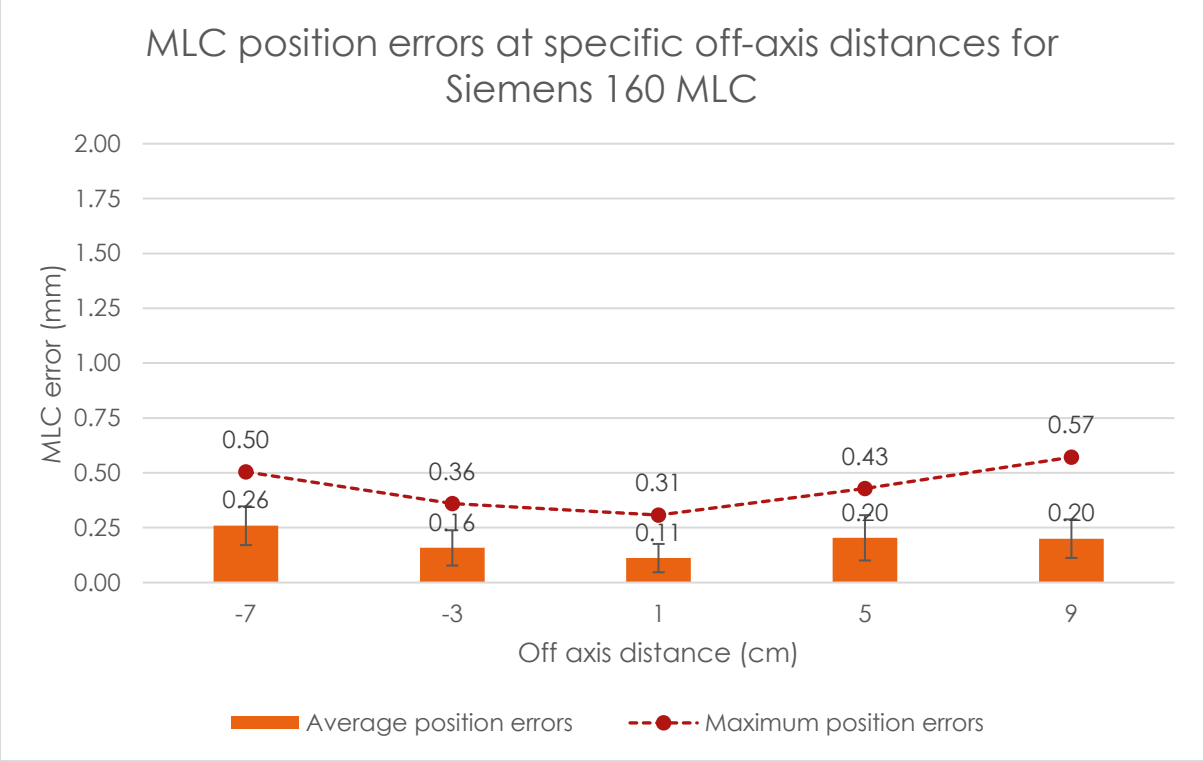

Figure 31: Graphic representation of the average MLC position errors at specific off-axis distances using Siemens 160 MLC.

For Siemens 160 MLC, the smallest position error seems to be closest to the central axis. All measured errors agreed well with expected values and were within regulatory tolerances of 2mm.

Stellenbosch University https://scholar.sun.ac.za

Similarly, figure 32 below shows the average width error, maximum width errors and width standard deviation (error bars) for all 6 Siemens 160 MLC linacs as a function of off-axis distance.

Figure 32: Graphic representation of the average MLC width errors at specific off-axis distances using Siemens 160 MLC.

For Siemens 160 MLC, the width error seems to be fairly constant across the imaged field of view. All measured errors agreed well with expected values and were within regulatory tolerances of 2mm.

Figure 33 below shows the average position error, maximum position errors and position standard deviation (error bars) for the single Varian Millennium 120 MLC linac as a function of off-axis distance.

Stellenbosch University https://scholar.sun.ac.za

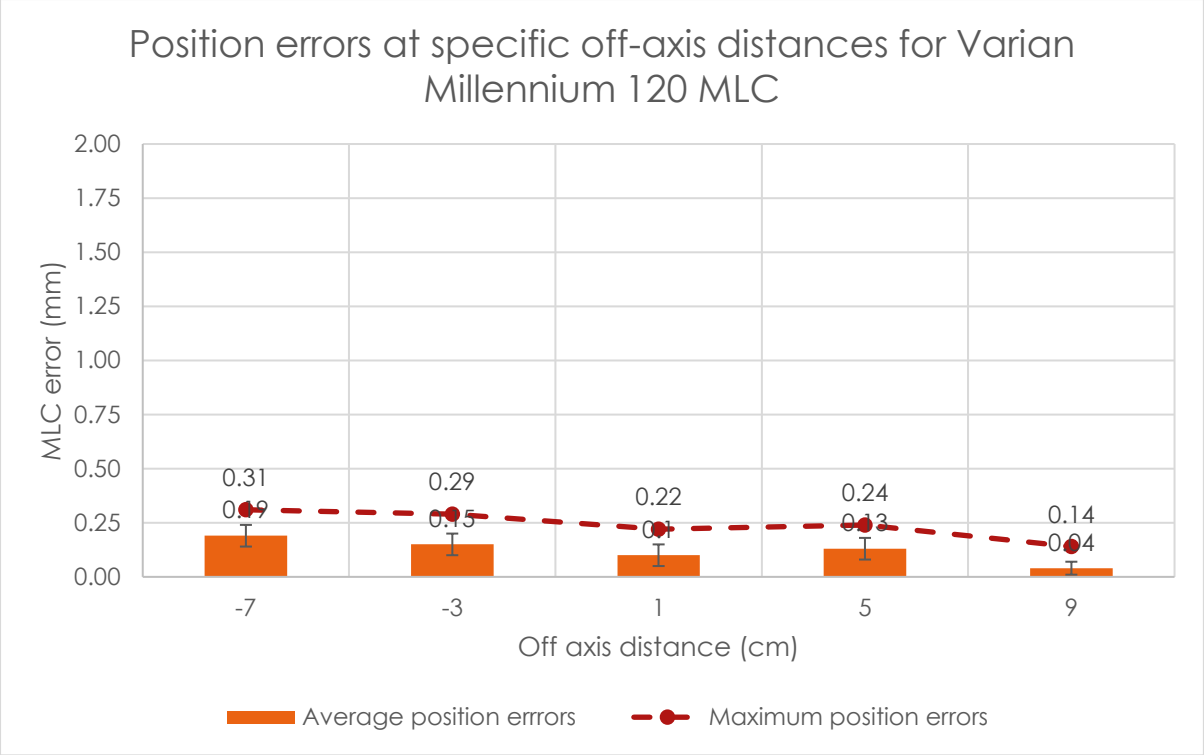

Figure 33: Graphic representation of the average MLC position errors at specific off-axis distances using Varian Millennium MLC.

For Varian millennium 120 MLC, the position error seems to be fairly constant across the imaged field of view. All measured errors agreed well with expected values and were within regulatory tolerances of 2mm.

Similarly, figure 34 below shows the average width error, maximum width errors and width standard deviation (error bars) of the single Varian Millennium 120 MLC linac as a function of off-axis distance.

Stellenbosch University https://scholar.sun.ac.za

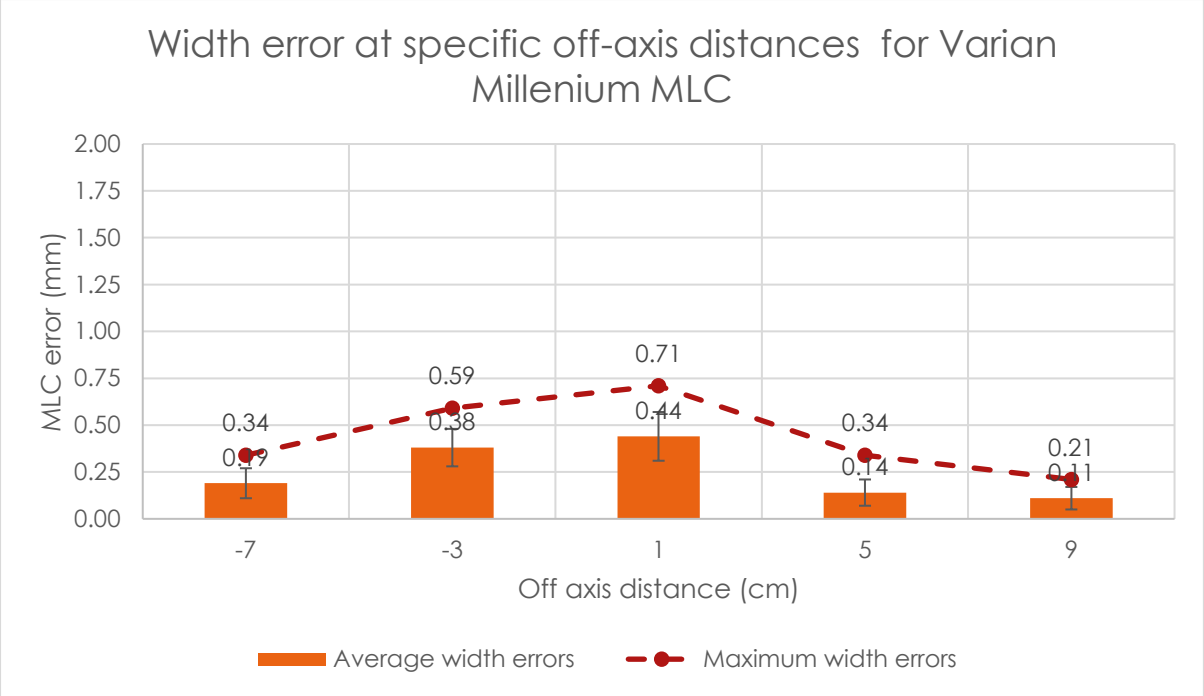

Figure 34: Graphic representation of the average MLC width errors at specific off-axis distances using Varian Millennium MLC.

For Varian millennium 120 MLC, the expected width differs most from the measured width on the central axis. All measured errors agreed well with expected values and were within regulatory tolerances of 2mm.

Figure 35 below shows the average position error, maximum position errors and position standard deviation (error bars) for the single Varian HDMLC linac as a function of off-axis distance.

Stellenbosch University https://scholar.sun.ac.za

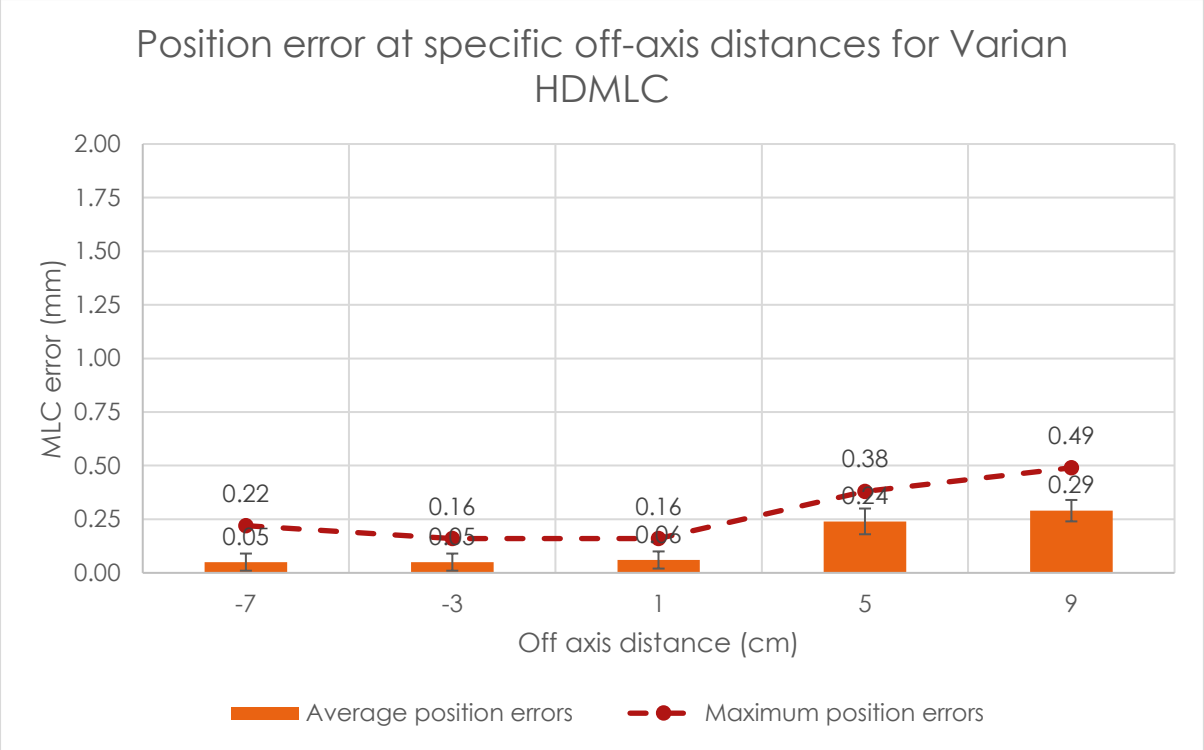

Figure 35: Graphic representation of the average MLC position errors at specific off-axis distances using Varian HDMLC.

For Varian HDMLC, the position error seems to be smaller across the left of the imaged field of view than on the right of the imaged field of view. All measured errors agreed well with expected values and were within regulatory tolerances of 2mm.

Similarly, figure 36 below shows the average width error, maximum width errors and width standard deviation (error bars) of the single Varian HDMLC linac as a function of off-axis distance.

Stellenbosch University https://scholar.sun.ac.za

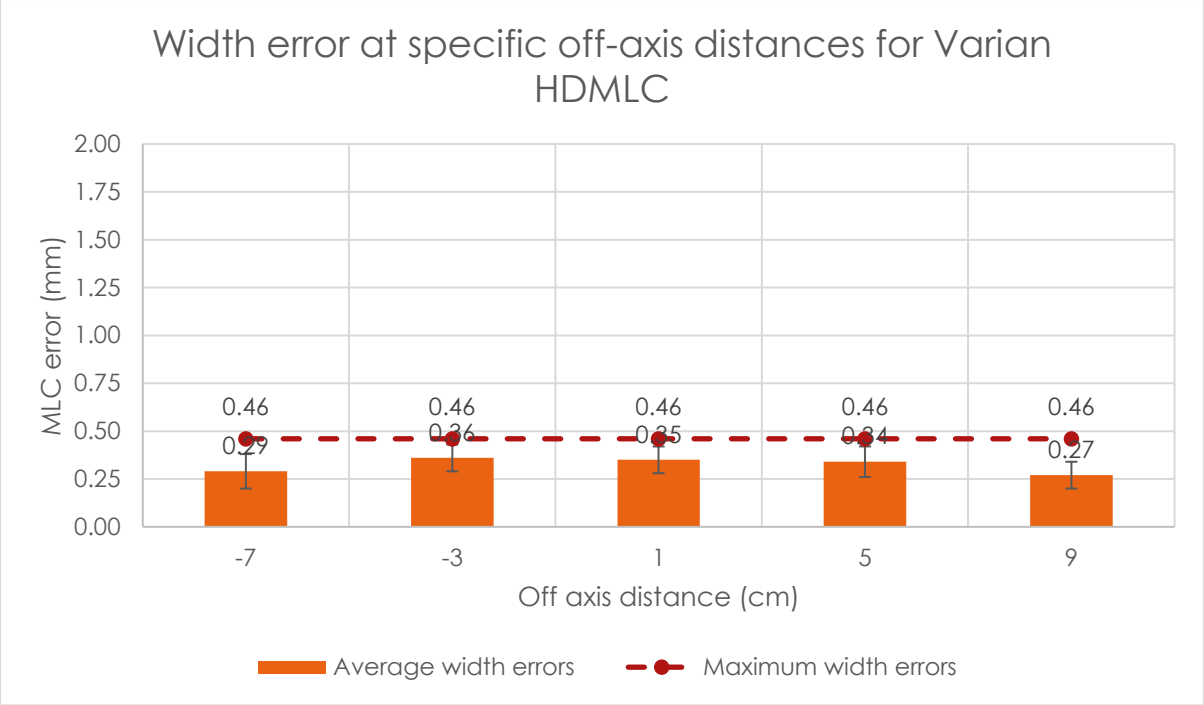

Figure 36: Graphic representation of the average MLC width errors at specific off-axis distances using Varian HDMLC.

For Varian HDMLC, the width error seems to be fairly constant across the imaged field of view. All measured errors agreed well with expected values and were within regulatory tolerances of 2mm.

Figure 37 below shows the average position error, maximum position errors and position standard deviation (error bars) for the single Varian Halcyon linac as a function of off-axis distance.

Stellenbosch University https://scholar.sun.ac.za

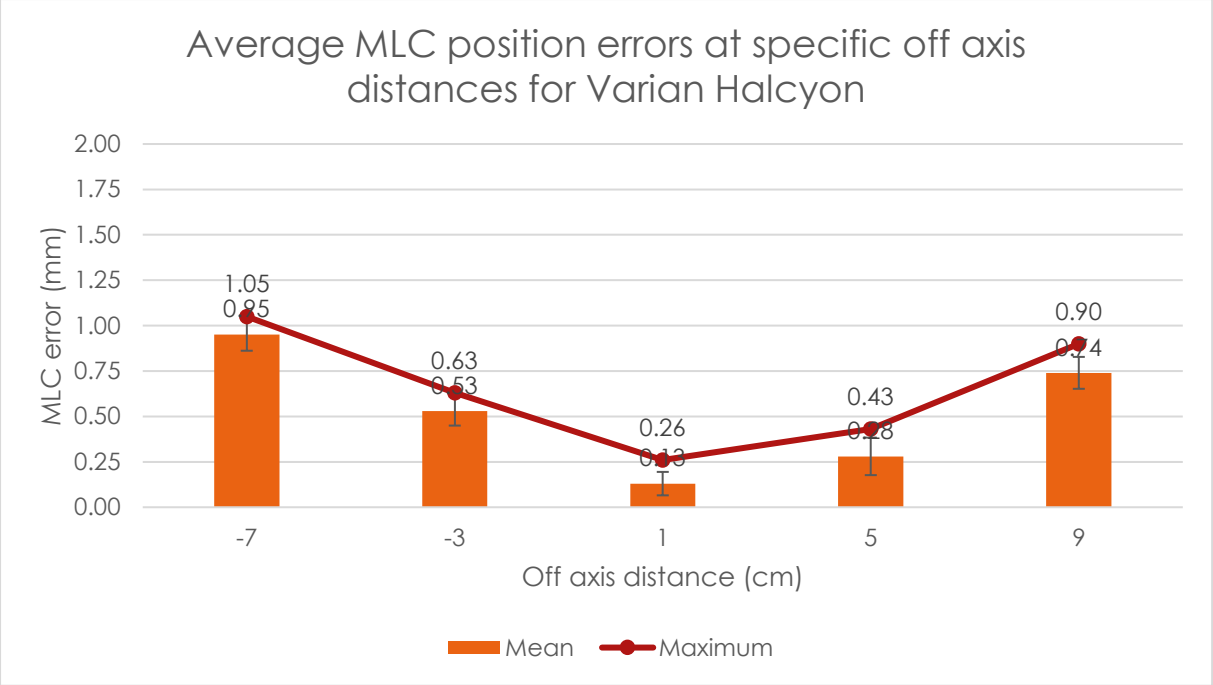

Figure 37: Graphic representation of the average MLC position errors at specific off-axis distances using Varian Halcyon MLC.

For Varian Halcyon MLC, the position error seems to be smallest at 5 cm to the right of the central axis and differs quite a lot from the expected position in the off-axis regions. All measured errors agreed well with expected values and were within regulatory tolerances of 2mm.

Similarly, figure 38 below shows the average width error, maximum width errors and width standard deviation (error bars) of the single Varian Halcyon linac as a function of off-axis distance.

Stellenbosch University https://scholar.sun.ac.za

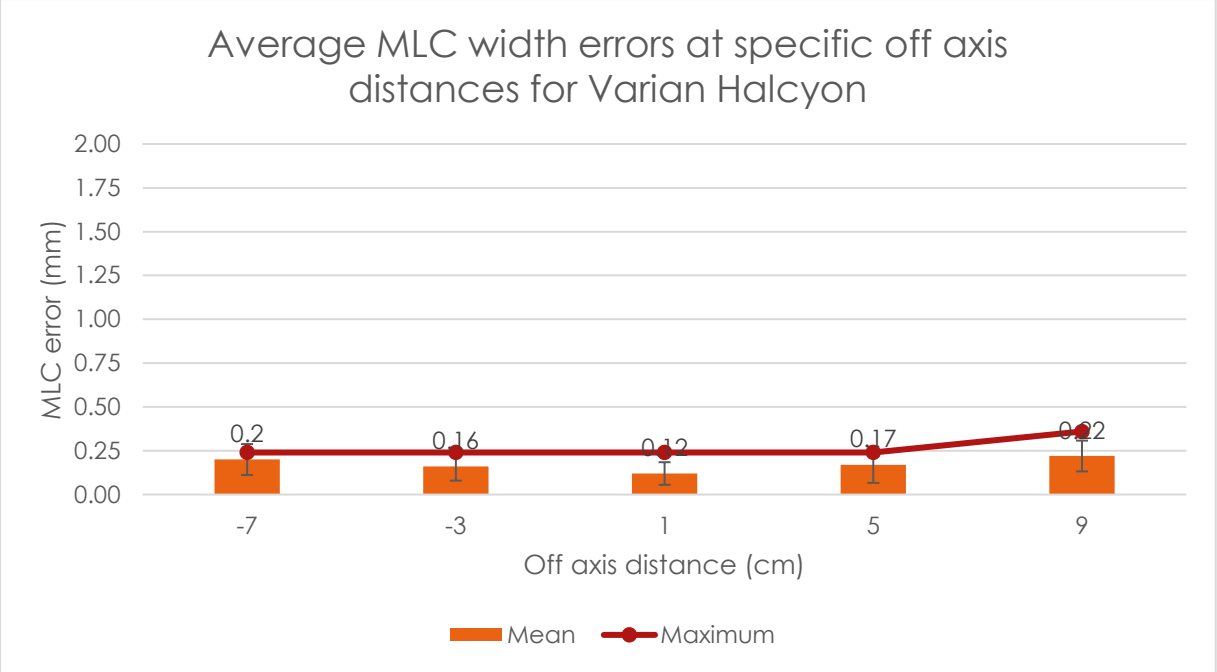

Figure 38: Graphic representation of the average MLC width errors at specific off-axis distances using Varian Halcyon MLC.

For Varian Halcyon MLC, the width error seems to be fairly constant across the imaged field of view. All measured errors agreed well with expected values and were within regulatory tolerances of 2mm.

Figure 39 below shows the average position error, maximum position errors and position standard deviation (error bars) for the 12 Elekta Agility linacs as a function of off-axis distance.

Stellenbosch University https://scholar.sun.ac.za

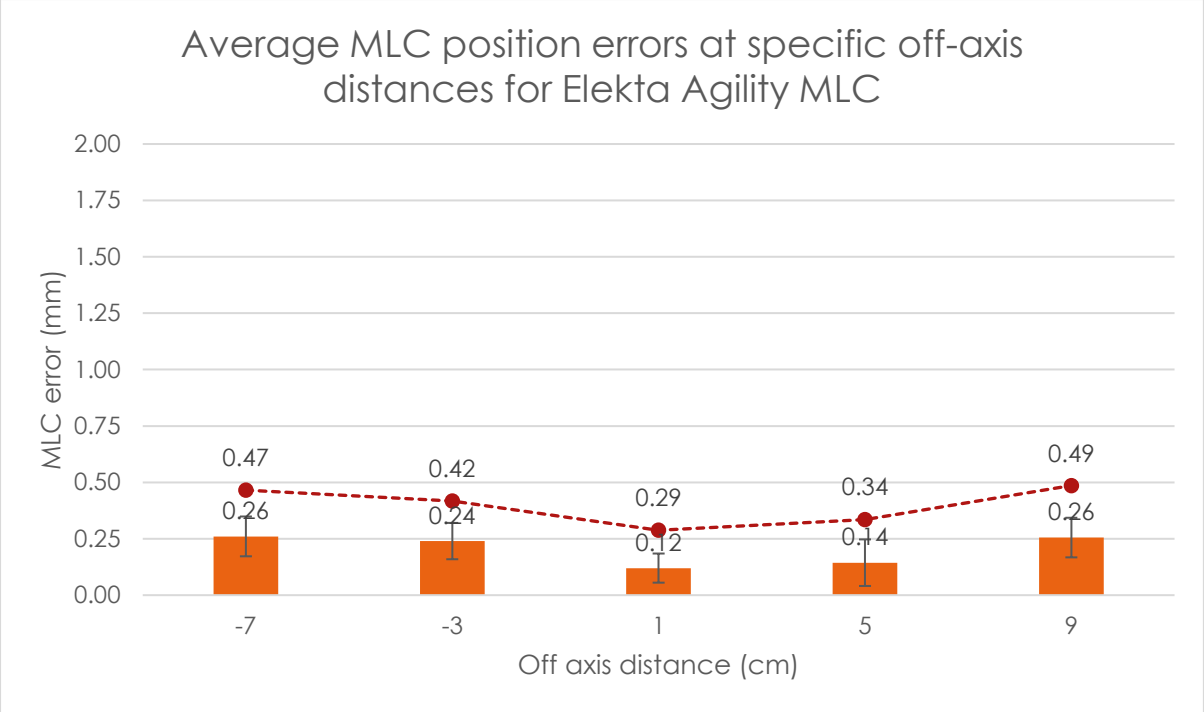

Figure 39: Graphic representation of the average MLC position errors at specific off-axis distances using Elekta agility MLC.

For Elekta Agility MLC, the position error seems the smallest on the central axis. All measured errors agreed well with expected values and were within regulatory tolerances of 2mm.

Similarly, figure 40 below shows the average width error, maximum width errors and width standard deviation (error bars) of the 12 Elekta Agility linacs as a function of off-axis distance.

Stellenbosch University https://scholar.sun.ac.za

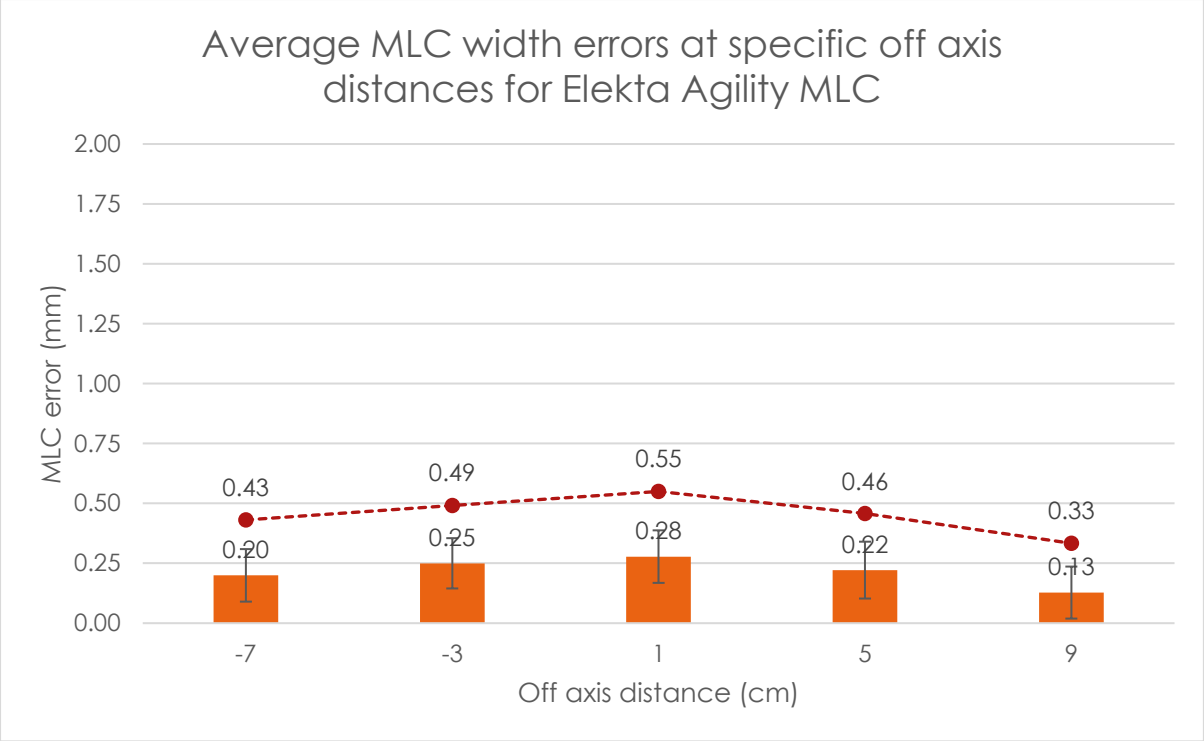

Figure 40: Graphic representation of the average MLC width errors at specific off-axis distances using Elekta agility MLC.

For Elekta Agility MLC, the width error seems the largest on the central axis. All measured errors agreed well with expected values and were within regulatory tolerances of 2mm.

Although most measured positions were quite close to the expected positions, the Varian Halcyon MLC differed significantly more in picket position compared to the other MLC types.

The configuration of this MLC is quite complex and differ significantly from the other MLC types as well. Additionally, this machine only has a 6FFF photon energy leading to a lower signal for off-axis pickets compared to those on the central axis.

This was additionally investigated as off-axis pickets might have a skewed maximum for flattening filter-free beams. A picket fence image was taken with an Elekta Versa HD accelerator of a 6MV and 6FFF beam right after one another and the results were compared. The average position difference of each of the pickets was in the order of 1-pixel size with a maximum difference of 0.3mm. A superimposed line profile of a single line on a single picket can be visualised below in figure 4.:

Stellenbosch University https://scholar.sun.ac.za

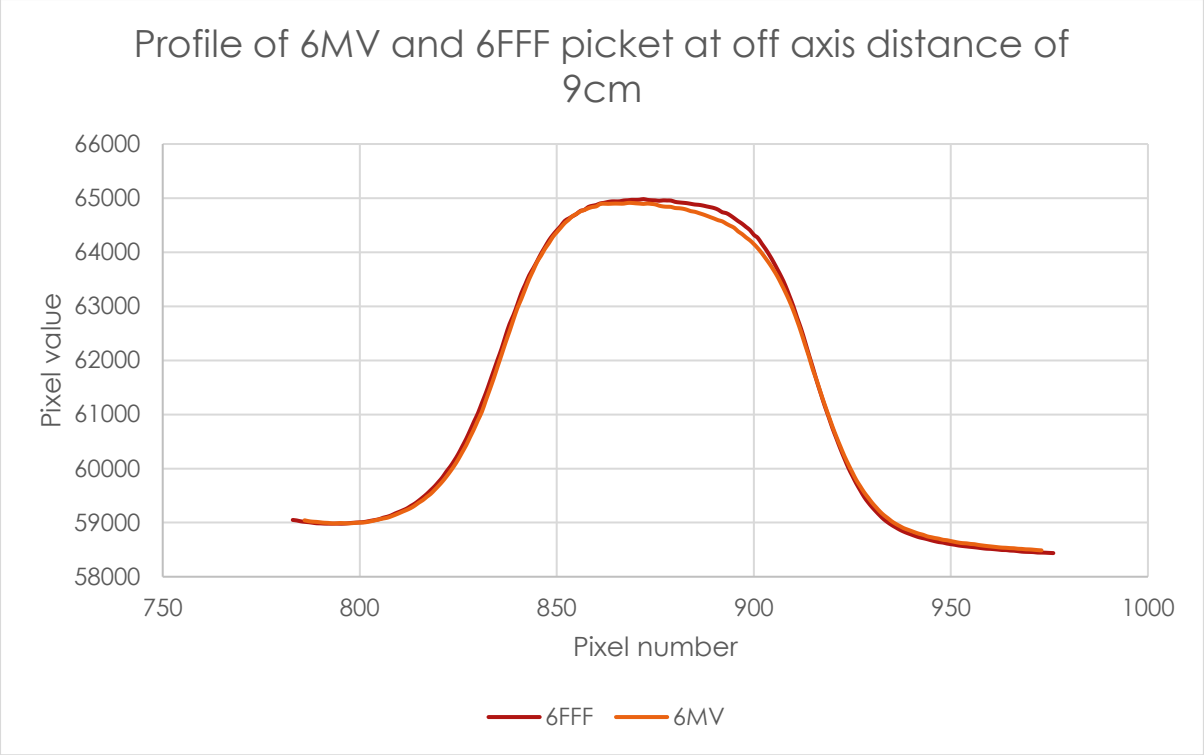

Figure 41: Graphic representation of a single-pixel profile of a 6MV and 6FFF picket taken at an off-axis distance of 9cm.

The compiled software deals with the variation in intensity adequately by finding the maximum and minimum per picket and not for the total image. Additionally, the picket centre is taken to be the midpoint between the 50% intensity values and not a physical point on the profile. If the profile is therefore skewed, this does not alter the found position of the centre of the picket by the software.

This might not be clinically significant if the TPS model for this unit can account for this variation for clinical cases.

Other than for these position errors on the Varian Halcyon MLC, the variation in MLC position and width accuracy across the useful field of view or any apparent trends that might be visual is not in a significant order compared to the inherent uncertainty due to limited resolution of the EPID. The differences or errors are in the order or smaller than 1 pixel.

Stellenbosch University https://scholar.sun.ac.za

Section 9: National survey of MLC data used for VMAT:

A survey was done of a group of participating LINACs in public and private sectors of radiotherapy in South Africa, by analysing the routine QA picket fence images delivered at several gantry angles and during an arc with the created software. Instructions were given on how the Picket fence was to be constructed, to maintain a standardized test among all LINACs. The maximum width and position errors were recorded for each image.

Figure 42 below shows the average difference in width error due to gravity at gantry angles 90º and 270º at various off-axis distances for a Varian Millennium MLC.

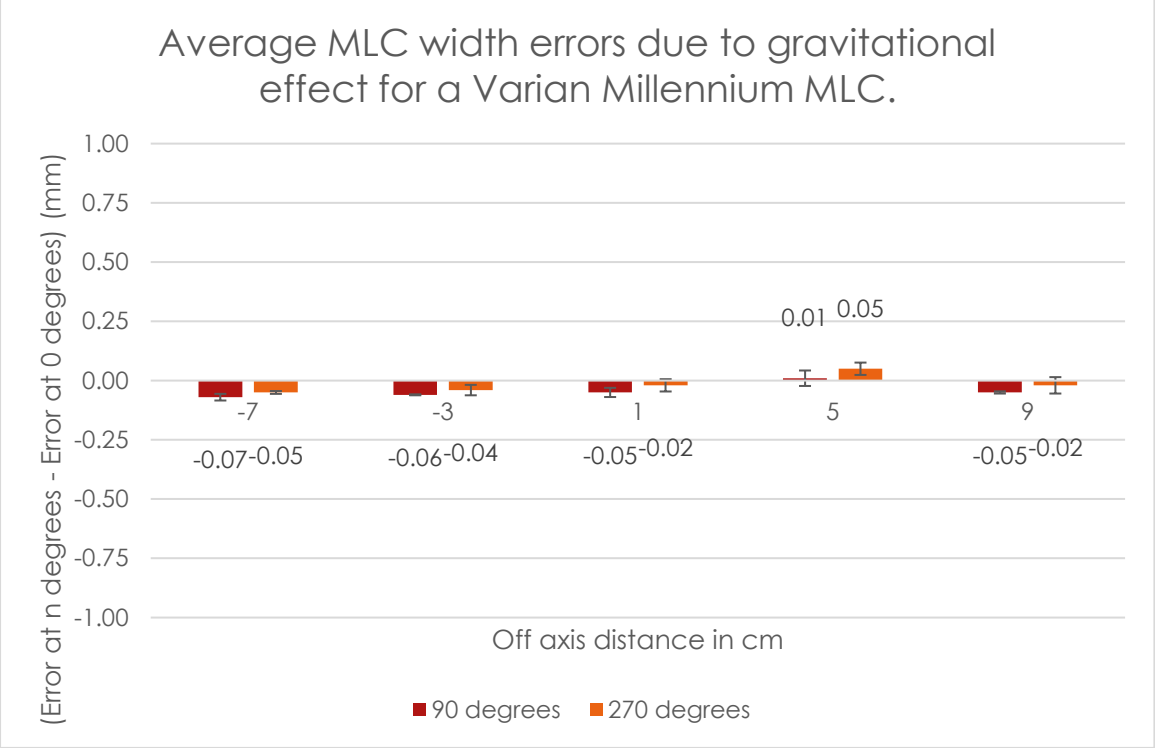

Figure 42: Graphic representation of the average MLC width errors at specific off-axis distances due to the effects of gravity for Varian Millennium MLC.

Figure 43 below shows the average difference in position error due to gravity at gantry angles 90º and 270º at various off-axis distances for a Varian Millennium MLC.

Stellenbosch University https://scholar.sun.ac.za

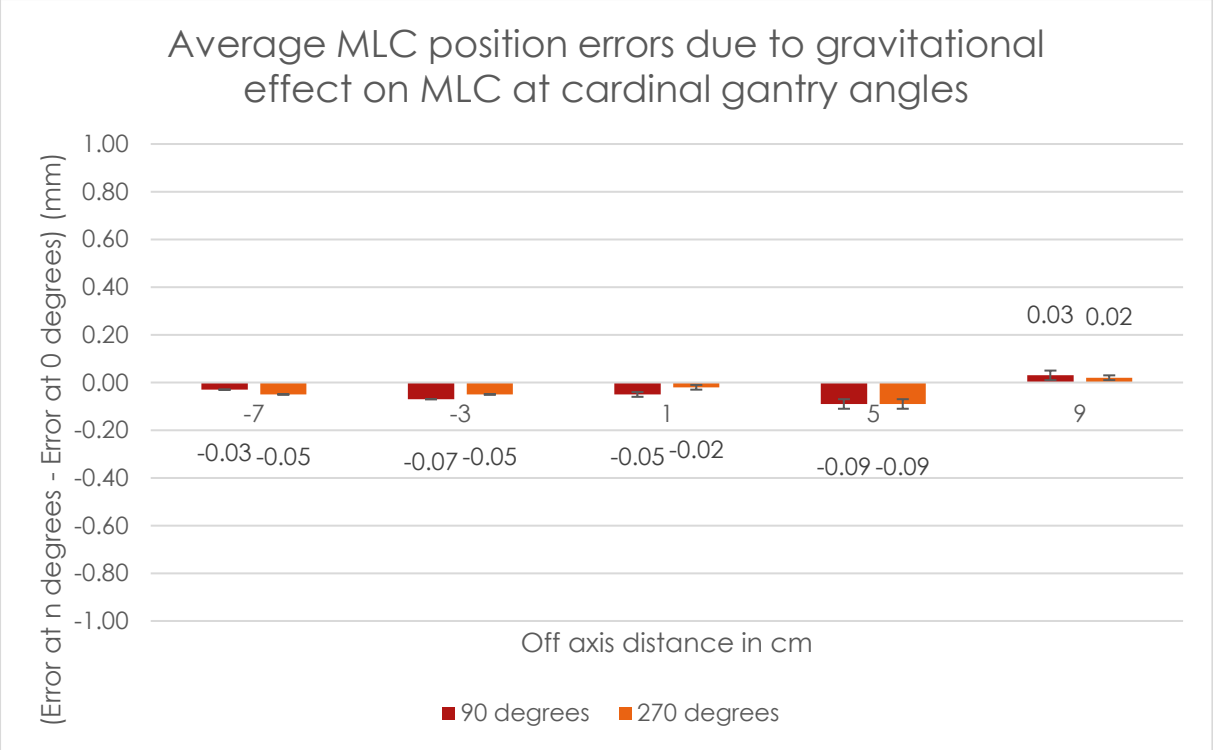

Figure 43: Graphic representation of the average MLC position errors at specific off-axis distances due to the effects of gravity for Varian Millennium MLC.

From the data presented, there seems to be a small gravitation effect on the Varian Millennium MLCs at gantry angles 90º and 270º at a maximum of 0.25 mm.

Figure 44 below shows the average difference in width error due to gravity at gantry angles 90º and 270º at various off-axis distances for a Varian HDMLC.

Stellenbosch University https://scholar.sun.ac.za

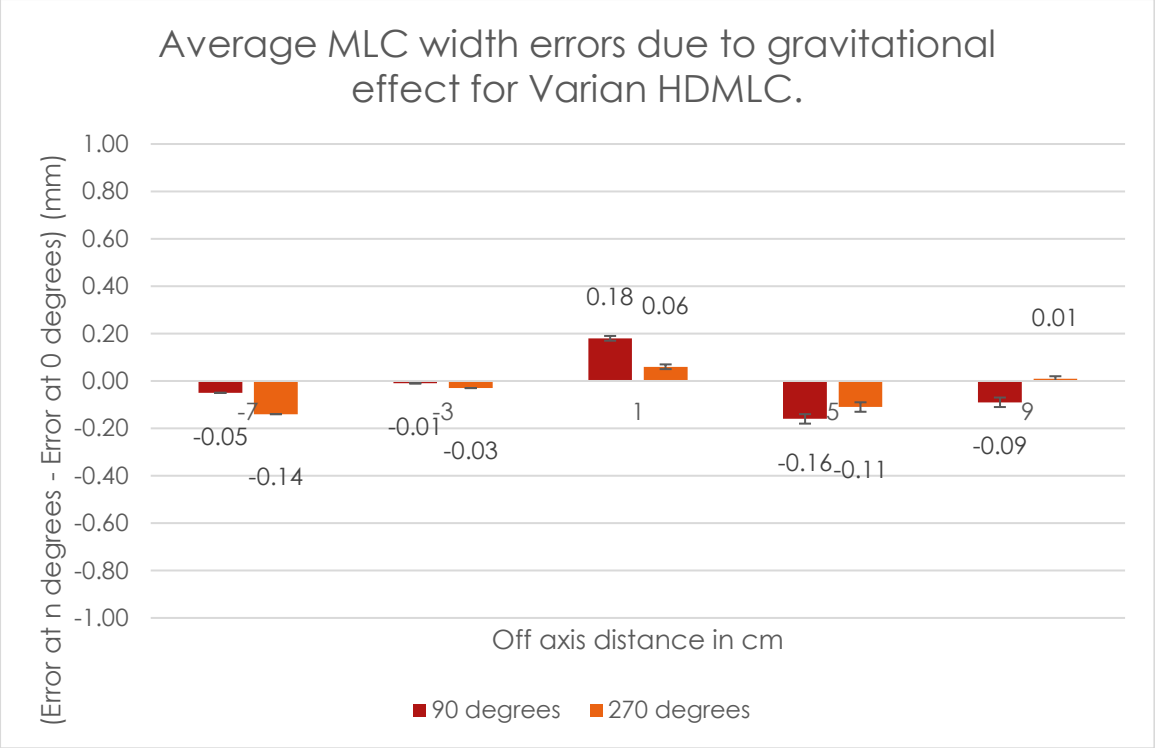

Figure 44: Graphic representation of the average MLC width errors at specific off-axis distances due to the effects of gravity for Varian HDMLC.

Figure 45 below shows the average difference in position error due to gravity at gantry angles 90º and 270º at various off-axis distances for a Varian HDMLC.

Stellenbosch University https://scholar.sun.ac.za

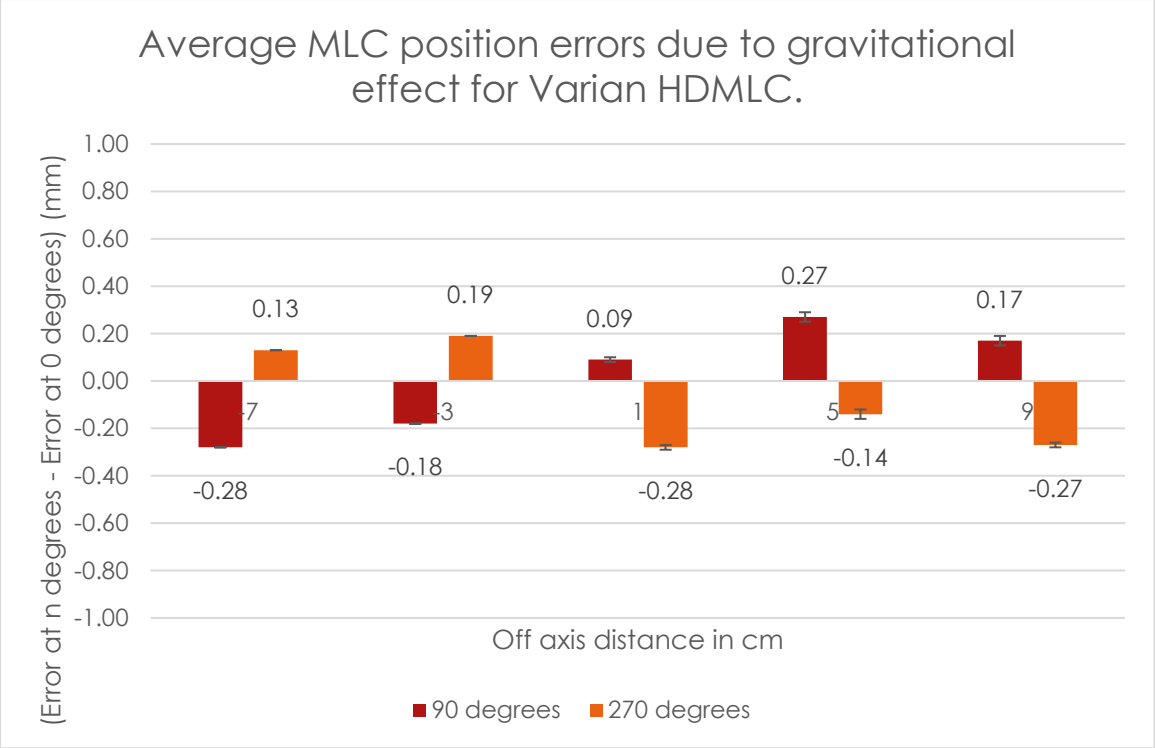

Figure 45: Graphic representation of the average MLC position errors at specific off-axis distances due to the effects of gravity for Varian HDMLC.

From the data presented, the Varian HDMLC seems to correct for the gravitational effect on the MLCs similarly to the Varian Millennium MLC with a maximum of 0.28 mm.

The HDMLC accuracy results are congruent with the work of Sharma, et al, who concluded that MLC accuracy on the isocentre plain was within 0.03cm for this MLC type over all gantry and collimator positions measured(33).

Figure 46 below shows the average difference in width error due to gravity at gantry angles 90º and 270º at various off-axis distances for an Elekta Agility MLC.

Stellenbosch University https://scholar.sun.ac.za

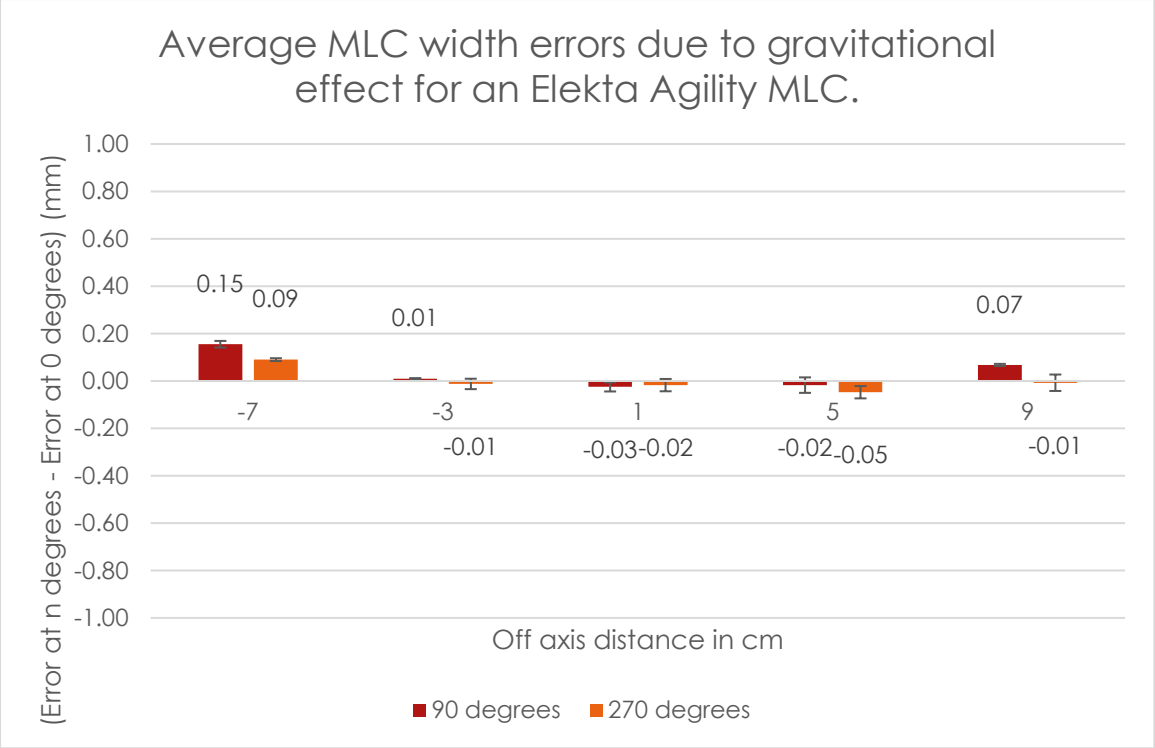

Figure 46: Graphic representation of the average MLC width errors at specific off-axis distances due to the effects of gravity for Elekta agility MLC.

Figure 47 below shows the average difference in position error due to gravity at gantry angles 90º and 270º at various off-axis distances for an Elekta Agility MLC.

Stellenbosch University https://scholar.sun.ac.za

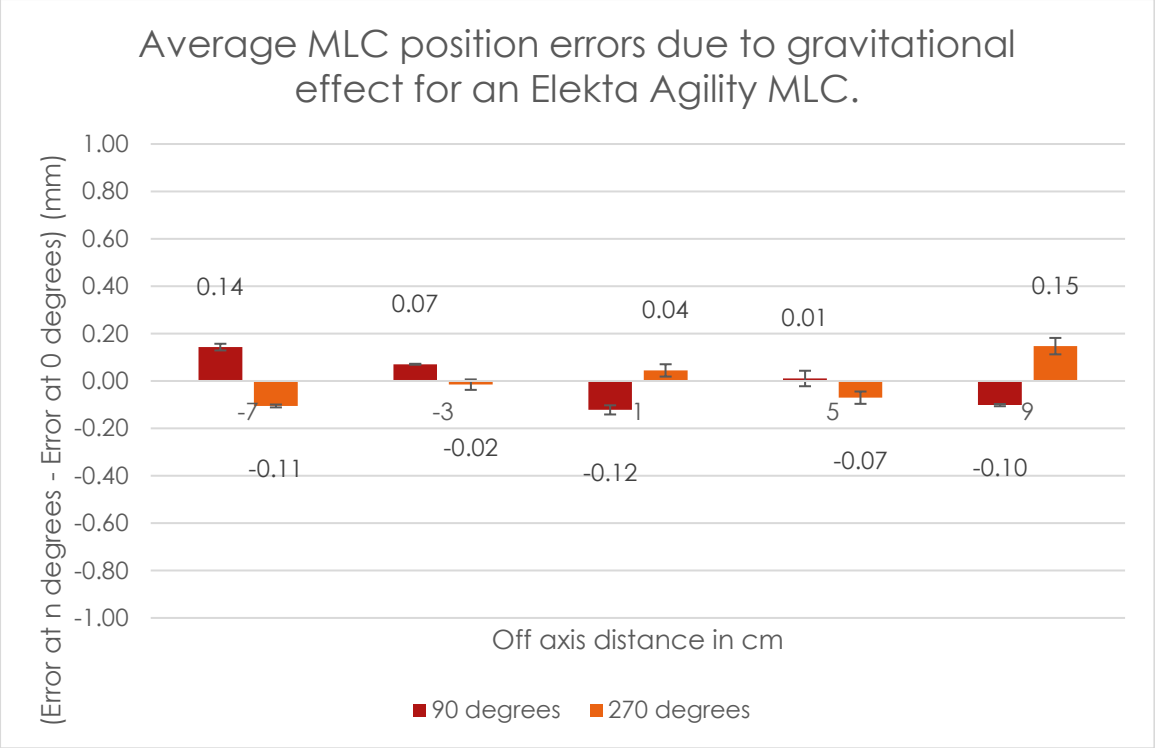

Figure 47: Graphic representation of the average MLC position errors at specific off-axis distances due to the effects of gravity for Elekta agility MLC.

The Elekta Agility MLCs seem to be slightly less influenced by gravity with a max difference of 0.15 mm when the picket fence is at zero gantry angle is compared to the picket fence at gantry angle 90º and 270º degrees. This might be due to its ability to better visualise and correct the actual leaf position using optical tracking.

Errors of size larger than 1 pixel size could only be found on the images acquired on with the Varian HDMLC. Any errors smaller than 1 pixel has too much uncertainty to associate any significance when comparing it to any other value smaller than 1 pixel.

Picket fence images from arc deliveries were only analysed in "relative" mode. This simply means that the distance from one picket to the next was not considered, and only if MLCs in a single picket were performing the same. This is because as the gantry arcs, the EPID sags additionally to the MLC. The errors from one picket to the next is therefore dependent on EPID sag, however, the errors on the MLCs from imaging the same picket experienced the same EPID sag. This was done to reduce the complexity of the software, its requirements and any additional calibrations required while maintaining the accuracy of what is known.

Stellenbosch University https://scholar.sun.ac.za

Figure 48 below shows an example of an arc PF taken on an Elekta Versa HD linac. The change in start and end positions of the pickets from top to bottom in the image indicates the variation in results of the MLC positions due to EPID sag that can be noticed by reference to the yellow line.

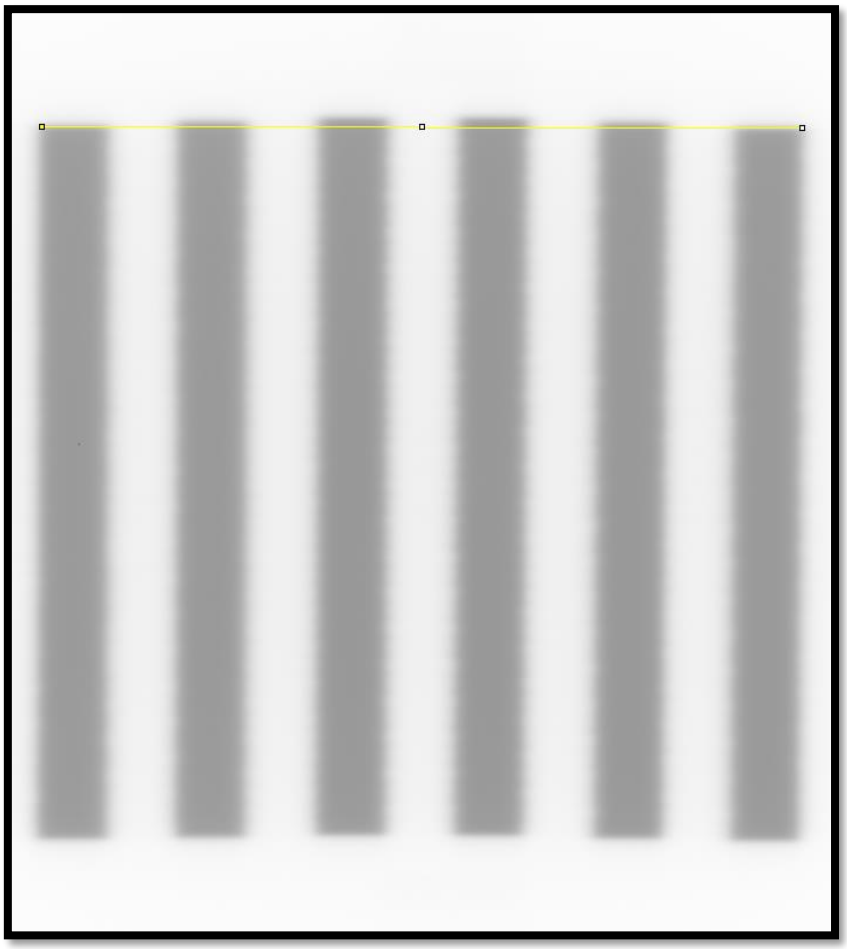

Figure 48: Arc picket fence image acquired on an EPID on an Elekta Versa HD accelerator.

Figure 49 below shows the mean and maximum relative position errors from the arc picket fence for the Elekta Agility MLC units that participated in this section.

Stellenbosch University https://scholar.sun.ac.za

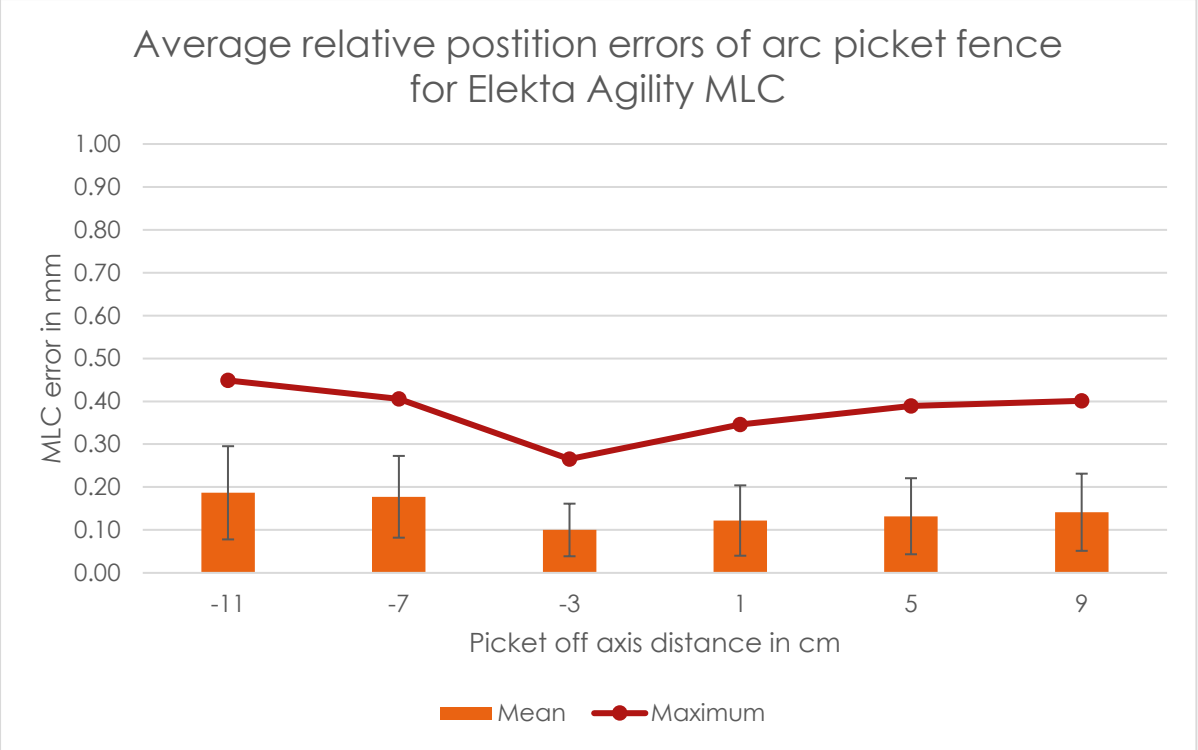

Figure 49: Graphic representation of mean and maximum relative position errors from the arc picket fence for the Elekta Agility MLC.

Figure 50 below shows the mean and maximum relative width errors from the arc picket fence for the Elekta Agility MLC units that participated in this section.

Stellenbosch University https://scholar.sun.ac.za

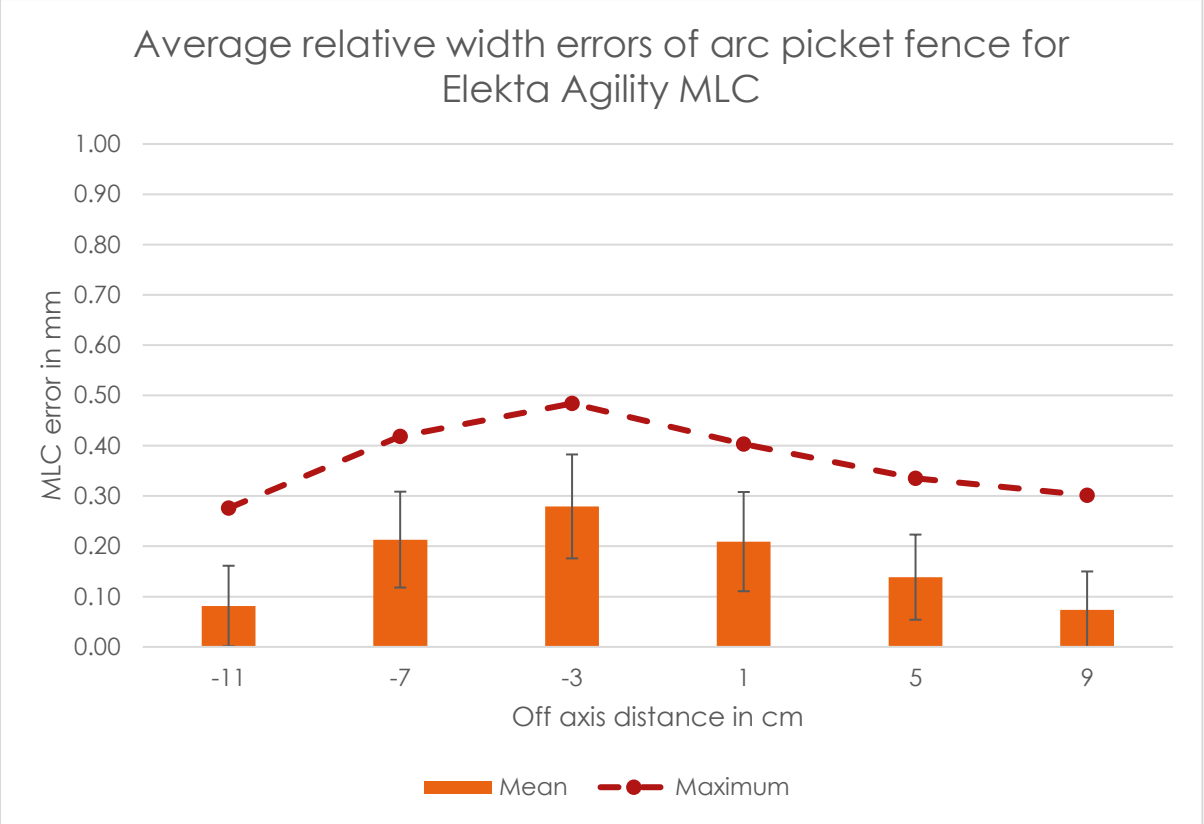

Figure 50: Graphic representation of mean and maximum relative width errors from the arc picket fence for the Elekta Agility MLC.

Section 10: National survey of micro-MLC data used for SRS:

The maximum width and position errors within the central 10x10 cm^2 were recorded for each image. Errors reported in this section are taken as the difference between the expected and the measured picket widths and positions.

Figure 51 below shows the average position error, maximum position errors and position standard deviation (error bars) for the single Varian HDMLC linac as a function of off-axis distance for the central 10cm of the field.

Stellenbosch University https://scholar.sun.ac.za

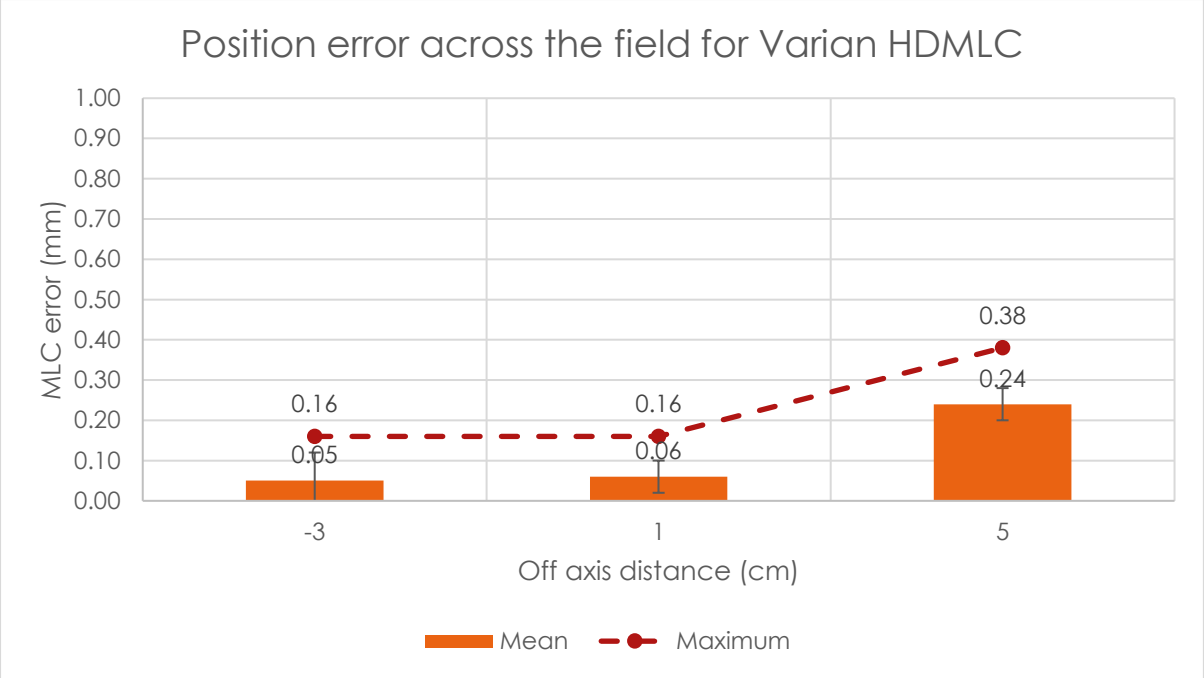

Figure 51: Graphic representation of the average MLC position errors at specific off-axis distances for Varian HDMLC.

Figure 52 below shows the average width error, maximum width errors and width standard deviation (error bars) for the single Varian HDMLC linac as a function of off-axis distance for the central 10cm of the field.

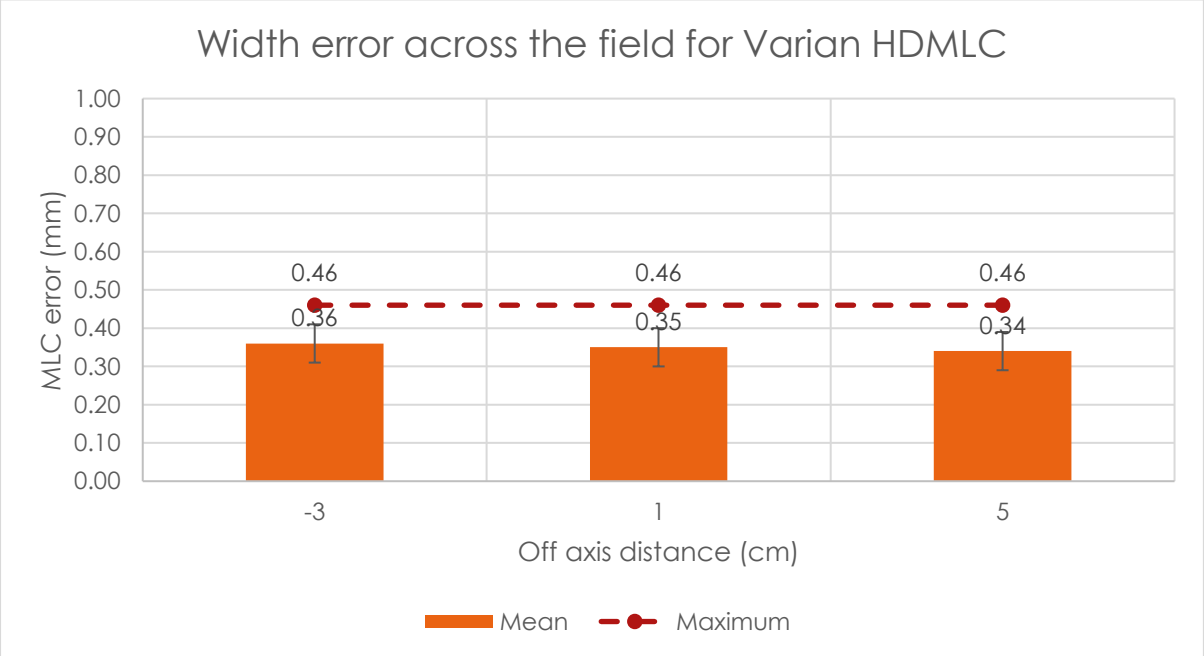

Figure 52: Graphic representation of the average MLC width errors at specific off-axis distances for Varian HDMLC.

Stellenbosch University https://scholar.sun.ac.za

From the data presented, the Varian HDMLC measured positions and width are close to the expected positions and widths and within the national regulatory tolerance for SRS linacs.

Figure 53 below shows the average position error, maximum position errors and position standard deviation (error bars) for the single Elekta Apex MLC as a function of off-axis distance for the central 10cm of the field.

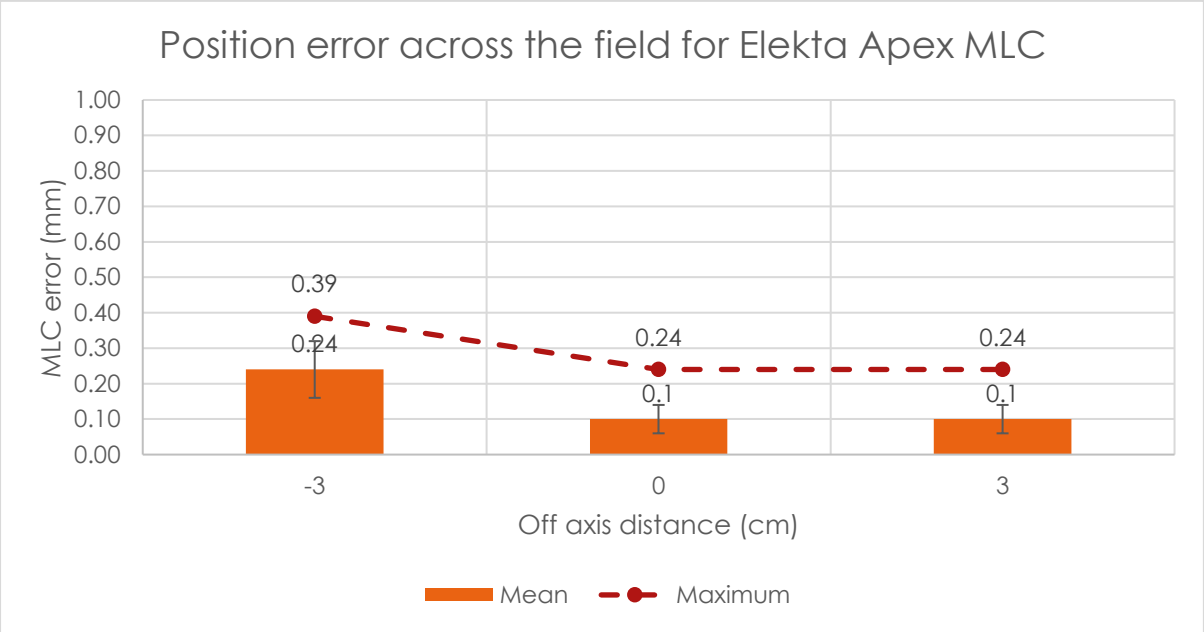

Figure 53: Graphic representation of the average MLC position errors at specific off-axis distances for Elekta Apex MLC.

Figure 54 below shows the average width error, maximum width errors and width standard deviation (error bars) for the single Elekta Apex MLC as a function of off-axis distance for the central 10cm of the field.

Stellenbosch University https://scholar.sun.ac.za

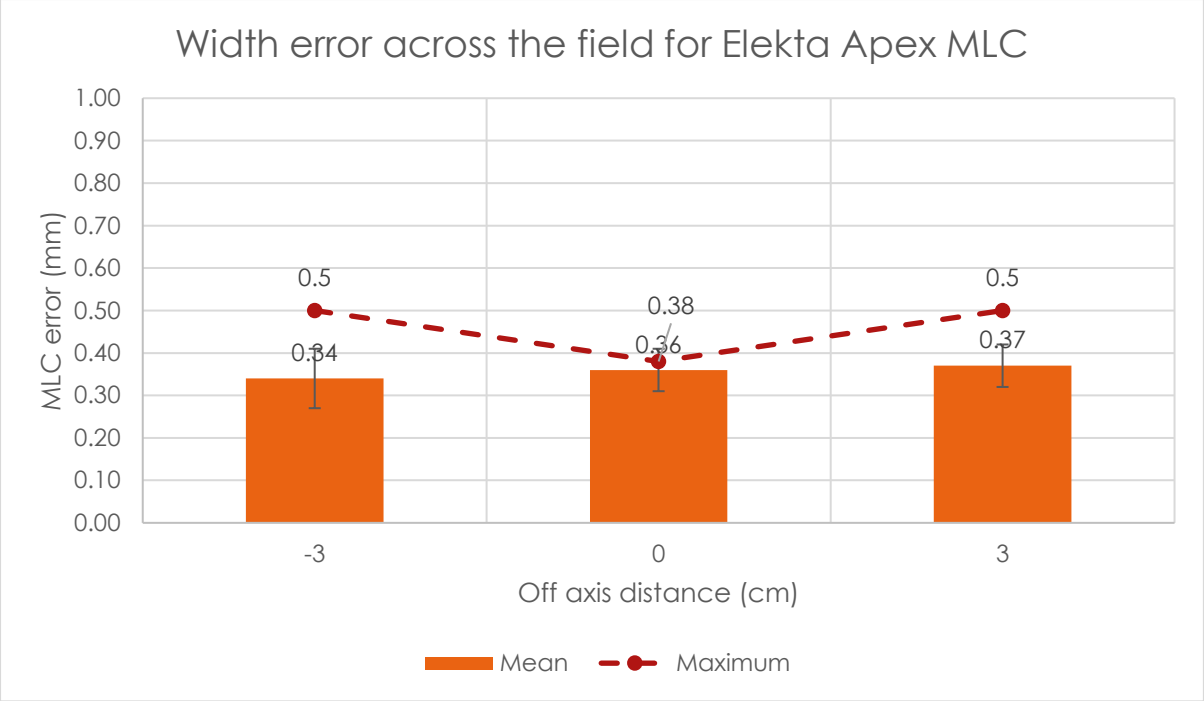

Figure 54: Graphic representation of the average MLC width errors at specific off-axis distances for Elekta Apex MLC.

From the data presented, the Elekta Apex MLC measured positions and width are close to the expected positions and widths and within the national regulatory tolerance for SRS linacs.

From this data, there does not seem to be a significant difference in MLC accuracy at a gantry angle of zero between standard and micro MLC systems from Elekta and Varian.

Not one of the micro MLC systems show better accuracy than non-micro MLC systems. This might be due to the limited resolution of the EPID, since most errors found on most of the MLC systems tested in this study are in the order of or smaller than 1 pixel.

Generally, the results show errors in modern MLC systems in the order on 1 pixel. Any errors measured that are smaller than 1 pixel inherently carries large uncertainty, and the significance of these errors are therefore not commented on. It would be poor practice to draw conclusions from data measured that have smaller errors than the resolution of the measurement device due to the large level of uncertainty in the data.

Stellenbosch University https://scholar.sun.ac.za

Conclusion:

This study demonstrates that it is possible to create a simple quantitative method to accurately and digitally measure the MLC positional error on most linac types by using clinically available EPID detectors and in-house created software at no additional cost. The data presented shows that the software is robust enough to handle EPID images from different vendors accurately and sensitive enough to find small MLC errors accurately. Baseline values could be established for all units of volunteers that participated in the study and can be viewed in Appendix A.

The validation data shows that by using simple methods of interpolation and analysis that are user-independent, errors smaller than the pixel size can be determined with nearly the same accuracy as commercially available software packages in a short period. Furthermore, the results of the software compare well with Elekta Icom logs. The validation data also agrees well with Varian trajectory logs, however, this is only since the measured errors are small. There remains uncertainty regarding the absolute error reported by the Varian trajectory logs since the errors are in the order of 10 times smaller than the EPID measured errors.

The method employed proved to be sufficiently robust to be able to use at various gantry angles, during an arc delivery and for flattening filter-free beams. Uncertainties in analysing picket fence testing results obtained during an arc are shown and discussed for VMAT capable machines. Two of the linacs that participated had EPID detectors that were calibrated to measure dose. As expected, this did not have an effect on the MLC positional measurements made and no difference was observed between units with EPIDs that are calibrated to measure dose and those that are not.

No pass/fail criteria section was added to the software as all measured errors should always be interpreted and analysed by a qualified Medical Physicist. In cases where the software is to be used clinically, the Medical Physicist will be able to determine if an error exists based on the measured data and from the presented data the course of action forward.

From the nationwide survey of MLC accuracy, incorporating different MLC types, different EPID imager types, different MP users with different levels of understanding and experience in MLC QA and differences in capability of the units, data shows that the MLC accuracy is comparable between different linac and MLC vendor types and mostly user independent. Within a specific vendor type, standard deviations are in the order of 1-pixel size, indicating that there is not much variation between leaf positions of a specific MLC

Stellenbosch University https://scholar.sun.ac.za

type. This might be a by-product of good quality and standardised MLC calibration procedures.

All units that participated in this study adhered to the national requirements for MLC QA at the time of measurement.

Additional investigation shows that the position results of the Varian Halcyon MLC differing from the conventional linacs is not due to the nature of the flattening filter beam. The data in this study is insufficient to make any other conclusions as to these results. A possibility would be the unconventional calibration procedures due to the unconventional design.

This study provides a background for more advanced testing of MLC than is currently the South African standard. It forms a starting point for transitioning to MLC QA with better accuracy and user independence.

Although this method is simple and provides an accurate solution for measuring the MLC error for static fields, the errors cannot be explicitly translated to dynamic deliveries such as VMAT or DMLC.

Known drawbacks of this study include incomplete data contributions from various units and an under-sampling of specific unit types (mostly Varian) as this study was based on cooperation from volunteers.

A clear guide to creating the fields over all vendor types as well as how to use the software can be viewed in appendix A in an attempt to provide a means for replication of the results.

Future work:

Future work on this topic includes the investigation of the accuracy of the Varian trajectory log files by comparison to a measurement of sufficient resolution, the investigation of dynamic MLC errors and their correlation to static MLC positioning errors and the determination of methods to express MLC errors about the actual radiation isocentre.

A special investigation is required for Varian Halcyon positioning of the MLC with attention given to differences between measured and planned fluences, especially in the off-axis region as well as an investigation into the calibration of this complex MLC system.

The clinical effect these errors have on patients and a discussion on adapting the tolerances of MLC QA for positional MLC measurements is needed.

Stellenbosch University https://scholar.sun.ac.za

Acknowledgements:

Philosopher, Ludwig Wittgenstein, once said knowledge is in the end based on acknowledgement.

It is with a proud heart and a profound sense of thankfulness that I would acknowledge all the knowledge imparted by those who saw the potential in me.

To my colleagues, thank you for the inspiration, coffee and tolerance.

To my supervisor, thank you for the guidance and support throughout the entire process.

To my wife, thank you for believing in me and always nudging me on.

To my parents, thank you for always accepting me, encouraging my inquisitive nature and nurturing my passions.

Lastly, to my Heavenly Farther, thank you for the ability and opportunity.

Stellenbosch University https://scholar.sun.ac.za

References:

1. Maidment A, Yaffe M. Diagnostic Radiology Physics A Handbook for Teachers and Students. 2014. 209–235 p.
2. What Is Cancer? [Internet]. [cited 2021 Feb 10]. Available from: https://www.cancer.gov/about-cancer/understanding/what-is-cancer
3. De Vita VT, Lawrence TS, Rosenberg SA. Cancer Principles & Practice of Oncology. 8th ed. De Vita VT, Lawrence TS, Rosenberg SA, editors. Philadelphia: Lippincott Williams & Wilkins; 2008.
4. Podgorsak EB. Radiation Oncology Physics : A Handbook for Teachers and Students. Vienna: International Atomic Energy Agency; 2005.
5. Gray Cancer Institute. The Novice`s guide to electron linear accelerators. Gray Cancer Institute; 1996. p. 1–7.
6. Systems TP. VMAT Information for Treatment Planning Systems. Crawley: ELEKTA LIMITED; 2014.
7. Khan FM. Physics of Radiation Therapy (3rd Edition). Lippincott Williams & Wilkins; 2003. p. 61–154.
8. Rowshanfarzad P, McGarry CK, Barnes MP, Sabet M, Ebert MA. An EPID-based method for comprehensive verification of gantry, EPID and the MLC carriage positional accuracy in Varian linacs during arc treatments. Radiat Oncol. 2014;9(1):1–10.
9. Rowshanfarzad P, Riis HL, Zimmermann SJ, Ebert MA. A comprehensive study of the mechanical performance of gantry, EPID and the MLC assembly in Elekta linacs during gantry rotation. Br J Radiol. 2015;88(1051).
10. Bushberg, JT, Siebert, JA, Leidholdt, EM, Boone J. The Essential Physics of Medical Imaging. 2011.
11. Gedraite ES, Hadad M. Investigation on the effect of a Gaussian Blur in image filtering and segmentation. Proc Elmar - Int Symp Electron Mar. 2011;(January 2011):393–6.
12. Susmitha A, Mishra I, Jain S, Asst S. Performance Analysis of Average and Median Filters for De noising Of Digital Images . 2016;1435–9.
13. Sánchez HJ. A new peak search routine for fast evaluation on small computers. Comput Phys. 1991;5(4):407.

Stellenbosch University https://scholar.sun.ac.za

14. Jarman KH. What It's Like to Be Normal: Probability Distributions and One Rule That Could Make You Wildly Popular. The Art of Data Analysis. 2013. 63–85 p.

15. Cherry S.R., Sorenson J.A. PME. Physics in Nuclear Medicine. 4th ed. Vol. 1, Statewide Agricultural Land Use Baseline 2015. Philadelphia: Elsivier; 2012.

16. Howard JP. Interpolation and Extrapolation. Comput Methods Numer Anal with R. 2018;(January):95–132.

17. Gerald J. Kutcher, Coia L, Gillin M, Hanson WF, Leibel S, Robert J M, et al. Comprehensive QA for radiation oncology: report of AAPM Radiation Therapy Comittee Task Group 40. Vol. 21, Medical Phys. 1994. p. 581–618.

18. Canadian Partnership foron Treatment Centres Medical Linear Accelerators and Multileaf Collimators. 2015; Available from: www.comp-ocpm.ca

19. Klein EE, Hanley J, Bayouth J, Yin FF, Simon W, Dresser S, et al. Task group 142 report: Quality assurance of medical accelerators. Med Phys. 2009;36(9):4197–212.

20. Multileaf Collimators. Vol. 1, South African Medical Physics Society (SAMPS) South African Association of Physicists in Medicine and Biology (SAAPMB) South African Standards for Quality Assurance in Radiotherapy (SASQART). 2015.

21. Volumetric Modulated Arc Therapy (VMAT) Designator Test Performance Tolerance Action. Vol. 1, South African Medical Physics Society (SAMPS) South African Association of Physicists in Medicine and Biology (SAAPMB) South African Standards for Quality Assurance in Radiotherapy (SASQART). 2015.

22. Böhm C, Hofer M, Böhm C, Hofer M. AAPM report 72: Basic Applications of Multileaf Collimators. Physical Unclonable Functions in Theory and Practice. Medical Physics Publishing; 2013. 53–68 p.

23. Lim TY, Dragojević I, Hoffman D, Flores-Martinez E, Kim GY. Characterization of the Halcyon TM multileaf collimator system. J Appl Clin Med Phys. 2019;20(4):106–14.

24. Thorman S. Elekta's New Agility MLC Solution Poised to Revolutionize Beam Shaping of Radiation Therapy Cancer Treatments. 2012.

25. Hadad K, Alipour H. Evaluation of MLC thickness and composite effects on collimation parameters using EGSnrc and IAEA phase space data. J Biomed Phys Eng. 2020;10(1):59–64.

26. Klüter S, Sroka-Perez G, Schubert K, Debus J. Leakage of the Siemens 160 MLC multileaf collimator on a dual energy linear accelerator. Phys Med Biol. 2011;56(2).

Stellenbosch University https://scholar.sun.ac.za

27. Que W, Kung J, Dai J. "Tongue-and-groove" effect in intensity modulated radiotherapy with static multileaf collimator fields. In: Physics in medicine and biology. 2004. p. 399–405.

28. Hariri S, Shahriari M. Suggesting a new design for multileaf collimator leaves based on Monte Carlo simulation of two commercial systems. J Appl Clin Med Phys. 2010;11(3):173–85.

29. LoSasso T, Chui CS, Ling CC. Physical and dosimetric aspects of a multileaf collimation system used in the dynamic mode for implementing intensity modulated radiotherapy. Med Phys. 1998;25(10):1919–27.

30. IMPAC Medical Systems I. Monaco Technical Reference: Post Modeling Adjustment of MLC Parameters. 2012. p. Document ID: LRMMON0003.

31. Rowshanfarzad P, Sabet M, Barnes MP, O'Connor DJ, Greer PB. EPID-based verification of the MLC performance for dynamic IMRT and VMAT. Med Phys. 2012;39(10):6192–207.

32. Roche M, Crane R, Powers M, Crabtree T. Agility MLC transmission optimization in the Monaco treatment planning system. J Appl Clin Med Phys. 2018;19(5):473–82.

33. Sharma DS, Dongre PM, Mhatre V, Heigrujam M. Physical and dosimetric characteristic of high-definition multileaf collimator (HDMLC) for SRS and IMRT. J Appl Clin Med Phys. 2011;12(3):142–60.

34. Galvin JM. The multileaf collimator: a complete guide. [Internet]. AAPM annual meeting. 1999. Available from: http://www.aapm.org/meetings/99AM/pdf/2787-9625.pdf

35. Graves MN, Thompson A V., Martel MK. Calibration and quality assurance for rounded leaf-end MLC systems. Med Phys. 2001;28(11):2227–33.

36. Young LA, Yang F, Cao N, Meyer J. Rounded leaf end modeling in Pinnacle VMAT treatment planning for fixed jaw linacs. J Appl Clin Med Phys. 2016;17(6):149–62.

37. Midi NS, Zin HM. Feasibility of using the linac real-time log data for VMAT treatment verification. J Phys Conf Ser. 2017;851(1).

38. Vatnitsky S, Rosenblatt E, International Atomic Energy Agency. IAEA-TECDOC-1588: Transition from 2-D Radiotherapy to 3-D Conformal and Intensity Modulated Radiotherapy. 2008;(May). Available from: http://www-pub.iaea.org/MTCD/publications/PDF/TE_1588_web.pdf

39. Sumida I, Yamaguchi H, Kizaki H, Koizumi M, Ogata T, Takahashi Y, et al. Quality assurance of MLC leaf position accuracy and relative dose effect at the MLC abutment

Stellenbosch University https://scholar.sun.ac.za

region using an electronic portal imaging device. J Radiat Res. 2012;53(5):798–806.

40. Antypas C, Floros I, Rouchota M, Armpilia C, Lyra M. MLC positional accuracy evaluation through the Picket Fence test on EBT2 films and a 3D volumetric phantom. J Appl Clin Med Phys. 2015;16(2):189–97.

41. Mamalui-Hunter M, Li H, Low DA. MLC quality assurance using EPID: A fitting technique with subpixel precision. Med Phys. 2008;35(6):2347–55.

42. Christophides D, Davies A, Fleckney M. EP-1519: Automatic detection of MLC position errors using an EPID based picket fence test. Radiother Oncol. 2016;119:S703–4.

43. Kantz S, Troeller Mcdermott A, Söhn M, Reinhardt S, Belka C, Parodi K, et al. Practical implications for the quality assurance of modulated radiation therapy techniques using point detector arrays. J Appl Clin Med Phys. 2017;18(6):20–31.

44. Rowshanfarzad P, Sabet M, O'Connor DJ, McCowan PM, McCurdy BMC, Greer PB. Detection and correction for EPID and gantry sag during arc delivery using cine EPID imaging. Med Phys. 2012;39(2):623–35.

45. Clarke MF, Budgell GJ. Use of an amorphous silicon EPID for measuring MLC calibration at varying gantry angle. Phys Med Biol. 2008;53(2).

46. Parent L, Seco J, Evans PM, Dance DR, Fielding A. Evaluation of two methods of predicting MLC leaf positions using EPID measurements. Med Phys. 2006;33(9):3174–82.

47. Varian Medical Systems T. Millennium mlc system and maintenance guide. 2003.

48. Lee JW, Chung JB, Lee DH, Park JH, Choe BY, Suh TS, et al. Discrepancy of intensity modulation radiation therapy dose delivery due to the dose-dynamic multi-leaf collimator gravity effect. J Korean Phys Soc. 2008;53(6):3436–43.

49. Picioli M, Torzsok K, Ruiz Plata A, Marangoni F, Broque H, Aponte J. PO-1029 The use of Elekta Agility MLC Dynamic log files for VMAT QA. Radiother Oncol. 2019;133(Mlc):S571.

50. Karan T, Kim S, Abbas A, Moseley DJ, Taremi MM, Yeung I. Dosimetric Discrepancies due to Positional Errors in MLC Movement During Stereotactic Lung VMAT. Int J Radiat Oncol. 2014;90(1):S190.

51. Calvo-Ortega JF, Teke T, Moragues S, Pozo M, Casals J. A varian dynalog file-based procedure for patient dose-volume histogram-based IMRT QA. J Appl Clin Med Phys. 2014;15(2):100–9.

52. Sakaria K, Shaheera Midi N, Zin HM. Picket fence test of Agility MLCs using linac log data. J Phys Conf Ser. 2019;1248(1).

Stellenbosch University https://scholar.sun.ac.za

53. Hirashima H, Nakamura M, Miyabe Y, Uto M, Nakamura K, Mizowaki T. Monitoring of mechanical errors and their dosimetric impact throughout the course of non-coplanar continuous volumetric-modulated arc therapy. Radiat Oncol. 2018;13(1):1–8.

54. Moiseenko V, Lapointe V, James K, Yin L, Liu M, Pawlicki T. Biological Consequences of Errors in MLC Calibration in the Context of IMRT Delivery and QA. Med Phys. 2011;38(6):3583.

55. Oliver M, Gagne I, Bush K, Zavgorodni S, Ansbacher W, Beckham W. Clinical significance of multi-leaf collimator positional errors for volumetric modulated arc therapy. Radiother Oncol [Internet]. 2010;97(3):554–60. Available from: http://dx.doi.org/10.1016/j.radonc.2010.06.013

56. Nithiyanantham K, Mani GK, Subramani V. Analysis of direct clinical consequences of MLC positional errors in volumetric-modulated arc therapy using 3D dosimetry system. 2015;16(5):296–305.

57. Strauss L, Shaw W, State F, Africa S, Strauss L, Shaw W. Considerations for the verification of volumetric modulated arc therapy-planned dose distributions. 2019;1–9.

58. Rowshanfarzad P, Sabet M, Barnes MP, O'Connor DJ, Greer PB. EPID-based verification of the MLC performance for dynamic IMRT and VMAT. Med Phys. 2012;39(10):6192–207.

59. Eckhause T, Al-Hallaq H, Ritter T, Demarco J, Farrey K, Pawlicki T, et al. Automating linear accelerator quality assurance. Med Phys. 2015;42(10):6074–83.

60. Li Y, Chen L, Zhu J, Wang B, Liu X. A quantitative method to the analysis of MLC leaf position and speed based on EPID and EBT3 fi lm for dynamic IMRT treatment with different types of MLC. 2017;(September):106–15.

Stellenbosch University https://scholar.sun.ac.za

Appendix A: Manual for acquisition and analysis with the software.

Design and rationale behind QAPRO picket fence:

The rationale behind using picket fence test for quality assurance of MLC:

The picket fence is the most popular quality assurance test for MLC leaf position accuracy. Both the full width at half maximum of the gaps and the separation of the gaps are measured as a measure of leaf position constancy and accuracy(60).

This is in line with current South-African standards and American standards for MLC QA(19)(20,21).

Several published studies have looked into the dosimetric impact of MLC errors and this has driven the increasing need for a way to quantitively check the MLC as part of routine quality assurance. One such study, published in 2015 by Karthikeyan Nithiyanantham et al., entitled "Analysis of direct clinical consequences of MLC position errors in volumetric-modulated arc therapy using 3D dosimetry system" concluded that **systematic** MLC errors beyond ±0.3 mm influenced the intensity-modulated dose distributions significantly(56).

Similar studies have been done locally at the University of the Free State in Bloemfontein, South Africa by Struss and Shaw, found that their VMAT plans exhibited significant dosimetric changes when **systematic** MLC errors of ±0.5 mm and more were introduced(57).

Design of the QAPRO Picket fence:

The QAPRO Picket fence was designed to test the MLC accuracy in the clinical range used and across a clinically large field of view with the ability to analyze the results digitally with as little as possible user influence.

A 2cm wide picket with 2cm gaps was chosen as this relates well to the general field sizes used in IMRT/VMAT deliveries. Using this gives the user an idea of the MLC errors for a clinically appropriate field. Errors found from the picket fence test can then, therefore, be directly translated to clinical situations.

Additionally, the QAPRO picket fence design incorporates a 20cm field of view. This means that the picket fence is aimed at testing the MLC positional accuracy off-axis as well as close to the central axis. This gives the user an idea of the full capability of the MLC

Stellenbosch University https://scholar.sun.ac.za

across a wide range of positions in the clinical field of treatment. The field of view was limited to 20cm due to the useful field of view of onboard imaging equipment.

The use of the onboard imager as an imaging modality was chosen due to its fast digitization capability, cost-effectiveness, excellent resolution, and the ability to use it at any gantry angle.

Stellenbosch University https://scholar.sun.ac.za

Creation and acquisition procedure for QAPRO Picket fence:

Picket fence at gantry zero:

Elekta:

When using an Elekta linear accelerator with an IviewGT MV imager, follow the following acquisition protocol for optimal results.

1. Create 6 static fields in Mosaiq with the following properties:

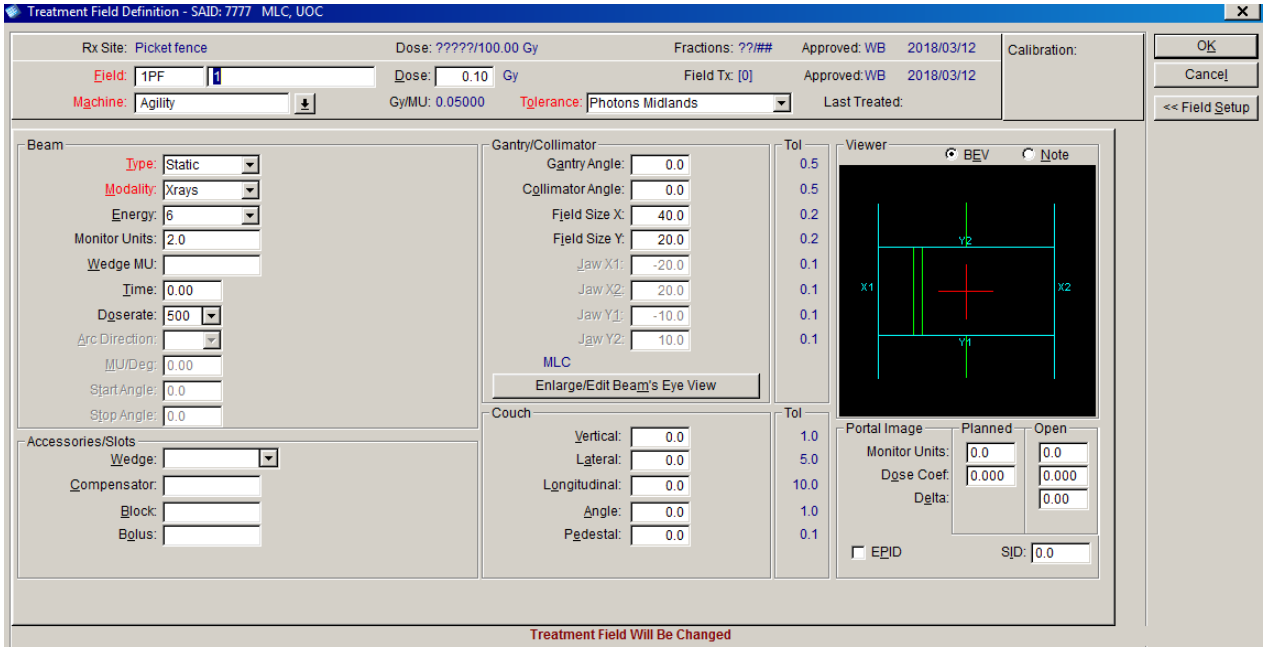

And the following MLC properties for fields 1-6 follow numerically with the simple MLC function as shown below to the values in the table.

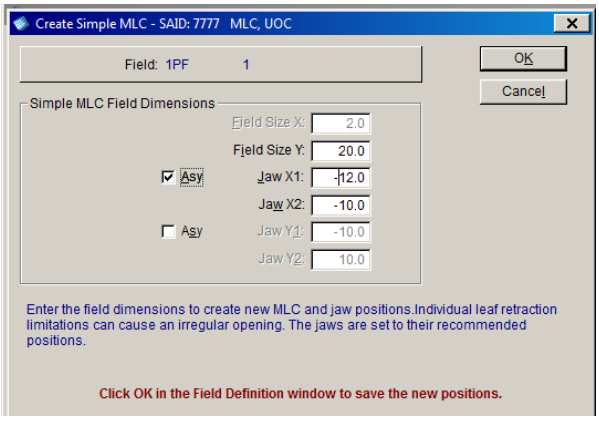

Stellenbosch University https://scholar.sun.ac.za

Jaw	Picket 1	Picket 2	Picket 3	Picket 4	Picket 5	Picket 6
X1 position	-12	-8	-4	0	4	8
X2 position	-10	-6	-2	2	6	10

2. After these fields have been created, MV images of these images are taken. The individual pickets can be imaged independently and added with independent software like ImageJ or the IviewGT software may be set to acquire a segmented image.

When taking a segmented image, open the patient on Mosaiq and click on the iCom button on the IviewGT software. The patient demographics will be imported to the IviewGT software. Click the iCOM button again to leave this page. If an acquisition window opens, click cancel and click the iCom button to return to the home screen of the IviewGT software. Select the field that was created. Click on the "Edit field" button and change the "iCom-Vx" parameter to "Double/Multiple" and then change the "IMRT segments" value to 6. Click the "OK" button.

Load the first beam to the linac. Ensure that the light field is within the imaging area of the detector for all pickets. On the "IviewGT" software, click the camera button with the "2/n" under it and deliver the segments one after the other without changing anything on the "IviewGT" software. Automatic field sequences may be created on Mosaiq to deliver the static fields back to back without human interference if it is preferred.

3. After acquiring the image, the image should be transferred to the Mosaiq server and the image should be available in the image tab of the Mosaiq patient. The image may then be exported to any computer.
4. The image exported is a DICOM image and can be opened and analyzed with the PicketPRO software.

Stellenbosch University https://scholar.sun.ac.za

Siemens:

When using a Siemens linear accelerator with an OptiVue 500/1000 MV imager, follow the following acquisition protocol for optimal results.

1. Create 6 static fields in Mosaiq with the following properties:

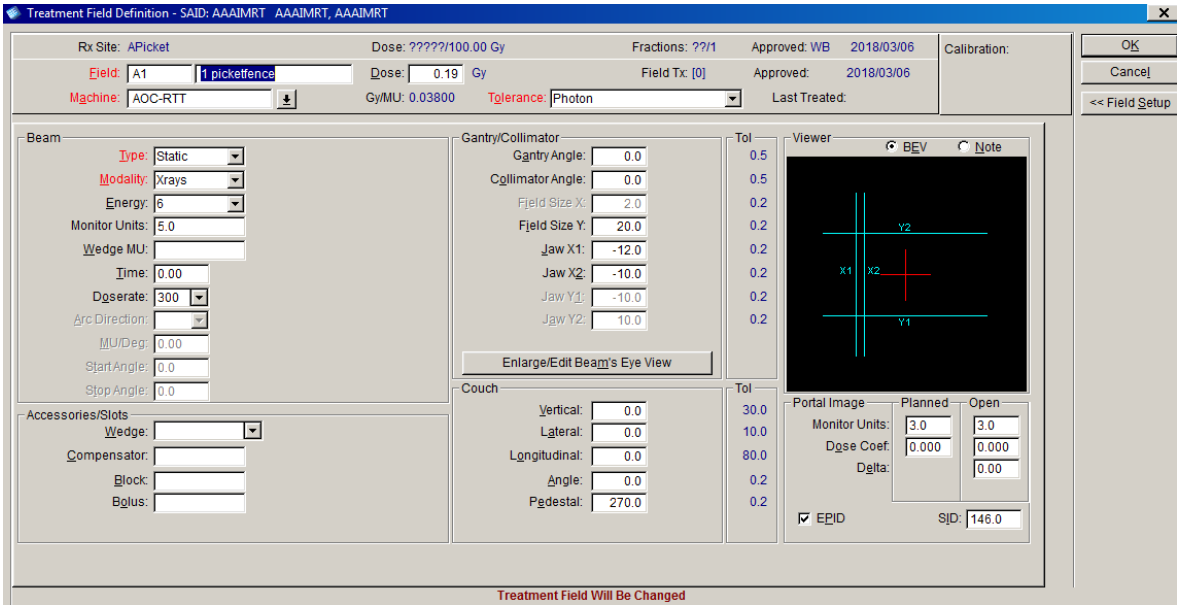

And the following MLC properties for fields 1-6 follow numerically with the **asymmetric Jaw** function as shown below to the values in the table.

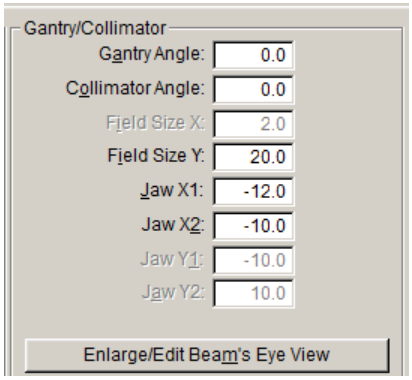

Jaw	Picket 1	Picket 2	Picket 3	Picket 4	Picket 5	Picket 6
X1 position	-12	-8	-4	0	4	8
X2 position	-10	-6	-2	2	6	10

Stellenbosch University https://scholar.sun.ac.za

Note that this only sets the Jaw positions and that Mosaiq does not allow us to set MLC positions for Siemens accelerators. For units such as the Primus, where there is no backup jaw in the MLC direction, the MLCs will follow the jaw prescription, however, for other units like the Oncor and the Artiste, MLC positions must be defined.

This can be done by logging into the Mosaiq of an Elekta Synergy (not versa) in your region and changing the machine to Synergy/Agility. The MLCs can then be enabled, and the **simple MLC** function is used to create the picket positions easily. The user should then log back into the Mosaiq of the Siemens unit and change the machine back to the Siemens unit. The MLC positions will now be defined and the linac will accept the fields for delivery.

2. After these fields have been created, MV images of these images are taken. The individual pickets can be imaged independently and added with the software.
    a. When taking the images, open the patient in Mosaiq.
    b. In most cases, the Artiste EPID images cannot be taken in QA mode and must be scheduled in clinical mode. A clinical log in is required on the Therapist.
    c. Log in to the Therapist in clinical mode.
    d. On Mosaiq go to "D and I".

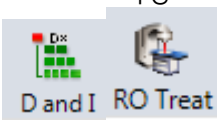

    e. Right-click on one of the fields to be delivered and select 'Treatment Calendar'

Stellenbosch University https://scholar.sun.ac.za

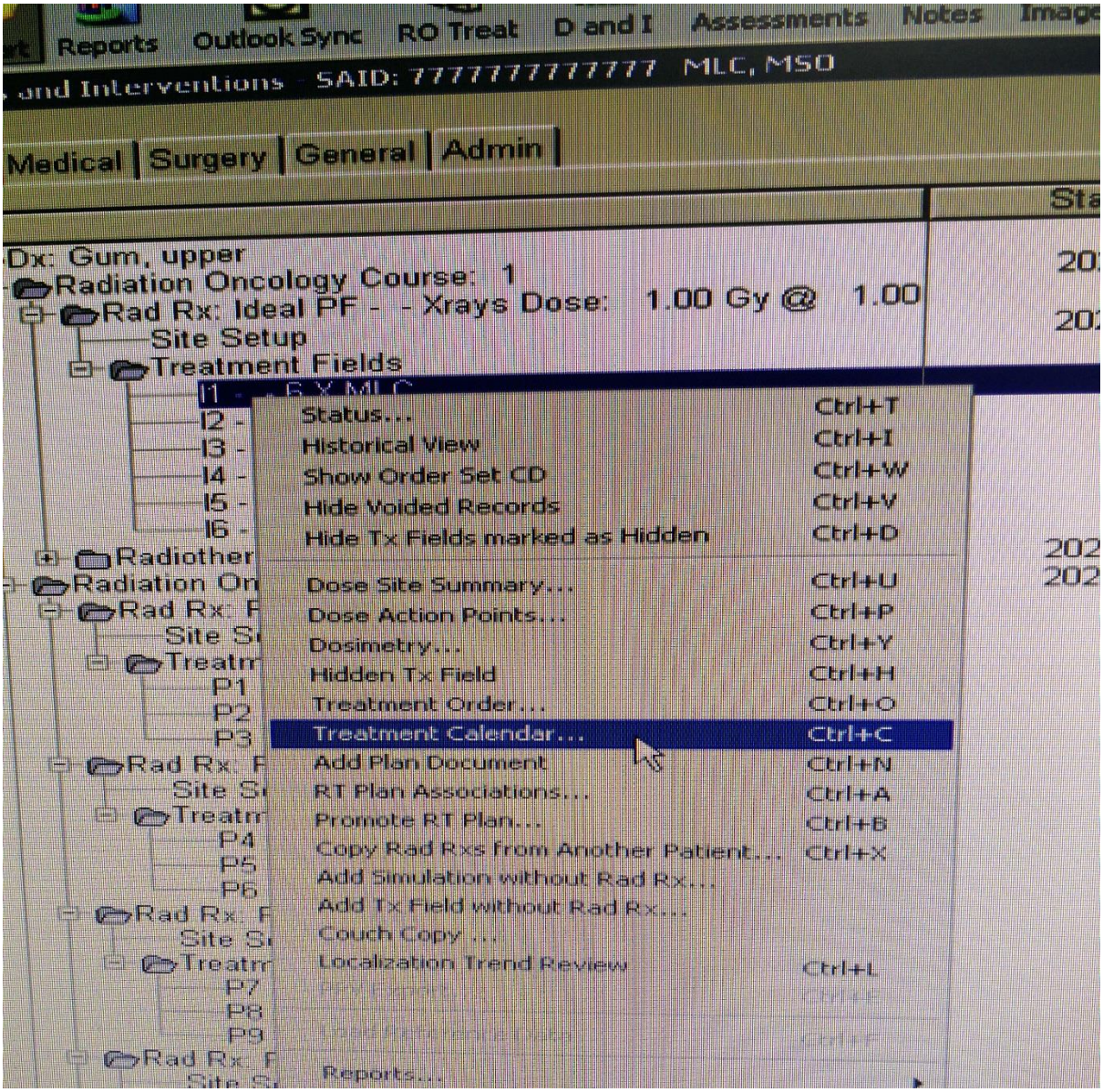

f. In the "insert sessions" workspace, select other and click on the insert sessions for course 1 button. A new session will be added to the calendar.

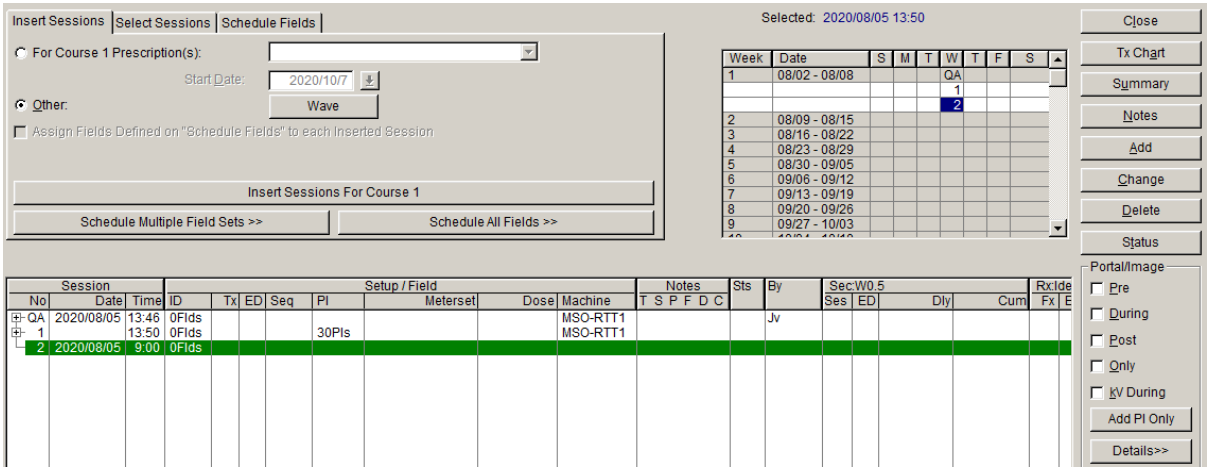

Stellenbosch University https://scholar.sun.ac.za

g. Right-click on the session and select 'Edit Treatment Calendar Session…'

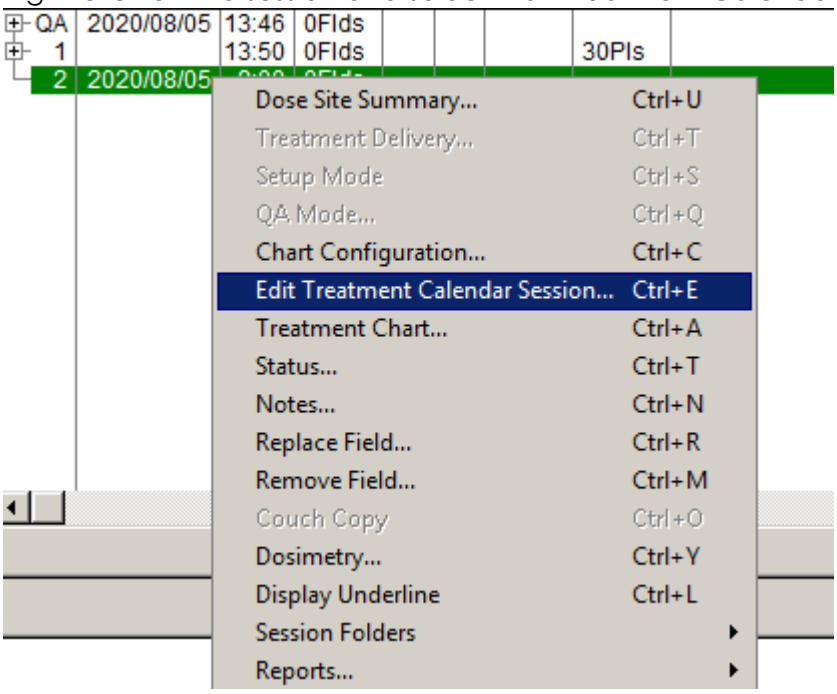

h. In this window, the treatment date can be changed. To add fields, click on 'Define' under the fields section

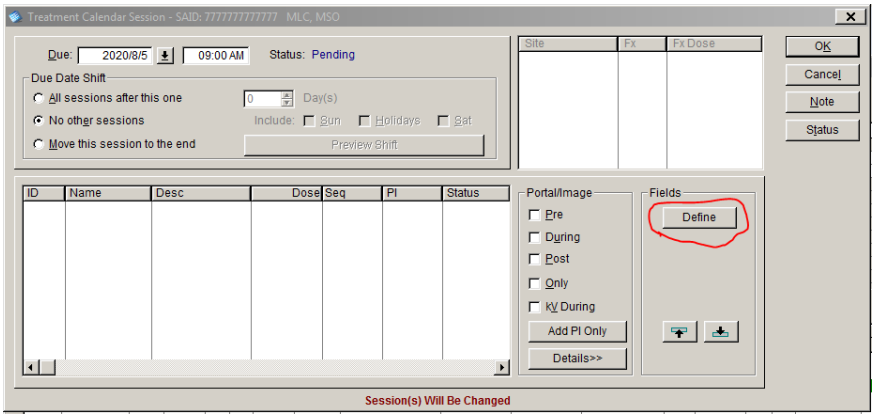

i. Select the fields that need to be delivered and click on Add>> to add them to this session. Click on OK when all fields have been added

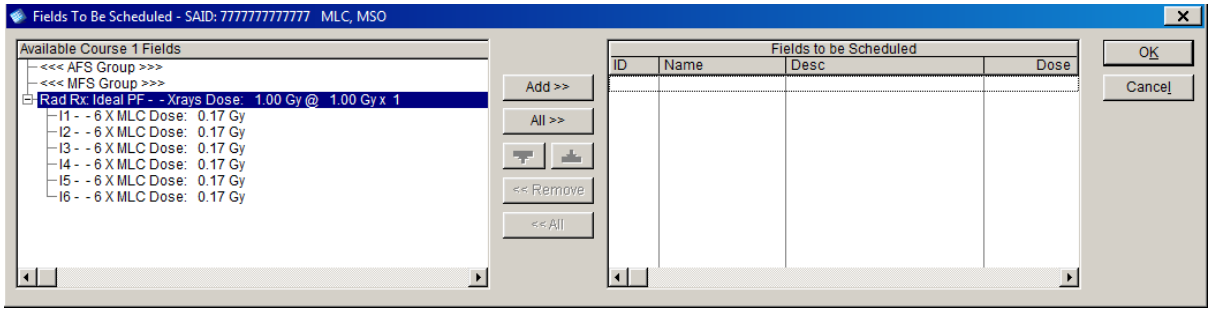

Stellenbosch University https://scholar.sun.ac.za

j. Highlight the first field by clicking on it and clicking on 'Details>>' under Portal/Image. Tick the Only box and select plan under it to change the field to a Portal field. Do this for all fields and click on OK

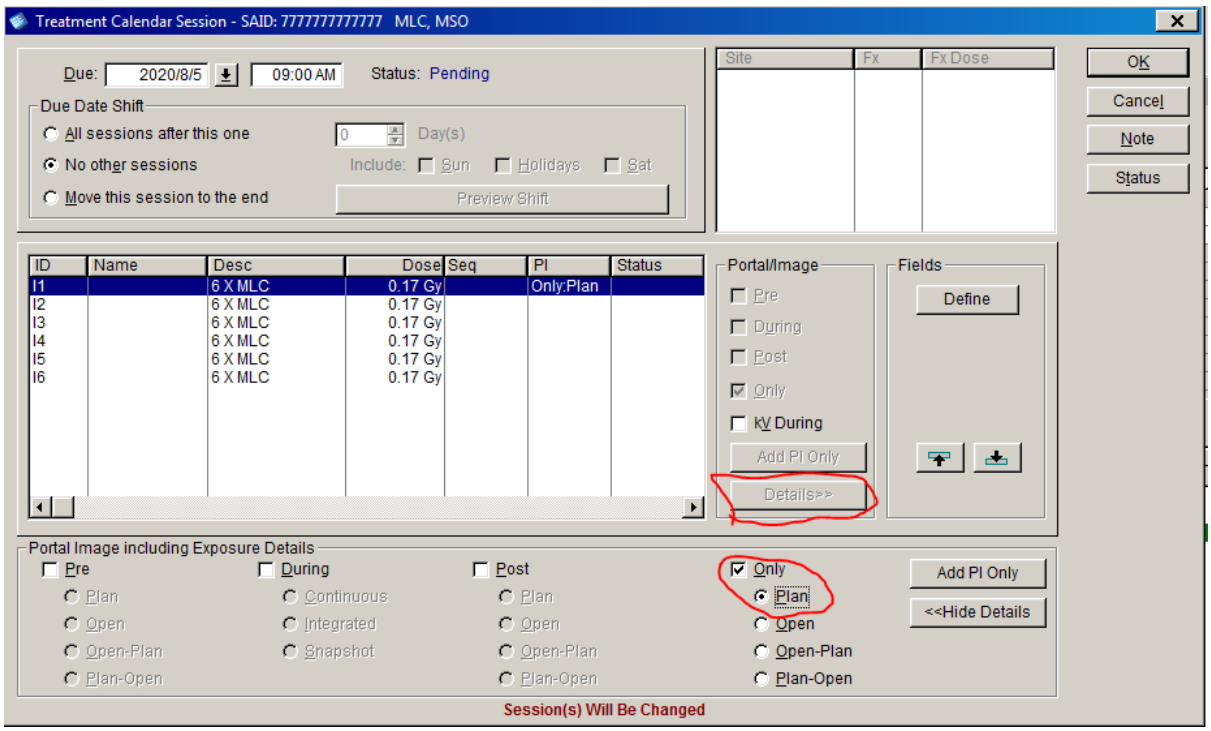

k. On the right click on 'Tx Chart' to exit the Treatment Calendar

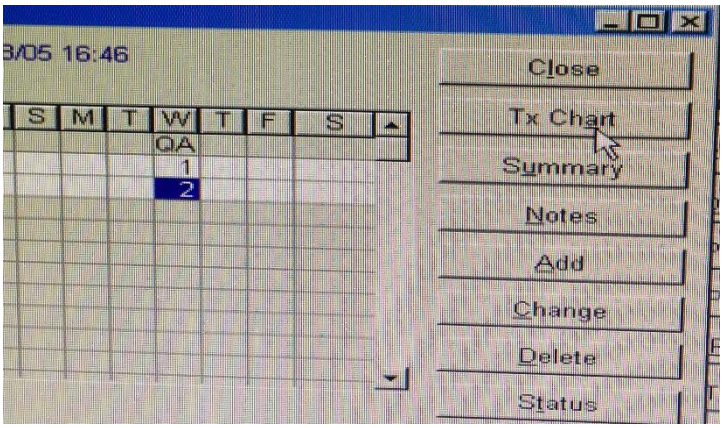

l. Select the session that was just added and click on Treat on the right

m. Select 'Send Plan' in the next window

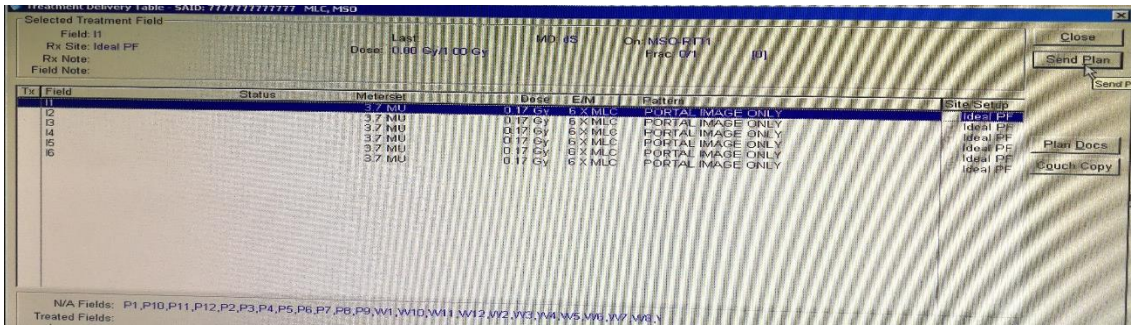

Stellenbosch University https://scholar.sun.ac.za

n. Move over to the Therapist and follow all steps to select the fields and send it to the Linac
o. Deliver each field with the EPID in the correct position. **The couch cannot be moved out of the field so make sure that it is raised high enough to ensure that all pickets pass completely through it. You can raise it close to the linac head to ensure this.**
p. Once all fields have been delivered close the treatment on the therapist and enter the patient browser.
q. Navigate to the correct patient and select the first picket image. Right-click on it and select Transfer.
r. In the send to window select the Mosaiq Dicom location for your department. Do this for all images to have the images in Mosaiq as DICOM images that can be exported and analysed in PicketPRO.

It is important to remember to add the MUs for open and plan ports and the SID in Mosaiq when you create the field or else the linac will not accept the request.

An exception to Portfilm function:

If the Portfilm function is not available (known to happen on Oncor and Artiste units), Create field type as "Setup", not "Static".

During the delivery, the couch angle/pedestal angle cannot be changed/overridden, instead lift the couch high enough that all beams go through the couch fully.

Stellenbosch University https://scholar.sun.ac.za

Varian Vitalbeam/Truebeam:

When using a Varian Vital- or Truebeam linear accelerator with an MV imager, follow the following acquisition protocol for optimal results.

- Create 6 static fields in Mosaiq with the following properties:

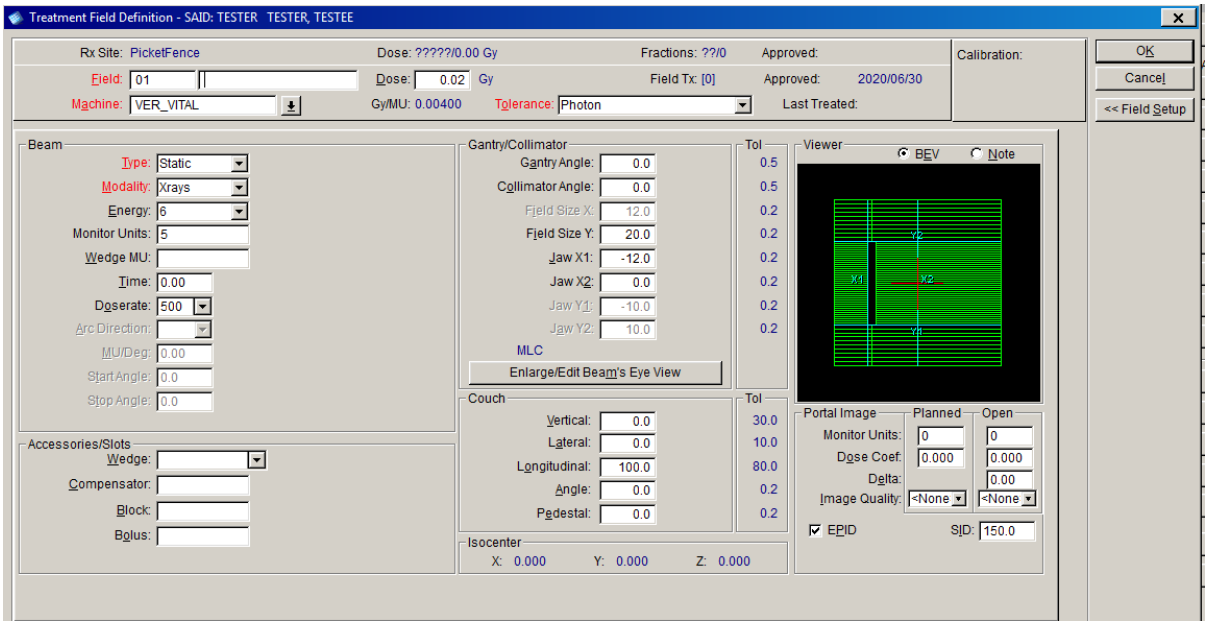

And the following MLC properties for fields 1-6 follow numerically with the simple MLC function as shown below to the values in the table.

Jaw	Picket 1	Picket 2	Picket 3	Picket 4	Picket 5	Picket 6
X1 position	12	8	4	0	-4	-8
X2 position	-10	-6	-2	2	6	10

After these fields have been created, MV images of these fields are taken. The individual pickets can be imaged independently and added with independent software like ImageJ or the Doselab software may be used to combine images.

To take the segmented images, open the patient in Mosaiq, and send them over to the treatment workstation. **The couch needs to be out gantry's way – push back couch**

Stellenbosch University https://scholar.sun.ac.za

1. Log in to Treatment Mode
2. To take the segmented images, open the patient in MOSAIQ and send them over to the treatment workstation
3. Complete the following steps to add a portal image if no image was preloaded
4. Highlight the first field and click ADD - Add Imaging
5. Modality – MV (Imaging screen)
6. Execution Phase – During
7. Modality Speci – Dosimetry
8. Select During, Dosimetry (as above) and Apply images to each field - click OK
9. Back to the treatment console screen
10. Click the acquire tick boxes next to the couch (first click on Acquire – bottom of the screen)

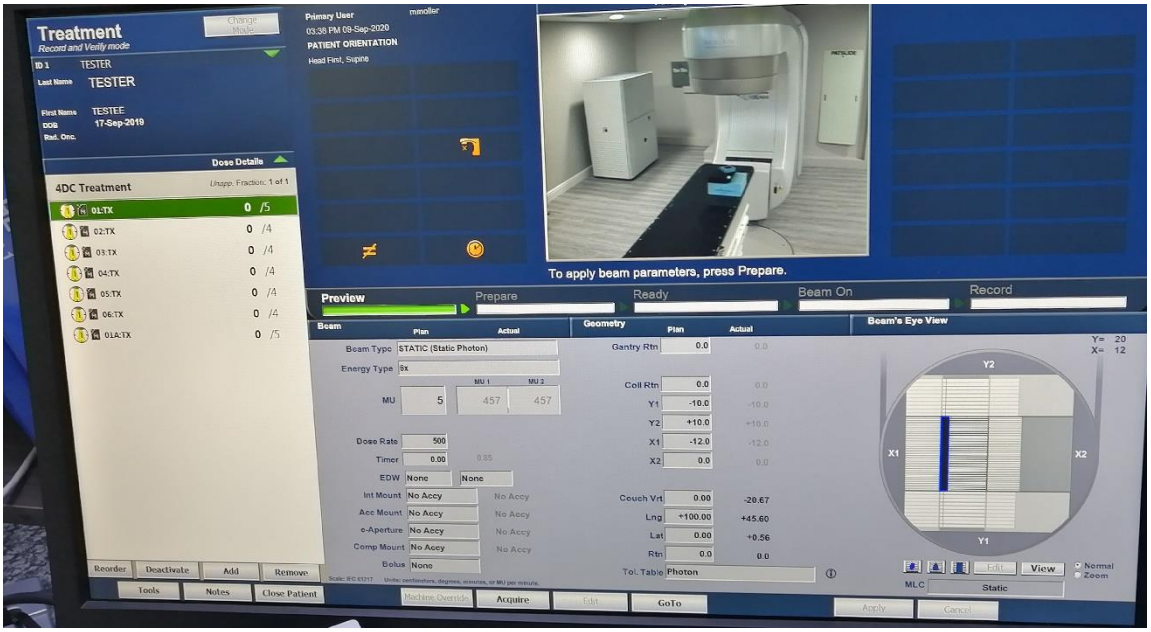

Stellenbosch University https://scholar.sun.ac.za

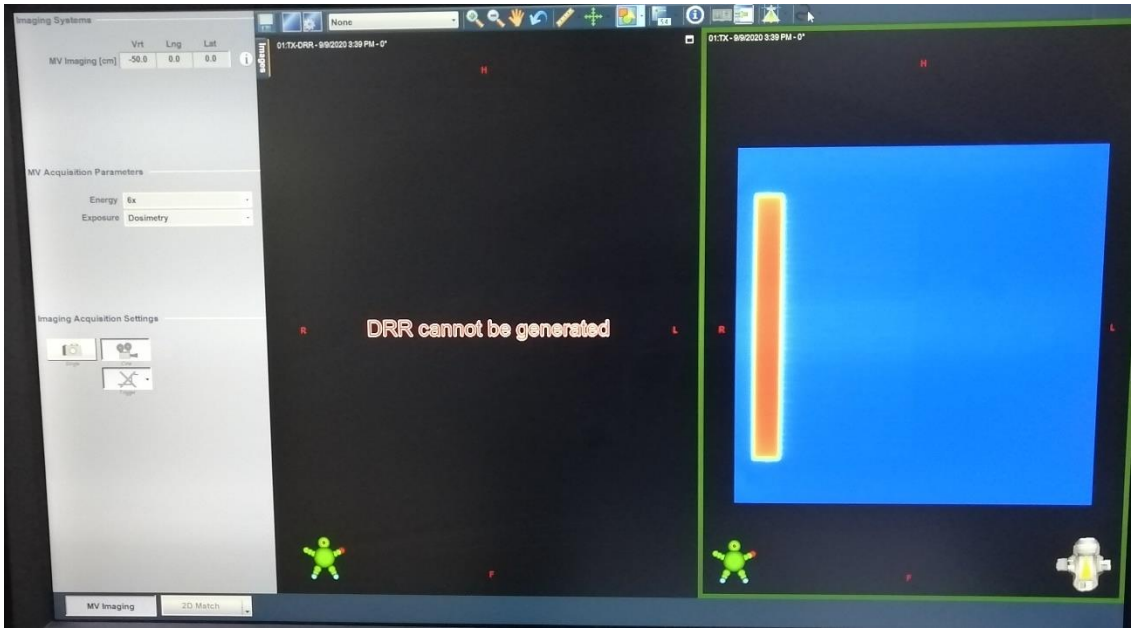

14. After delivery is complete click Close Plan
15. Sign Off
16. Images will be saved back to Mosaiq by the date and time of the image acquisition
17. The image exported is a DICOM image and can be opened and analyzed with the PicketPRO software.

Stellenbosch University https://scholar.sun.ac.za

Varian Halcyon:

Since the Varian Halcyon cannot function with any other R&V system other than Aria, the Varian Halcyon picket fence must be created and delivered from Eclipse & Aria.

1. Open patient TESTER, TESTEE.
2. Since units can be changed without altering MLC positions if the units have the same MLC, you can copy the "PF HAL_OUT" plan under the "Halcyon" course and just change the unit.
3. If this does not work for some unknown reason, the individual pickets can be created as separate static fields. You can use the MLC shape tool. It becomes an available option when the BEV window is active and the MLC is selected for the specific field.

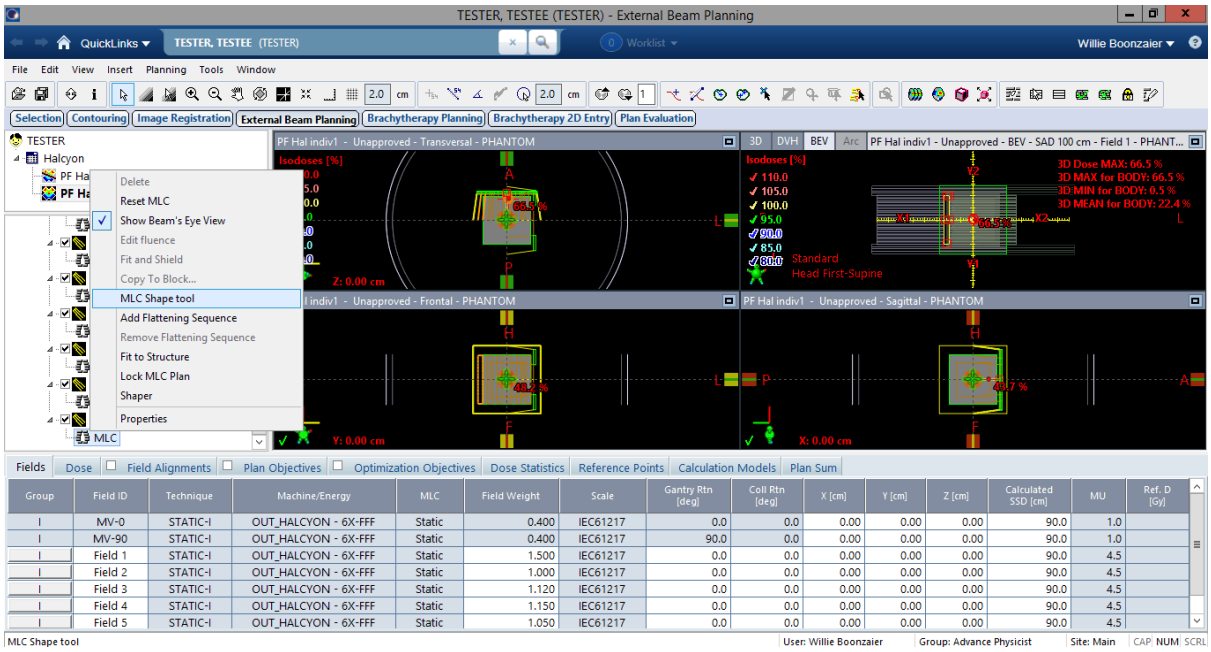

Group	Field ID	Technique	Machine/Energy	MLC	Field Weight	Scale	Gantry Rtn [deg]	Coll Rtn [deg]	X [cm]	Y [cm]	Z [cm]	Calculated SSD [cm]	MU	Ref. D [Gy]
I	MV-0	STATIC-I	OUT_HALCYON - 6X-FFF	Static	0.400	IEC61217	0.0	0.0	0.00	0.00	0.00	90.0	1.0	
I	MV-90	STATIC-I	OUT_HALCYON - 6X-FFF	Static	0.400	IEC61217	90.0	0.0	0.00	0.00	0.00	90.0	1.0	
I	Field 1	STATIC-I	OUT_HALCYON - 6X-FFF	Static	1.500	IEC61217	0.0	0.0	0.00	0.00	0.00	90.0	4.5	
I	Field 2	STATIC-I	OUT_HALCYON - 6X-FFF	Static	1.000	IEC61217	0.0	0.0	0.00	0.00	0.00	90.0	4.5	
I	Field 3	STATIC-I	OUT_HALCYON - 6X-FFF	Static	1.120	IEC61217	0.0	0.0	0.00	0.00	0.00	90.0	4.5	
I	Field 4	STATIC-I	OUT_HALCYON - 6X-FFF	Static	1.150	IEC61217	0.0	0.0	0.00	0.00	0.00	90.0	4.5	
I	Field 5	STATIC-I	OUT_HALCYON - 6X-FFF	Static	1.050	IEC61217	0.0	0.0	0.00	0.00	0.00	90.0	4.5	

4. Make sure that both the "Rectangular" and "asymmetric options are chosen.

Stellenbosch University https://scholar.sun.ac.za

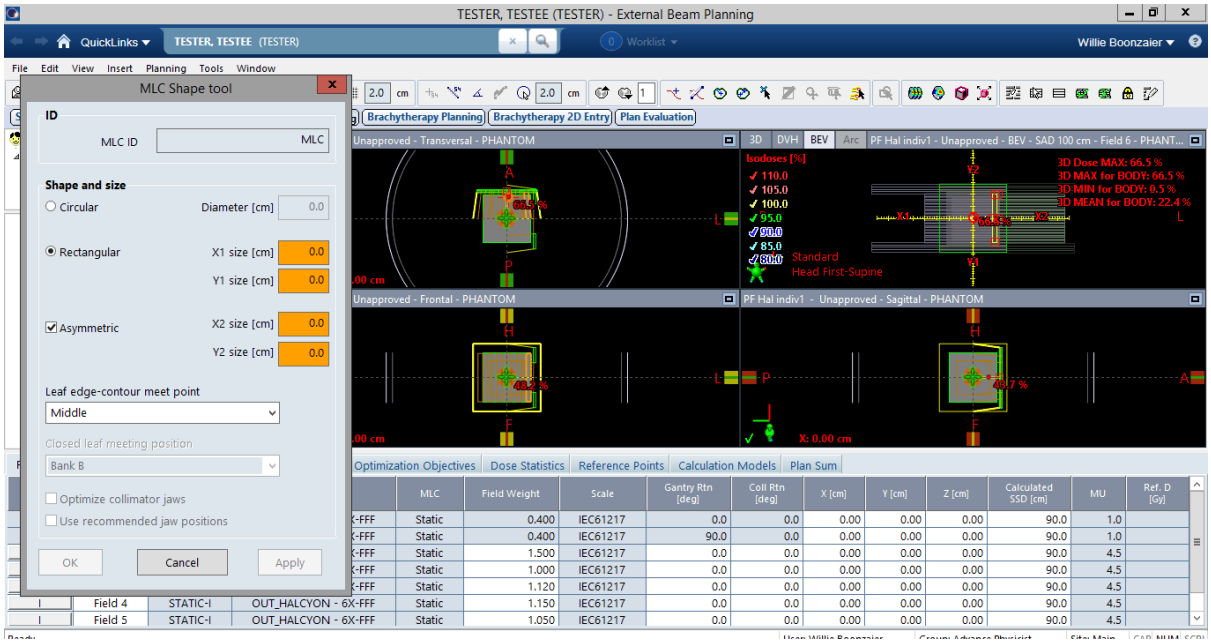

5. Use the table below for X1, X2, Y1, and Y2 values for all pickets.

	Value in cm					
Option	Picket 1	Picket 2	Picket 3	Picket 4	Picket 5	Picket 6
X1	12	8	4	0	-4	-8
X2	-10	-6	-2	2	6	10
Y1	10	10	10	10	10	10
Y2	10	10	10	10	10	10

6. If you have created all pickets, you can use the "Merge Subfields" option in the "Planning" menu to merge all fields into a single dynamic MLC field and recalculate the dose.

Stellenbosch University https://scholar.sun.ac.za

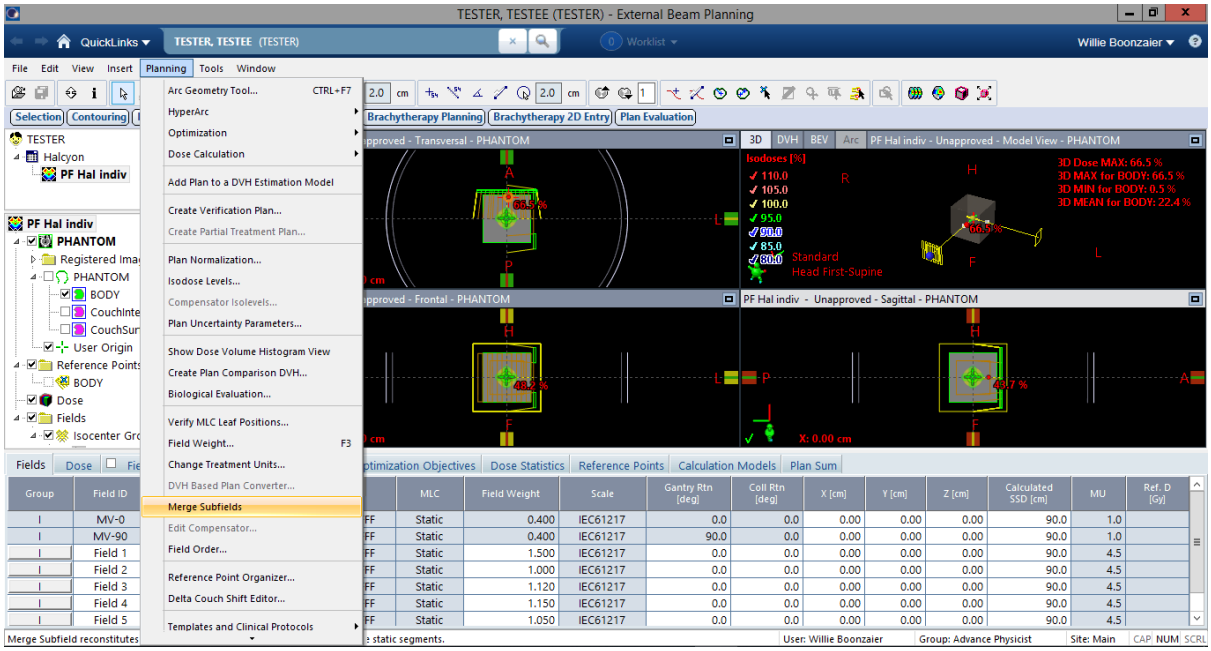

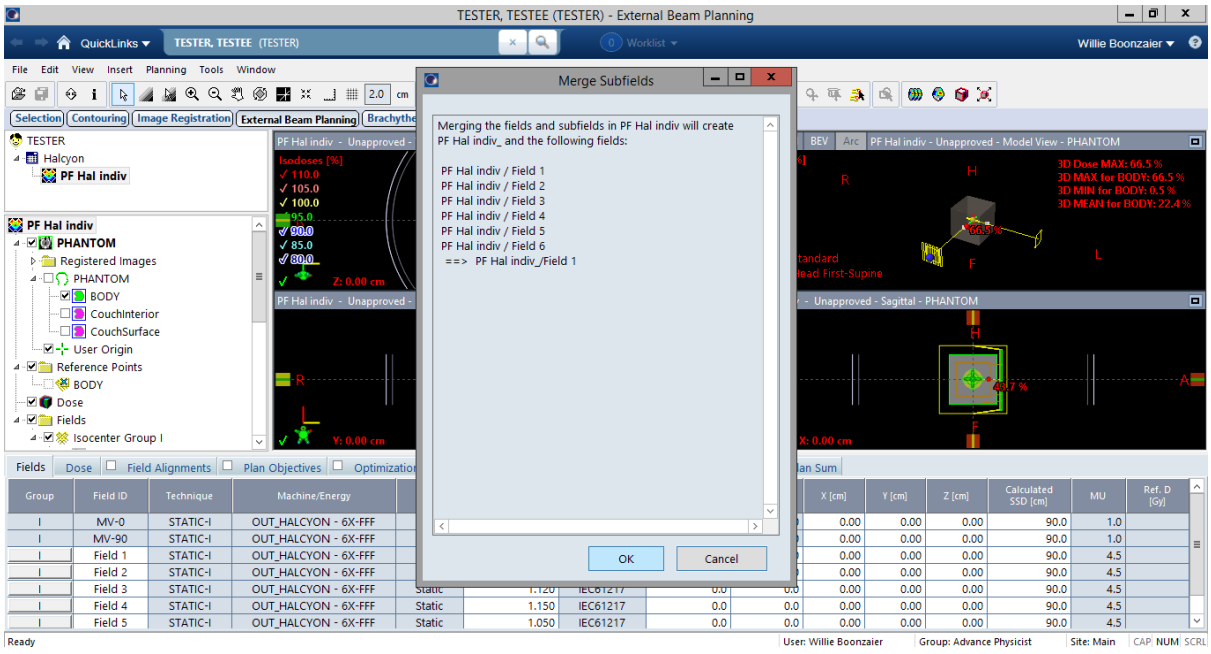

Stellenbosch University https://scholar.sun.ac.za

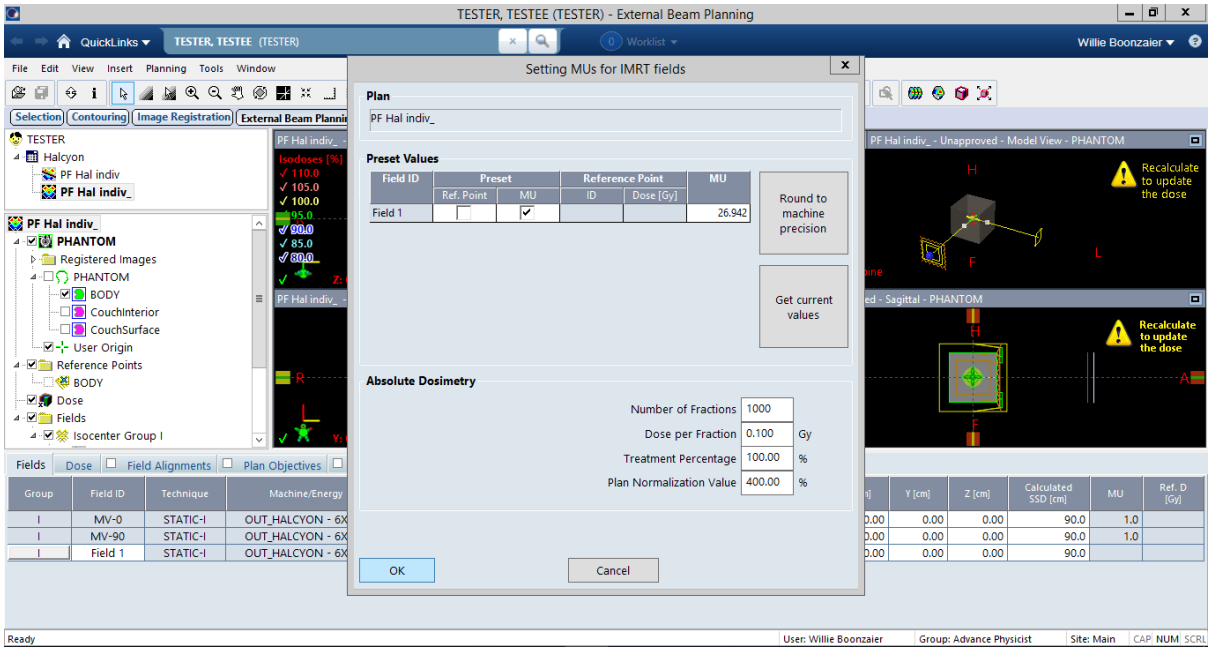

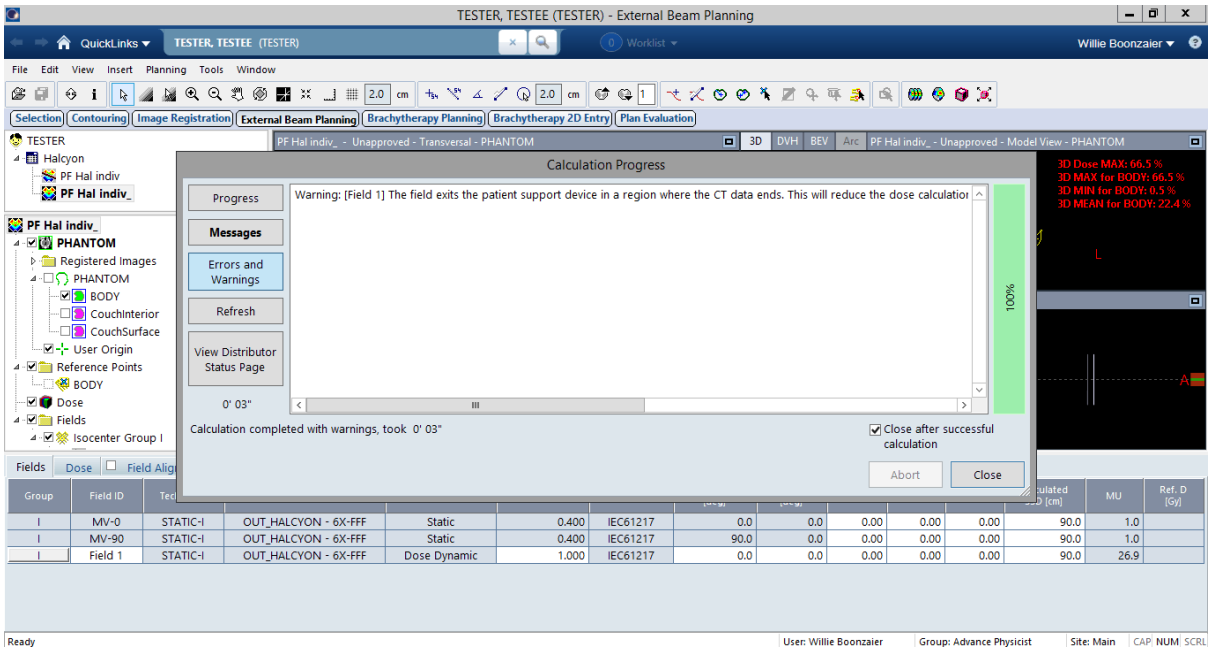

7. To deliver and image it, deliver the pattern as an IMRT patient using portal dosimetry.
8. After this has been completed, use a DICOM export filter to export the acquired image from Eclipse to your PC. The filter settings should be set up as below with a link to the PC and folders used:

Stellenbosch University https://scholar.sun.ac.za

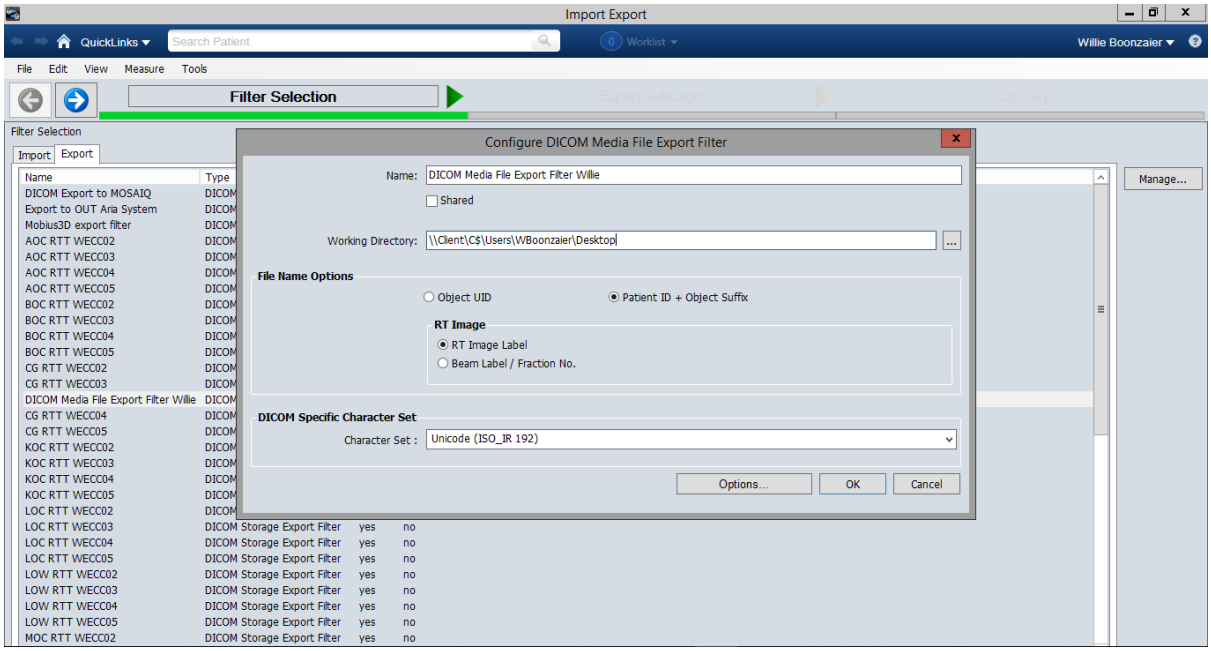

Stellenbosch University https://scholar.sun.ac.za

Picket fence at various gantry angles and picket fence during arc:

For these two tests, the beam limiting devices (MLCs and Jaws) are prepared the same as for the Picket fence at gantry angle zero. The only difference in these two tests compared to the Picket fence at gantry angle zero is the introduction of gantry angles or arcs.

Picket fence at various gantry angles:

For this test, 6 static fields can be created as for the Picket fence at gantry angle zero, however, for this test, the gantry angle of all the pickets should be changed to the same angle (non-zero) and the gantry angles can be alternated monthly.

This test is designed to pick up single MLC errors from the bank as well as MLC over or under travel at a certain gantry angle.

Note that once again it is possible to deliver these static beams in an automatic field sequence to speed up the workflow.

Picket fence during arc delivery:

For this test, the MLCs and Jaw characteristics are again the same as in the other picket fence tests. The delivery type is changed to "Arc", the start and stop angles adjusted to divide a full rotation (360 degrees) into 6 arcs of equal weight, and the monitor units set to 20 MU per arc.

This test is designed to pick up single MLC errors from the bank but not MLC over or under travel during VMAT delivery.

Note that it is not possible to deliver arcs in an automatic field sequence and that the arcs should be delivered one after the other while the EPID is allowed to automatically detect the start and the stop of segments and sum the segments into a single image.

Stellenbosch University https://scholar.sun.ac.za

Analysis of QAPRO Picket fence using PICKETPRO:

After successfully installing the QAPRO software to the PC to be used, the following procedure can be used to analyse the picket fence images.

Using the PICKETPRO for picket fence analysis:

1. Open the QAPRO software.

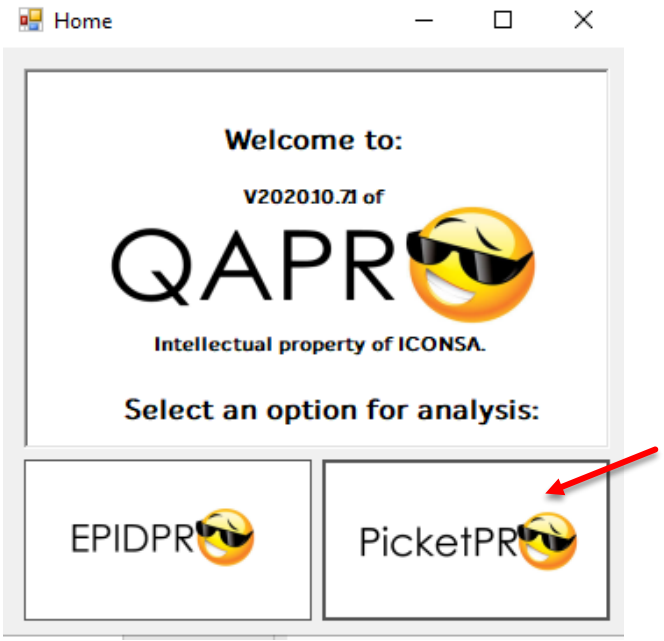

2. Select the PICKETPRO option in the home window.
3. The following window will appear.

4. Select the correct linac model from the drop-down list. **Note that if the wrong model is selected, you may have problems importing your image.**

Stellenbosch University https://scholar.sun.ac.za

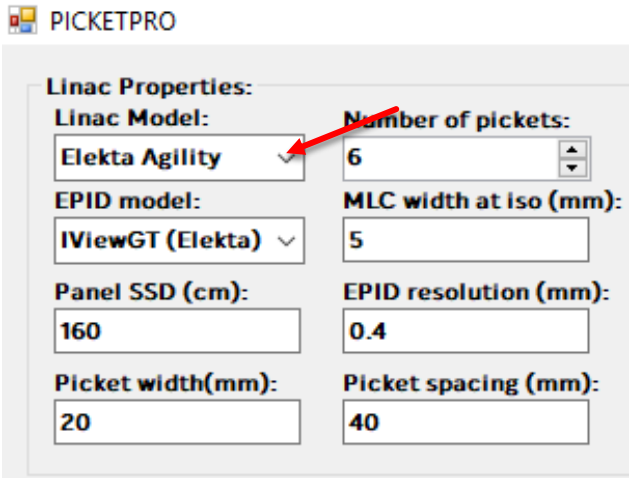

5. Click on the open button and use the open file dialogue to navigate to the appropriate image and open it. Wait as it might take several minutes. Note that DICOM images from onboard imagers are very large as the files are encrypted and contain data for over a million pixels.

Stellenbosch University https://scholar.sun.ac.za

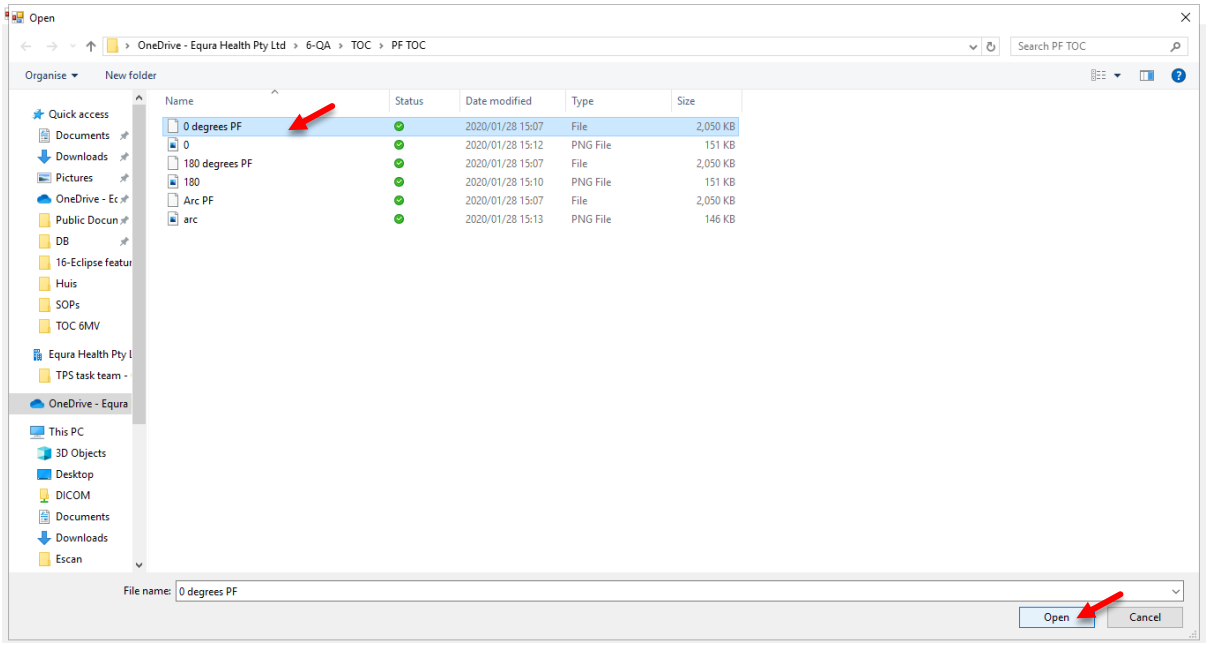

6. If you have 1 image with all 6 pickets on, move on to step 7. If your pickets are on individual images, use the add image button to add each of the other pickets to the first picket one by one.

Stellenbosch University https://scholar.sun.ac.za

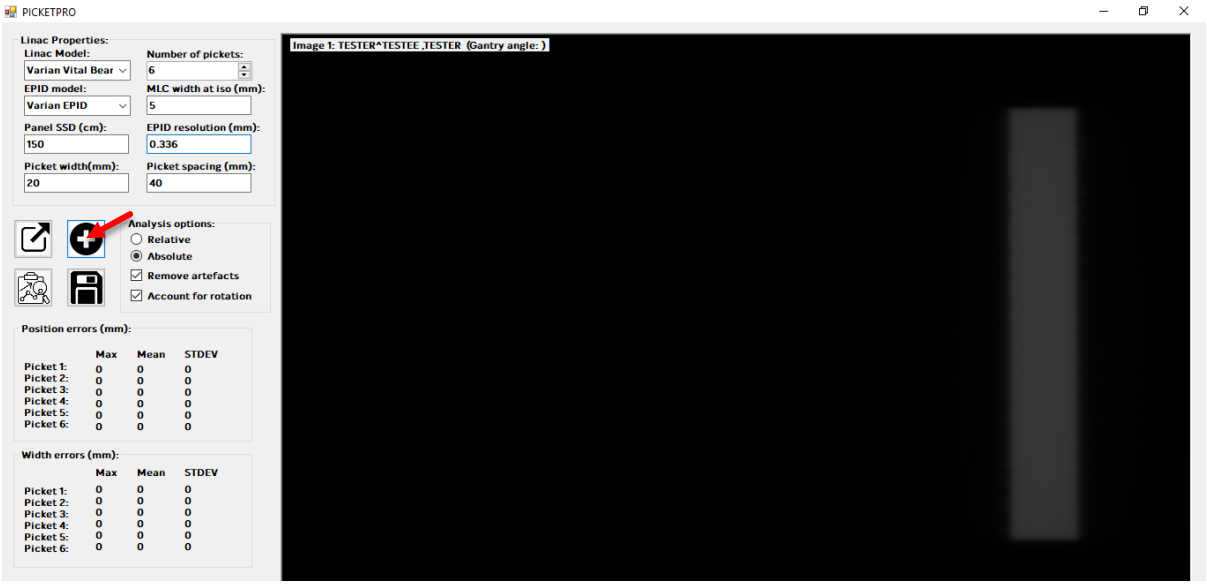

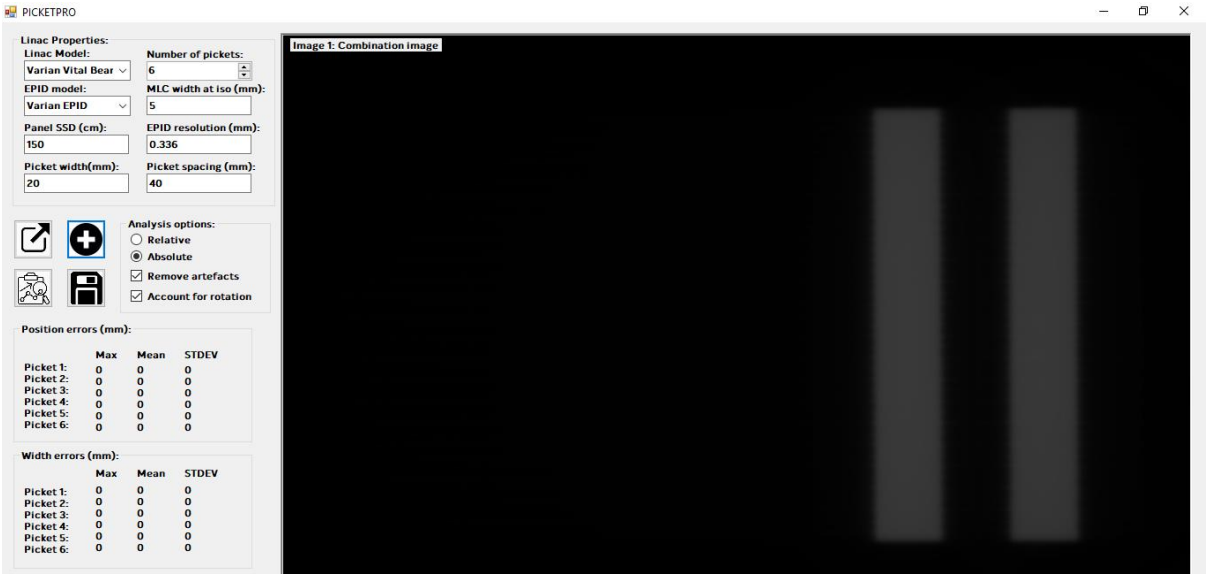

7. If the image is displayed in the PictureBox, ensure that all of the Linac and analysis parameters are correct.

    a. The panel SSD when imaging should be used for all units except Halcyon. For Halcyon, use 100cm.
    b. The EPID resolution depends on the model of EPID used when imaging. The true EPID resolution should be used and not the digital resolution. Use the table below to check if your resolution is correct.

Stellenbosch University https://scholar.sun.ac.za

EPID model	Resolution of a pixel (mm)
IviewGT (Elekta)	0.4
Optivue 1000 (Siemens)	0.4
Varian aS1000	0.336
RDS MV imager (Halcyon)	0.22

c. The "Remove artefacts" option should always be checked. This employs a median filter to get rid of image, and electronic noise.
d. The "Absolute analysis" should always be used with the exception if the gantry is moving during the acquisition of the picket fence as for the arc picket fence. In this solitary case, the relative analysis should be used to eliminate the influence of EPID sag on the MLC results.
e. "Account for rotation" accounts for collimator rotation and may be used or not used as decided by the user.

8. When you have checked all of the parameters, click on the analysis button. This will start the analysis. You can track the analysis with the feedback bar at the bottom of the PictureBox.

Stellenbosch University https://scholar.sun.ac.za

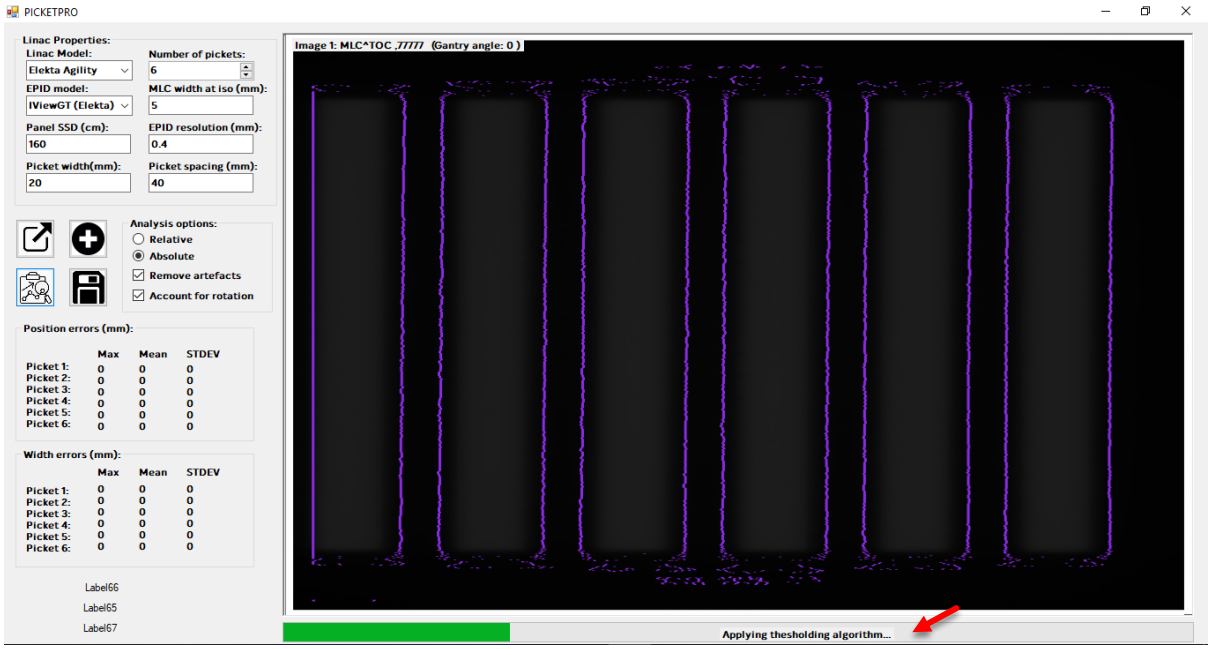

9. After the analysis has been completed, visually inspect the processed image to evaluate if the software found true MLC errors. False errors can cause unreliable results. False errors can happen due to a variety of reasons but mostly occur due to imager or imaging artefacts.

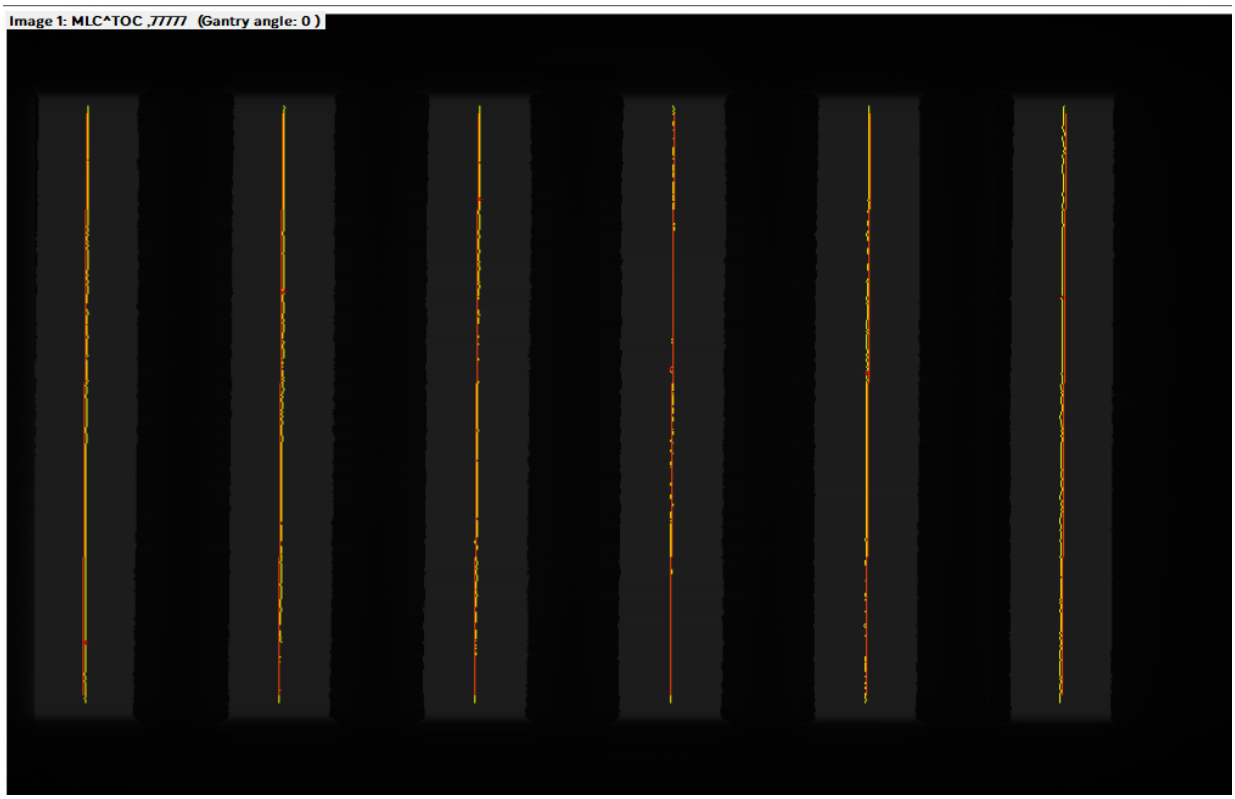

10. Maximum errors provide only the single leaf with the largest error. These can be random or systematic errors. Mean errors provide information regarding the systematic errors and the state of the system. A small standard deviation error

Stellenbosch University https://scholar.sun.ac.za

indicates that all the MLCs are performing in the same way. For a baseline on what to expect from your system, study Appendix A.

Position errors (mm):

	Max	Mean	STDEV
Picket 1:	0.5	0.36	0.08
Picket 2:	0.49	0.3	0.09
Picket 3:	0.36	0.22	0.07
Picket 4:	0.27	0.05	0.04
Picket 5:	0.38	0.23	0.07
Picket 6:	0.62	0.44	0.09

Width errors (mm):

	Max	Mean	STDEV
Picket 1:	0.38	013	013
Picket 2:	0.25	01	0.07
Picket 3:	0.38	018	01
Picket 4:	0.38	018	011
Picket 5:	0.38	018	0.09
Picket 6:	0.25	0.04	0.07

Stellenbosch University https://scholar.sun.ac.za

Baseline expected values for each machine type:

Below are screenshots are taken from the ideal picket fence of each of the units that were validated. The absolute analysis option was used in all cases, excluding the arc picket fence.

Stellenbosch University https://scholar.sun.ac.za

Elekta Agility:

Gantry angle =0 degrees.

Stellenbosch University https://scholar.sun.ac.za

Gantry angle = 90 degrees.

Stellenbosch University https://scholar.sun.ac.za

Arc picket fence:

Stellenbosch University https://scholar.sun.ac.za

Siemens Artiste MLC160:

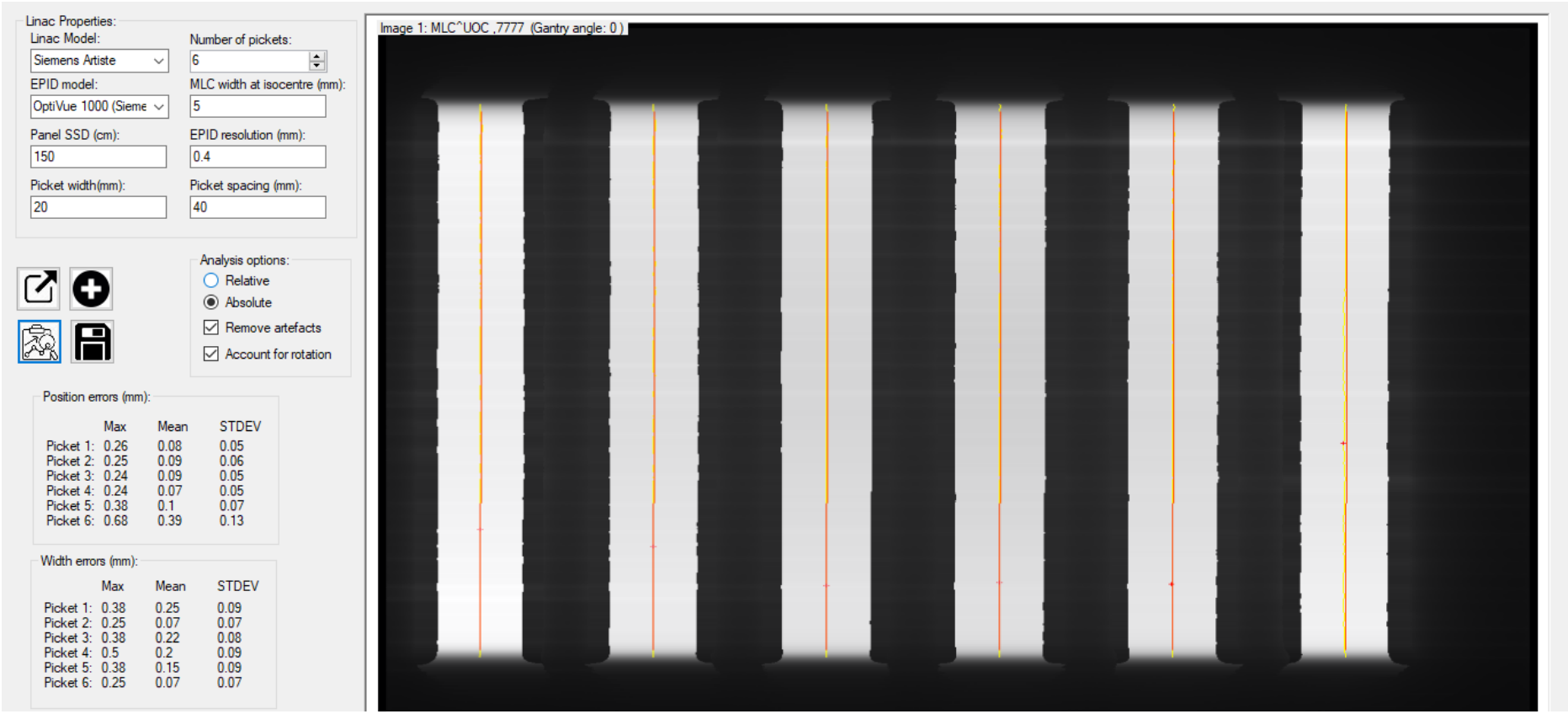

Stellenbosch University https://scholar.sun.ac.za

Varian Vital beam Millennium 120 MLC:

Stellenbosch University https://scholar.sun.ac.za

Varian Halcyon:

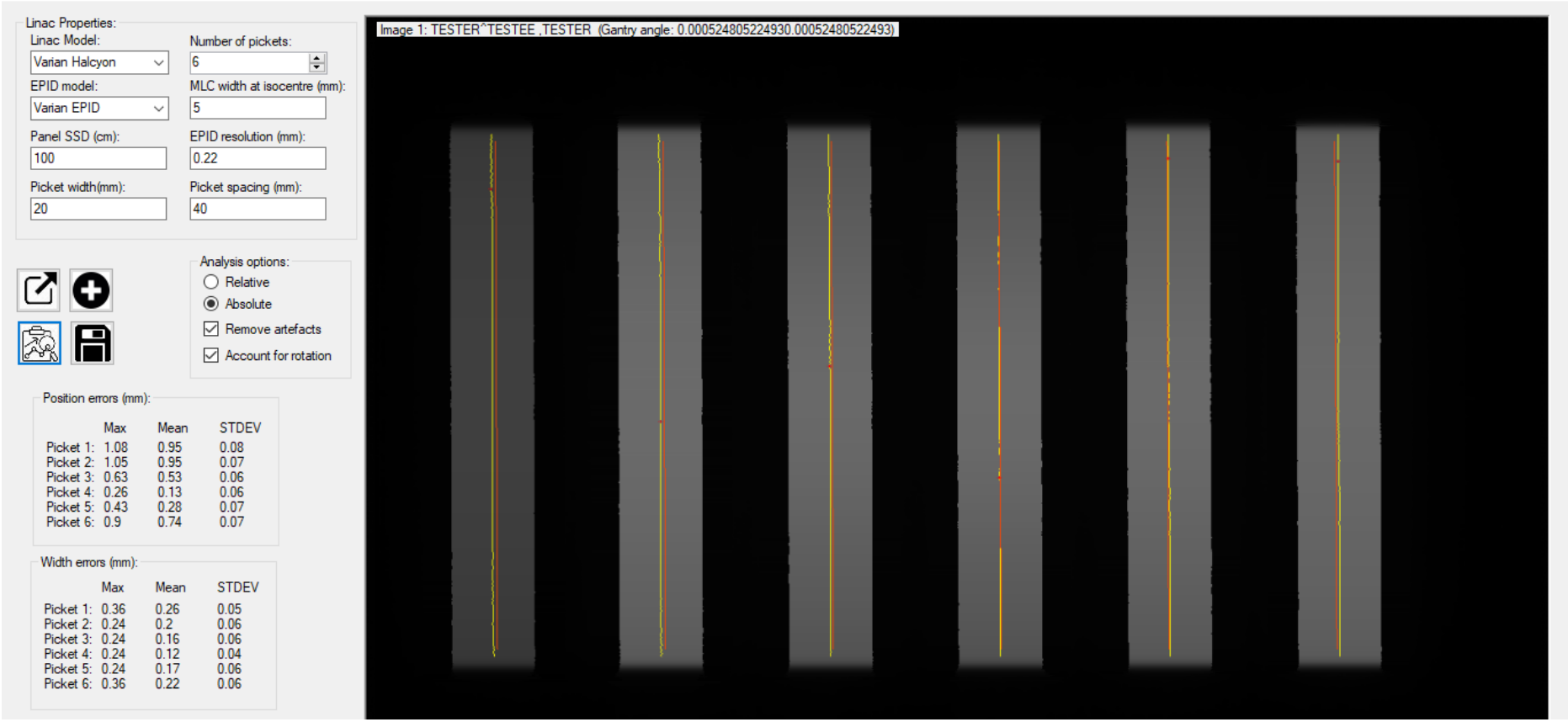

Stellenbosch University https://scholar.sun.ac.za

Appendix B: Layout of software created

This appendix outlines the flow of the program created.